

From the Dept. Dermatology, Venereology & Allergy  
University Medical Center Mannheim  
(Director: Prof. Dr. med. S. Goerdts)

# Liver-specific endothelial mechanisms of melanoma metastasis

Inaugural dissertation for  
obtaining the doctoral degree of the  
combined Faculty of Mathematics, Engineering  
and Natural Sciences  
of the Ruprecht – Karls –University Heidelberg

Presented by  
Verena Häfele

Oral examination: 15.11.2023

Inaugural dissertation  
For  
Obtaining the doctoral degree  
Of the  
Combined Faculty of Mathematics, Engineering and Natural Sciences  
Of the  
Ruprecht – Karls –University  
Heidelberg

Presented by  
M. Sc. Verena Häfele

Born in: Karlsruhe  
Oral examination: 15.11.2023

# **Liver-specific endothelial mechanisms of melanoma metastasis**

Referees: Prof. Dr. Peter Angel

Prof. Dr. med. Cyrill Géraud

“I am among those who think that  
science has great beauty.”

Marie Curie

Parts of this thesis have been published:

*“Hepatic Endothelial Notch Activation Protects against Liver Metastasis by Regulating Endothelial-Tumor Cell Adhesion Independent of Angiocrine Signaling”*

Sebastian A. Wohlfeil\*, Verena Häfele\*, Bianca Dietsch, Kai Schledzewski, Manuel Winkler, Johanna Zierow, Thomas Leibing, Mona Malek Mohammadi, Joerg Heineke, Carsten Sticht, Victor Olsavszky, Philipp-Sebastian Koch, Cyrill Géraud\*, Sergij Goerd\*

Cancer Res (2019) 79 (3): 598–610.

\*Equally contributing first and last authors.

*“Angiogenic and molecular diversity determine hepatic melanoma metastasis and response to anti-angiogenic treatment.”*

Sebastian A. Wohlfeil, Verena Häfele, Bianca Dietsch, Céline Weller, Carsten Sticht, Anna Sophia Jauch, Manuel Winkler, Christian David Schmid, Anna Lena Irkens, Ana Olsavszky, Kai Schledzewski, Philipp-Sebastian Reiners-Koch, Sergij Goerd & Cyrill Géraud

Journal of Translational Medicine, volume 20, Article number: 62 (2022)

# Table of Contents

1. Abstract .....	- 1 -
2. Zusammenfassung.....	- 3 -
3. Introduction.....	- 5 -
3.1. Cutaneous melanoma .....	- 5 -
3.1.2 Epidemiology of cutaneous melanoma.....	- 5 -
3.1.3 Intrinsic and extrinsic risk factors of malignant melanoma .....	- 5 -
3.1.4 MAPK pathway signaling in malignant melanoma.....	- 6 -
3.1.5 Staging of cutaneous melanoma.....	- 7 -
3.1.6 Melanoma therapy.....	- 8 -
3.1.6.1 BRAF/MEK inhibitor.....	- 8 -
3.1.6.2 Immune checkpoint inhibition .....	- 8 -
3.1.6.3 Anti-cytotoxic T-lymphocyte-associated protein 4 (CTLA-4) antibodies.....	- 9 -
3.1.6.4 Anti-programmed cell death protein 1 (PD-1) antibodies .....	- 9 -
3.1.6.5 Immune checkpoint therapy .....	- 9 -
3.1.6.6 Combination therapy .....	- 10 -
3.2 Metastasis of cutaneous melanoma .....	- 10 -
3.2.1 Seed and soil hypothesis .....	- 11 -
3.2.2 The metastatic cascade and malignant melanoma.....	- 12 -
3.2.2.1 Epithelial-mesenchymal transition (EMT) .....	- 13 -
3.2.2.2 Dissemination and invasion of surrounding tissue .....	- 14 -
3.2.2.3 Surviving in the circulation .....	- 15 -
3.2.2.4 Tumor cell arrest and extravasation .....	- 15 -
3.2.2.5 Survival and adaptation to the microenvironment.....	- 16 -
3.2.2.6 Angiogenesis.....	- 17 -
3.2.3 The hepatic vascular niche .....	- 17 -
3.2.3.1 Formation of a premetastatic niche.....	- 17 -
3.2.4 Exosomes in melanoma metastasis .....	- 18 -
3.2.5 Role of liver resident cells in metastasis. ....	- 18 -
3.2.6 Histopathological growth patterns of hepatic metastases .....	- 19 -
3.2.7 Notch signaling in metastasis.....	- 19 -
3.3 The Liver .....	- 20 -
3.3.1 Hepatocytes.....	- 21 -
3.3.2 Hepatic stellate cells.....	- 22 -
3.3.3 Kupffer cells.....	- 23 -
3.3.4 LSEC .....	- 23 -

3.3.4.1 Origin .....	- 23 -
3.3.4.2 Morphology and Location .....	- 24 -
3.3.4.3 LSEC functions .....	- 25 -
3.3.4.3.1 Endocytic functions of LSEC .....	- 25 -
3.3.4.3.2 Leukocyte trafficking .....	- 26 -
3.3.4.3.3 Angiocrine signaling .....	- 26 -
3.3.4.3.4 Immunological functions of LSEC .....	- 26 -
3.3.4.4 LSEC and their role in liver regeneration.....	- 27 -
3.3.4.5 LSEC disfunction and liver fibrosis.....	- 27 -
3.3.4.6 LSEC and their role in metastasis. ....	- 28 -
3.4 Models of melanoma metastasis .....	- 28 -
3.4.1 Xenotransplantation models .....	- 28 -
3.4.2 Syngeneic transplantation model.....	- 29 -
3.4.3 Genetically engineered mouse models .....	- 29 -
3.5 Aim of the Thesis .....	- 30 -
4. Material and methods.....	- 32 -
4.1. Material .....	- 32 -
4.1.1. Chemicals, solvents, and reagents .....	- 32 -
4.1.2. Buffers and media/recipes .....	- 34 -
4.1.3. Kits .....	- 35 -
4.1.4. Unconjugated antibodies .....	- 36 -
4.1.5. Conjugated antibodies .....	- 37 -
4.1.6. Primers for Genotyping .....	- 37 -
4.1.7 Consumables .....	- 38 -
4.1.8. Technical equipment .....	- 39 -
4.1.9 Software .....	- 41 -
4.1.10 Mouse strains .....	- 41 -
4.1.11 Cell lines.....	- 42 -
4.2 Methods .....	- 42 -
4.2.1 Cell culture.....	- 42 -
4.2.1.1 Cell lines.....	- 42 -
4.2.1.2 Thawing of cells .....	- 43 -
4.2.1.3 Freezing of cells .....	- 43 -
4.2.1.4 Splitting.....	- 43 -
4.2.1.5 Seeding of cells.....	- 44 -
4.2.1.6 Harvesting cells.....	- 44 -

4.2.2 Preparation of murine melanoma cell lines for <i>in vivo</i> experiments.....	- 44 -
4.2.2.1 B16F10 <i>luc2</i> .....	- 44 -
4.2.2.2 WT31 .....	- 44 -
4.2.2.3 RET.....	- 45 -
4.2.2.4 D4M3.A.....	- 45 -
4.2.2.5 HcMel12 .....	- 45 -
4.2.2.6 MC38 .....	- 45 -
4.2.3 Animal experiments .....	- 45 -
4.2.3.1 Animal housing and breeding.....	- 45 -
4.2.3.2 Generation of liver-specific endothelial Notch1 overexpression mice .....	- 46 -
4.2.3.3 Generation of WLS <sup>HEC-KO</sup> mice.....	- 46 -
4.2.3.4 Liver colonization assays .....	- 46 -
4.2.3.4.1 Intralial injection of cells .....	- 46 -
4.2.3.4.2 Intravenous injection of WT31 cells.....	- 47 -
4.2.3.5 Bioluminescence Imaging.....	- 47 -
4.2.3.6 Dissection of mouse organs, cryopreservation and paraffin embedding .....	- 47 -
4.2.3.7 Blood parameters.....	- 48 -
4.2.4 Molecular biology methods.....	- 48 -
4.2.4.1 Genotyping .....	- 48 -
4.2.4.2 Polymerase chain reaction (PCR) .....	- 48 -
4.2.4.3 Agarose gel electrophoresis .....	- 49 -
4.2.4.4 RNA isolation .....	- 49 -
4.2.4.5 RNA sequencing.....	- 49 -
4.2.5 Histological methods.....	- 50 -
4.2.5.1 Hematoxylin & Eosin (H&E) Staining .....	- 50 -
4.2.5.2 Immunofluorescence staining of cryosections.....	- 50 -
4.2.5.3 Immunofluorescence staining of paraffin-embedded sections. ....	- 51 -
4.2.6 Image acquisition and analysis.....	- 51 -
4.2.6.1 Brightfield images.....	- 51 -
4.2.6.2 Image acquisition and processing of routine histology stainings .....	- 51 -
4.2.6.3 Confocal microscopy .....	- 51 -
4.2.6.4 Image analysis with Image J .....	- 52 -
4.2.7 Statistical analysis.....	- 52 -
5. Results .....	- 53 -
5.1 Murine Melanoma cell lines differ in their hepatic metastatic efficiency. ....	- 53 -
5.2 Histomorphological analysis of hepatic metastases of WT31, B16F10 <i>luc2</i> and RET cells. ....	- 56 -

5.3 Hepatic metastases differ in their vascular density but share a common endothelial expression profile on intratumoral blood vessels. ....	57 -
5.4 RNA sequencing of melanoma cell lines .....	64 -
5.5 Summary .....	66 -
5.6 Hepatic melanoma metastasis in genetically modified mice overexpressing the notch1 intracellular domain in LSEC.....	66 -
5.7 Generation of NICD <sup>OE-HEC</sup> mice.....	67 -
5.8 Hepatic endothelial activation of NICD protects from liver metastasis.....	67 -
5.9 Phenotypic characterization of adult NICD <sup>OE-HEC</sup> mice.....	70 -
5.10 Characterization of the hepatic endothelium of NICD <sup>OE-HEC</sup> mice.....	72 -
5.11 Metabolic zonation is impaired in NICD <sup>OE-HEC</sup> mice.....	77 -
5.12 Metastatic susceptibility is not altered in WLS <sup>HEC-KO</sup> mice.....	78 -
5.13 Expression of adhesion molecules in NICD <sup>OE-HEC</sup> mice. ....	79 -
5.14 Summary .....	80 -
6. Discussion.....	82 -
6.1 Mouse models of malignant melanoma .....	82 -
6.2 Capillarization of intratumoral blood vessels.....	83 -
6.3 Angiogenic processes in liver metastasis .....	83 -
6.4 Tumor-intrinsic mechanisms of melanoma metastasis .....	83 -
6.5 Tumor-extrinsic mechanisms of hepatic metastasis .....	84 -
6.5.1 Clec4g, as an endothelial subtype-specific promoter .....	85 -
6.5.2 Metabolic and endothelial zonation of NICD <sup>OE-HEC</sup> mice.....	85 -
6.5.3 Role of adhesion molecules in organotropic metastasis.....	87 -
6.6 Summary and Outlook.....	87 -
References.....	89 -
Acknowledgements .....	109 -
Appendix.....	110 -
List of Figures.....	110 -
List of Tables.....	111 -
List of Abbreviations.....	112 -

## 1. Abstract

Cutaneous melanoma arises from melanocytes in the skin and is a highly aggressive cancer that metastasizes early and has a poor prognosis. In recent years treatment of malignant melanoma has been revolutionized by the introduction of immune checkpoint inhibition (ICI) and targeted therapies. However, not all patients have the same prognosis and benefit from immunotherapy. Especially patients with liver metastases are associated with a poor prognosis and a poor response to ICI and targeted therapy of v-Raf murine sarcoma viral oncogene homolog B1 (BRAF)-mutated melanoma.

In 1889 Stephen Paget postulated in the „seed and soil“-hypothesis that circulating tumor cells are homed to selected sites. And indeed, melanoma metastasis is remarkably organ specific (organotropism). Organotropism can be explained by tumor cell intrinsic factors and by microenvironmental, organ-specific cues. In the organ-specific niche endothelial cells (EC) build the first line of contact for circulating tumor cells. The vascular niche might favor or suppress tumor cell arrest and extravasation.

The vascular niche in the liver is composed of liver sinusoidal endothelial cells (LSEC). LSEC form a sinusoidal discontinuous endothelium that lacks a basement membrane and contains fenestrations without diaphragms.

In this thesis I analyzed the organ-specific, endothelial-dependent mechanisms as well as tumor intrinsic mechanisms of malignant melanoma cell dissemination to the liver. In an experimental liver colonization model the hematogenous spread of tumor cells was mimicked. Murine melanoma cell lines, heterogenous in their underlying driver mutations, were injected into the spleen of C57BL/6 mice to induce liver metastasis. Additionally, the melanoma cell line WT31 harboring a human neuroblastoma Ras viral oncogene homolog (Nras) mutation was injected into the tail vein leading amongst other organs to liver colonization. Melanoma cell lines differed in their metastatic efficiency and high and intermediate metastatic melanoma cell lines were further analyzed. A common histopathological growth pattern of the high and intermediate metastatic melanoma cell lines was identified. Although, these cell lines differed in their vascular density, tumor endothelial cells shared a common expression profile.

In the second part of my thesis, the influence of notch overexpression in hepatic endothelial cells (HEC) using genetically modified NICD<sup>OE-HEC</sup> mice was studied. Notch 1 intracellular domain (NICD) overexpression in HEC significantly protected from liver metastasis in two models of malignant melanoma and in a model of colorectal cancer. Further, alterations in endothelial and metabolic zonation were detected and the expression of adhesion molecules

was altered in NICD<sup>OE-HEC</sup> mice. Downregulation of intercellular adhesion molecule 1 (ICAM1) was identified as a potential mechanism of protection from liver metastasis in NICD<sup>OE-HEC</sup> mice.

## 2. Zusammenfassung

Das maligne Melanom der Haut entsteht aus Melanozyten, den pigmentbildenden Zellen der Haut. Der schwarze Hautkrebs ist ein hochaggressiver Krebs, der bereits in einem frühen Stadium Metastasen ausbildet und mit einer ungünstigen Prognose einhergeht. Die Einführung der Immuntherapie und zielgerichteter Therapien hat die Behandlung des malignen Melanoms revolutioniert. Trotz der Fortschritte in der modernen Medizin profitieren nicht alle Patienten in gleichem Maße davon. Insbesondere Patienten mit Metastasen in der Leber haben noch immer eine ungünstige Prognose und sprechen schlechter auf die verfügbaren Immuntherapien, sowie auf zielgerichtete Therapien des BRAF-mutierten Melanoms an.

Bereits 1889 postulierte der englische Arzt Stephen Paget in der sogenannten „seed and soil“-Hypothese, dass zirkulierende Tumorzellen bestimmte Zielorgane selektieren. Betrachtet man das Metastasierungsmuster des malignen Melanoms so fällt auf, dass die Metastasierung kein zufälliger Prozess ist, sondern dass bestimmte Organe besonders häufig von Metastasen betroffen sind. Sowohl tumorintrinsic Faktoren als auch organspezifische Faktoren spielen hierbei eine Rolle. Organspezifische Nischen werden durch Endothelzellen gebildet, die Zellen, die auch als erstes mit zirkulierenden Tumorzellen in Kontakt kommen. Die sogenannte vaskuläre Nische spielt eine entscheidende Rolle bei der Unterdrückung der zirkulierenden Tumorzelle oder dem Auswachsen einer Metastase.

In der Leber wird die vaskuläre Nische von den Lebersinusendothelzellen gebildet, die ein sinusoidales, diskontinuierliches Endothel bilden, welches keine Basalmembran besitzt, aber endotheliale Fenestrations ohne Diaphragma.

In der vorliegenden Arbeit wurden organspezifische, endothel-abhängige sowie tumorintrinsic Mechanismen der organspezifischen Metastasierung des malignen Melanoms in die Leber untersucht. Als experimentelles Modell der Leberkolonisierung diente ein Modell der Milzinjektion von murinen Melanomzelllinien, sowie ein Modell der intravenösen Injektion einer Melanomzelllinie. Die intravenöse Injektion führte neben der Leberkolonisierung auch zur Kolonisierung weiterer Organe. Die verwendeten murinen Melanomzelllinien unterschieden sich hinsichtlich ihres genetischen Hintergrunds und verschiedener bekannter Mutationen des malignen Melanoms, zum Beispiel Mutationen des humanen NRAS Gens. Im Experiment zeigten sich Unterschiede hinsichtlich der Effizienz der Leberkolonisierung und die murinen Zelllinien mit hoher und mittlerer Effizienz wurden näher untersucht. Die analysierten Zelllinien zeigten ein gemeinsames histologisches Wachstumsmuster. Trotz Unterschiede in der vaskulären Dichte, konnte ein gemeinsames Expressionsmuster der Tumorendothelien identifiziert werden.

Im zweiten Teil der Arbeit werden organ-spezifische, endothel-abhängige Mechanismen der hepatischen Metastasierung am Beispiel der Überexpression des Notch-Signalweges untersucht. Endotheliale Überexpression der Notch1 intrazellulären Domäne in Lebersinusendothelzellen führte zu einer verminderten Metastasierung in die Leber in zwei Modellen des malignen Melanoms und in einem Modell des Kolonkarzinoms. Des Weiteren konnten Veränderungen der endothelialen und metabolischen Zonierung in der Leber festgestellt werden, sowie eine veränderte Expression von Adhäsionsmolekülen. Die Reduktion des Adhäsionsmoleküls ICAM1, wurde als potenzieller Mechanismus einer verminderten Adhäsion und Retention der Tumorzellen in der Leber identifiziert.

### **3. Introduction**

#### **3.1. Cutaneous melanoma**

Cutaneous melanoma is an aggressive cancer arising from melanocytes in the skin. Melanocytes are located in the basal layer of the epidermis and produce melanin, a dark pigment, responsible for the skin color [1]. The malignancy is very aggressive and can metastasize to multiple organ sites, leading to a high mortality [2]. Cutaneous melanoma is the 17<sup>th</sup> most common cancer worldwide and the main cause for skin-cancer related death (<https://www.wcrf.org/cancer-trends/skin-cancer-statistics>).

##### **3.1.2 Epidemiology of cutaneous melanoma**

Melanoma incidence is strongly linked to geographic location and skin pigmentation. Geographic areas with a high sun-exposure, such as Australia and North America, show high incidences in malignant melanoma. In the United states over 98 % of diagnosed malignant melanoma occur in white people [3]. In general, white people have a 10-fold increased risk of developing malignant melanoma in comparison to black, Asian or Hispanic populations [4].

Worldwide the incidence of malignant melanoma is rising. Along with an increase in incidence, there is also an increase in mortality, albeit at a lower degree. Cutaneous melanoma mostly affects young and middle-aged people with a median age at diagnosis of 57 years [5], [6]. The most frequent sites of primary melanoma at diagnosis are the face, neck, limbs and the back [7].

##### **3.1.3 Intrinsic and extrinsic risk factors of malignant melanoma**

Malignant melanoma is considered a multi-factorial disease arising from a combination of genetic, epigenetic, and environmental factors. Regarding environmental factors, the most important risk factor for developing cutaneous melanoma is ultraviolet (UV)-exposure. A major determinant for the risk of developing malignant melanoma is a history of intermittent unprotected sun exposure [8]. Especially sunburns in early childhood are linked with a high risk of developing cutaneous melanoma [9]. Further, artificial UV-exposure, such as tanning bed sessions or photochemotherapy for example in the treatment of psoriasis have been linked to a higher risk of developing cutaneous melanoma [10], [11].

The most important intrinsic risk factors are skin pigmentation, number of melanocytic nevi and a genetic predisposition.

In 1975 the American dermatologist Thomas B. Fitzpatrick developed a scale to link the skin type to its response to UV-exposure. The Fitzpatrick skin spectrum has been validated as a predictive risk factor for the development of cutaneous melanoma [12]. The lower the

Fitzpatrick skin type, or in other words the paler the skin and the more sensitive to UV-light, the higher the risk of developing skin cancer [13].

Nevi on the skin are accumulations of melanocytes. They can be congenital or acquired. A high number of cutaneous nevi and also the size of cutaneous nevi are associated with a high risk of malignant melanoma [14]–[16].

Further, genetic inheritance can be a causative risk factor of malignant melanoma. About 8 to 12% of melanoma patients have a family history of the disease [17], [18]. Hereditary malignant melanoma shows a clear pattern of autosomal-dominant inheritance with multiple family members being affected in more than one generation [19]. The most common genetic abnormality linked to familial melanoma is a mutation in the cyclin-dependent kinase inhibitor 2A (CDKN2A/p16) gene [20]. Other genetic mutations linked to inheritable melanoma are mutations of cyclin-dependent kinase 4 (CDK4), telomerase reverse transcriptase (TERT) and the protection of telomere-1 (POT1) [20].

#### **3.1.4 MAPK pathway signaling in malignant melanoma.**

In more than 50% of cutaneous melanoma activated mutations of the protooncogene BRAF are present [21]. Elderly patients with a longer history of chronic UV-exposure typically have a high mutational load with common mutations in BRAF, neurofibromin-1 (NF-1) and Neuroblastoma RAS viral oncogene homolog (NRAS) [22], [23]. Younger patients with a limited or intermittent sun exposure are typically linked to the BRAF V600E mutation and a lower mutational load [22], [24].

The BRAF V600E mutation is the most common BRAF mutation in malignant melanoma [25]. Due to a mutation in exon 15, valine is substituted by glutamic acid in the second placement of codon 600 of B-Raf kinase. This substitution causes a conformational switch of the catalytic domain of B-Raf, resulting in a constitutively active form with enhanced catalytic activity [26], [27]. Mutations of BRAF result in abnormal mitogen-activated protein kinase (MAPK) signaling.

The MAPK pathway is activated by extracellular signals that bind to cell membrane receptors, for example G-protein coupled receptors or receptor tyrosine kinases (RTKs). This leads to activation and guanosine triphosphate (GTP)-binding of rat sarcoma protooncogene (RAS). Activated RAS binds to the membrane and activates its effector proteins, the so called rapidly growing fibrosarcoma (Raf) proteins. There are three different isoforms of Raf proteins: a-Raf, b-Raf and c-Raf. Activation of Raf proteins results in the phosphorylation of a series of kinases among them mitogen-activated protein kinase kinase 1 (MEK1) and MEK2, which further phosphorylate extracellular signal-related kinase 1 (ERK1) and ERK2. Activated ERK regulates gene expression of metabolism, cytoskeletal functions, proliferation, differentiation, senescence and cellular death [28]. Collective mutations of BRAF lock the protein in its active

state and increase kinase activity [29]. This leads to a permanent increased activation of the MAPK pathway, resulting in an increase in oncogenic signaling. Another common cause of aberrant MAPK pathway signaling in malignant melanoma is mutation of NRAS [30]. Most common are missense mutations of NRAS in codon 12, 31, and 61, all of them leading to an increase in GTPase activity [26]. However, BRAF and NRAS mutations seem to be mutually exclusive, as less than 1 % of melanoma patients have co-mutations [31].

Mutations of the MAPK pathway alone are not sufficient for melanoma progression as they are detected in early melanogenesis and in a high percentage of melanocytic naevi. Additional mutations, such as deletion of phosphatase with tensin homolog (PTEN), autophagy related 5 (ATG5), or CDKN2A are needed for melanoma progression [32].

### **3.1.5 Staging of cutaneous melanoma**

The prognosis of cutaneous melanoma directly correlates with vertical tumor thickness, the Breslow depth. The Breslow depth in turn correlates with time of progression. Therefore, an early detection and rapid treatment is decisive in melanoma therapy. Melanoma patients are classified in four stages depending on primary tumor size, presence or absence of regional lymph node metastases, and presence or absence of distant metastases. The criteria for melanoma staging were identified by the American Joint Committee on Cancer and are continuously evolving [33].

Stage 1 comprises patients with low-risk primary tumors and absence of regional lymph node metastases and distant metastases. Primary lesions smaller than 1 mm without invasion of the reticular dermis or subcutaneous fat and further without epithelial ulceration are defined as stage 1A. Stage 1B is defined as primary lesion between 1 mm and 2 mm and with or without epithelial ulceration and invasion of the reticular dermis or subcutaneous fat. This very early diagnosis of melanoma has a favorable prognosis and surgical resection is the therapy of choice [33].

Stage 2 melanoma comprises high-risk primary tumors without evidence of regional lymph node metastases or distant metastases. Primary tumors have a size bigger than 1 mm and show ulceration of the overlying epithelium or a size between 2 mm and 4 mm with or without epithelial ulceration [33].

Stage 3 melanoma is defined as patients with documented lymph node metastases or the presence of in-transit or satellite metastases. The risk is further defined by the number and size of lymph node metastases, the number of affected lymph nodes and the presence of epithelial ulceration at the primary lesion [33].

Stage 4 melanoma compromises all patients with distant metastases [33]. Stage 4 melanoma patients have a poor prognosis and the relative 5-year survival rate for stage 4 patients diagnosed between 2011 and 2017 was 30% [34].

In the clinical setting certain diagnostic measures are applied to correctly identify the patient's tumor stage. Ultrasound may be used to detect lymph node metastases. Besides, magnetic resonance imaging (MRI) and computed tomography (CT) scans may be applied to detect brain or organ metastases. Local guidelines help physicians to choose the right diagnostic tool.

### **3.1.6 Melanoma therapy**

#### **3.1.6.1 BRAF/MEK inhibitor**

To target BRAF-mutated melanoma selective BRAF inhibitors have been developed, among them vemurafenib, dabrafenib and encorafenib [35]–[39]. These BRAF inhibitors were designed to bind the adenosine triphosphate (ATP)-binding pocket of the active conformation of BRAF [40]. Clinical trials with BRAF inhibitors in metastatic melanoma showed a good response and prolonged overall survival in comparison to chemotherapy [41]–[43]. However, upon 6-7 months approximately 50% of patients showed disease progression [43], [44]. Several mechanisms can mediate resistance to BRAF inhibitors, but most commonly resistance is mediated by reactivation of the MAPK pathway. Another challenge of BRAF monotherapy is the paradoxical activation of the MAPK pathway in wildtype cells, resulting in hyperproliferative cutaneous events, such as squamous cell carcinoma and keratoacanthoma [45], [46].

Clinical models showed that BRAF inhibitor resistance is associated with rapid recovery of MAPK signaling. To induce apoptosis in BRAF V600E mutated melanoma a complete inhibition of the pathway is necessary [47]. To maximize the effect of inhibition of the MAPK pathway a combination of BRAF inhibitors and MEK inhibitors was implemented. In organotypic cell culture models it has been shown that a combination of inhibition of BRAF and MEK enhanced apoptosis and the development of resistance was delayed [47].

For the treatment of BRAF-mutated metastatic malignant melanoma three combinations of BRAF/MEK inhibitors are approved by the United States Food and Drug Administration (US FDA) and are used in the clinics [48]–[50].

#### **3.1.6.2 Immune checkpoint inhibition**

Despite the recognition that melanoma is an immunogenic tumor, the standard of care in metastatic melanoma was chemotherapy until 2011 [51]. The first available immunological therapy was high-dose interleukin-2, which could induce a long-lasting response in a small subset of patients but also led to severe side-effects [52]. Therefore, the introduction of ICI was a real gamechanger in melanoma therapy and increased overall survival in patients with

metastatic melanoma. Nowadays, ICI is the standard of care for patients with metastatic melanoma [53].

### **3.1.6.3 Anti-cytotoxic T-lymphocyte-associated protein 4 (CTLA-4) antibodies**

T-Lymphocytes require two signals to be activated. The first signal comes from the interaction between the T-cell receptor and the antigen presented by the major histocompatibility complex (MHC)-receptor on the antigen presenting cell [54]. The second signal is provided by the interaction between the cluster of differentiation (CD)28 receptor on the T- lymphocyte and the CD80 and CD86 molecules expressed on the surface of the antigen presenting cell. However, CD28 on the T-cell surface can be replaced by cytotoxic T-lymphocyte-associated protein 4 (CTLA-4), an inhibitory receptor with higher affinity to CD80 and CD86 [54]. In a physiological setting CTLA-4 plays an important role in immunotolerance. Activation of CTLA-4 reduces T-helper cell activity and induces regulatory T-cells [54]. Forkhead box P3 (FOXP3) transcription factor is a transcriptional master regulator of the T-cell lineage and CTLA-4 is one of the target genes of FOXP3 [55]. Blocking CTLA-4 with specific antibodies therefore leads to two effects: T-helper cell activity is increased, and regulatory T-cells are inhibited.

### **3.1.6.4 Anti-programmed cell death protein 1 (PD-1) antibodies**

Programmed cell death protein 1 (PD-1) is another receptor on the surface of T-lymphocytes. It serves as an immune checkpoint in the periphery to inhibit lymphocyte activity when the specific immune response has already been established [54]. The PD-1 receptor is highly expressed on regulatory T-cells, but also on other activated lymphocytes, such as B-cells and natural killer cells (NK-cells) [56].

PD-1 is especially relevant in the exhaustion of specific T-lymphocytes that are chronically exposed to an antigen, such as cancer antigens but also during chronic viral infection [54]. Blocking PD-1 with specific antibodies has several effects. First, the exhaustion of T-lymphocytes induced by chronic antigen stimulation is blocked and therefore T-lymphocytes are reactivated [54]. Second, PD-1 blockade increases NK cell toxicity in the tumors and additionally antibody activity mediated by B-cells is increased [56], [57].

### **3.1.6.5 Immune checkpoint therapy**

Clinical trials with anti CTLA-4 antibody (Ipilimumab) and anti PD-1 antibodies (nivolumab and pembrolizumab) led to significant advantages regarding clinical response and overall survival of melanoma patients. However, treatment with immune checkpoint inhibitors is challenging and can be associated with potentially life threatening side effects of adverse immune events, such as hepatitis, colitis, endocrinopathies, fatigue and anemia [58]–[61].

The encouraging results of treatment with anti-CTLA-4 antibodies or PD-1 antibodies led to the first clinical studies with combinations of the two immunotherapeutic drugs. Combination

of Ipilimumab and Nivolumab could increase the 4-year overall survival rate to 53% of patients with metastatic melanoma [62]. Ipilimumab, nivolumab, pembrolizumab as well as combination of ipilimumab and nivolumab were approved for clinical use by the regulatory authorities. Still, only 50% of patients benefit from immunotherapy, and immune-related toxicity remains a major challenge in the treatment of melanoma patients [63].

#### **3.1.6.6 Combination therapy**

Both immunotherapy and targeted therapy improved the treatment response of metastatic melanoma. However, while the targeted therapy has high response rates, the duration of response is short-lived [64]. Immunotherapy on the other hand provides a more durable response, but not all patients benefit from it [63]. Therefore, combination of immunotherapy and targeted therapy were applied in clinical trials. A meta-analysis of different clinical studies showed that the combination of PD-1/ programmed death ligand 1 (PD-L1), BRAF and MEK inhibition increased progression-free survival in patients with stage III-IV BRAF V600 mutation-positive advanced and metastatic melanoma [65], [66]. In 2020 the combination of PD-L1 checkpoint inhibitor Atezolizumab with the targeted therapies Vemurafenib and Cobimetinib (MEK-inhibitor) has been approved by the FDA for treatment of advanced and metastatic melanoma (<https://www.gene.com/media/press-releases/14868/2020-07-30/fda-approves-genentechs-tecentriq-plus-c>).

### **3.2 Metastasis of cutaneous melanoma**

Cutaneous melanoma metastasizes to different organ sites at different frequencies. The most common sites of malignant melanoma metastasis are the skin (18%), the lung (10-40%), lymph nodes (5-35%), the liver (14-20%) and the brain (2-20%) [67], [68]. Further, overall survival of melanoma patients can be linked to the metastatic site [67], [69]. Patients with an isolated subcutaneous metastasis or skin metastasis have the best prognosis. Patients with metastases in distant lymph nodes and patients with isolated lung metastases have a favorable prognosis, whereas metastases in the liver, bone, or brain are correlated with a poor prognosis [70]. Additionally, cutaneous melanoma patients with liver metastases are known to show a poor response to immunotherapy and targeted therapy [69], [71], [72].

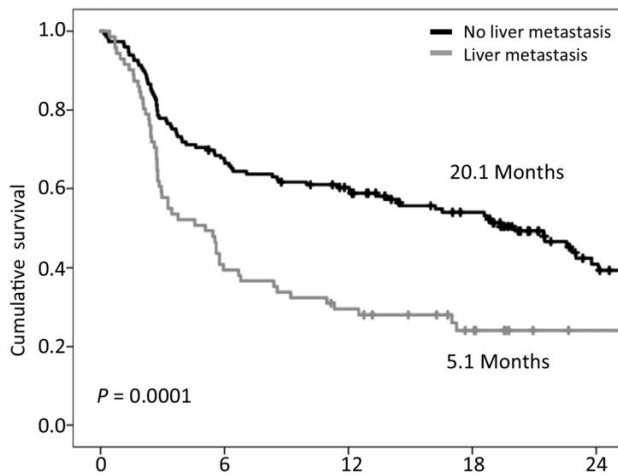


**Figure 1 Cumulative survival in malignant melanoma in presence or absence of liver metastasis.** Kaplan-Meier curve (progression free survival) of patients with (grey) and patients without liver metastases (black) is shown. Y-Axis: cumulative survival and X-Axis: time in month. Liver metastases are a negative prognostic factor in malignant melanoma and progression free survival is decreased in patients with liver metastases (5.1 months vs. 20.1 months median progression free survival). Figure taken from Tumei *et al.* [69] with kind permission of Cancer Immunology research.

### 3.2.1 Seed and soil hypothesis

In 1889 Stephen Paget postulated that metastasis was not a random event, but that the tumor (“seed”) spreads preferentially to the microenvironment (“soil”) of selected organs, also named metastatic-tropism [73]. According to the “seed-and-soil” hypothesis the organ microenvironment plays a crucial role in metastasis. Several experimental studies highlighted the importance of the tumor microenvironment. Kinsley *et al.* transplanted small fragments of lung or different organs, including kidney, spleen, thyroid, heart, and skin in syngeneic mice. After 10 days lung-homing melanoma cells were injected into the vasculature. Remarkably, metastases were only detected in the lung and transplanted lung of the animals, whereas other organs were free of metastases [74].

Organotropism of metastasis can be explained by the unique vascular signature of each organ. Endothelial cells express different adhesion molecules in different organs, thereby providing a unique signature or “address” for each organ [75]. Tumor cells expressing the corresponding ligand, can be homed to selected organs. An example is the expression of C-X-C motif chemokine receptor 4 (CXCR4) by breast tumors. Tissues expressing the corresponding ligand C-X-C motif chemokine ligand (CXCL12) including lung, liver, lymph node, and bone marrow are common sites of breast cancer metastasis [76].

Others argue that the metastatic pattern of a tumor is determined by the anatomy of the vasculature and lymphatic drainage of the site of the primary tumor. Disseminating tumor cells

follow the circulation and arrest non-specifically in the first organ they encounter. Additionally, anatomical and mechanical factors need to be considered regarding the metastatic pattern. A prime example is the liver, as a metastatic site of hematogenous spread of gastrointestinal tumors, due to the unique venous drainage from the portal vein [77], [78].

However, none of these hypotheses are mutually exclusive and might also depend on the primary tumor and its biology.

### 3.2.2 The metastatic cascade and malignant melanoma

Cancer metastasis arises from a series of sequential steps. Tumor cells invade in the surrounding tissue, enter the circulation, arrest at a distant site and grow out to form first micro metastases and then macroscopically visible metastases. However, this is not a unidirectional process. Rather there is interaction between the primary tumor, the disseminating tumor cells and the microenvironment of the metastatic site [79]. Malignant melanoma cells possess different biological features to successfully form metastases. In the following the different steps of the metastatic cascade, and the mechanisms of melanoma cells to overcome barriers will be described.

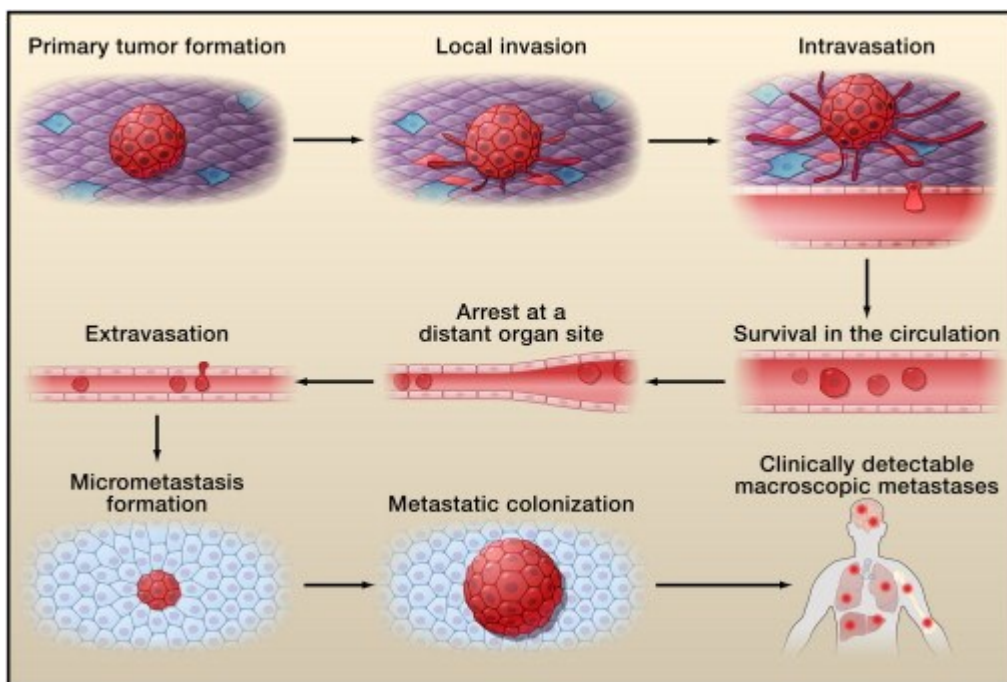


**Figure 2 The metastatic cascade.** Metastatic colonization requires several critical steps following a specific order, the so-called metastatic cascade. Upon primary tumor formation, tumor cells invade locally and enter the circulation. Circulating tumor cells arrest at distant organ sites, extravasate from the vasculature and form a micrometastasis which finally grows out into a macroscopic visible metastasis. Figure taken from Valastyan & Weinberg [80] with kind permission from Cell.

### 3.2.2.1 Epithelial-mesenchymal transition (EMT)

Most solid tumors arise from epithelial tissue, which is characterized by strong cell adhesion and is separated from the stromal tissue by a basal membrane [81]. During the process of tumor cell invasion tumor cells are released from their neighbor cells and overcome the barrier of the basement membrane. During this process epithelial-mesenchymal-transition (EMT) plays a critical role [82], [83]. EMT describes a process whereby epithelial cells take on the characteristics of mesenchymal cells, which facilitates cellular invasion. EMT is characterized by the loss of cell polarization and downregulation of epithelial proteins, including proteins that regulate cell-cell adhesion such as E-cadherin and catenins, but also occludins, claudins, and cytokeratins [83], [84]. Mesenchymal proteins are upregulated during EMT. These include N-cadherin, vimentin, tenascin C, laminin beta 1, collagen type V1 alpha, and various proteinases [83], [84]. EMT inducing pathways involve receptor tyrosine kinases (RTKs), the transforming growth factor  $\beta$  (TGF $\beta$ )-superfamily, wingless-related integration site (wnt) signaling, notch pathway [85], [86], and nuclear factor  $\kappa$ -light-chain-enhancer of activated B cells (NF $\kappa$ B) [87]. All of them are pathways that play an important role during development and stem cell renewal [88], [89].

EMT promotes metastasis in several ways. Tumor cell invasion is supported by the loss of cell-cell adhesion. E-cadherin is expressed in melanocytes and involved in cell-cell adhesion, but also in the regulation of melanocyte proliferation [90]. E-Cadherin loss results in reduced adhesion of melanocytes, an increased expression of N-Cadherin [91], and upregulation of cell surface molecules such as melanoma cell adhesion molecule (MCAM/MUC-18) [92]. N-cadherin has been shown to promote migration of melanoma cells [93]. Blocking N-cadherin with a monoclonal antibody results in a reduced transendothelial migration efficacy of melanoma cells [94], [95].

Another commonly observed property of cells, that have undergone EMT is the secretion of matrix metalloproteinases (MMPs). MMPs remodel the extracellular matrix of the tumor microenvironment. In melanoma cells the expression of MUC-18 has been associated with activity of MMP-2, increasing the invasive phenotype [96].

Loss of E-Cadherin also has an impact on intracellular signaling. E-cadherin spans the cell membrane and consists of an extracellular, a transmembrane and an intracellular domain. The cytoplasmic domain functions in intracellular signaling, for example RTK-signaling by the modulation of the activity of the epidermal growth factor receptor (EGFR) [97].

Regarding EMT, one must keep in mind that melanocytes originate from the neural crest and migrate to the epidermis during embryogenesis. Therefore, even so they express E-Cadherin, melanocytes are no typical epithelial cells. Already in benign melanocytic lesions high levels

of vimentin, a mesenchymal protein can be found [98]. Further, nevi showed a high expression of slug, a gene of the neural lineage [99]. Because of the origin of melanocytes fewer molecular changes are needed for EMT and this might be one explanation why melanoma cells have such a high metastatic potential [2].

### **3.2.2.2 Dissemination and invasion of surrounding tissue**

The ability to migrate is essential for the invasion of tissue and vessels. By a continuous cycle of actin polymerization and depolymerization membrane protrusions are formed. These protrusions adhere to the extracellular matrix and endothelial cells resulting in cell locomotion.

Adhesion to the extracellular matrix is mediated via integrin- and focal adhesion kinase (FAK)-containing complexes. Cell contraction is mediated by actin-myosin 2 and the release of adhesion at the trailing edge results in locomotion. Membrane protrusions are coordinated by the cofilin pathway, which is controlled by Ras homologous (Rho) family GTPases [100]. In line with this, in melanoma cells it has been shown that locomotion is driven by activation of the GTPase Rac through a complex containing Neural Precursor Cell Expressed, Developmentally Down-Regulated 9 (NEDD9), which has been shown to be amplified in metastatic melanoma [101].

Another important adhesion molecule in melanoma cells is L1 cell adhesion molecule (L1-CAM). In human primary melanoma the expression of L1-CAM is linked to metastatic melanoma and albeit the expression in nevi is low, it drastically increases in primary and metastatic melanoma [102]. The extracellular domain of L1-CAM contains six IgG-like domains and five fibronectin type-III-like repeats [103] and can form either homophilic or heterophilic interactions, thereby contributing to melanoma cell aggregation and attachment to endothelial cells via interaction with  $\alpha v \beta 3$ . The integrin  $\alpha v \beta 3$  is highly expressed on melanoma cells but not on endothelial cells [104]. *In vitro*  $\alpha v \beta 3$  of melanoma cells is required to bind to L1-CAM on an endothelial layer and to form protrusions. These protrusion showed a high expression of  $\alpha v \beta 3$  and formed pseudopods to penetrate the epithelial layer [104]. The binding of  $\alpha v \beta 3$  to L1-CAM on epithelial cells seems to play an important role in transendothelial migration. Further, L1-CAM has a dual role as its expression on melanoma cells and epithelial cells promotes metastasis [2].

Tumor cells can either migrate as single cells or as a collective in form of clusters, sheets and files. If tumor cells invade collectively, different clones with different properties can collaborate and thereby provide an advantage of migration and survival [81], [100]. Single tumor cells can migrate in two different modes: Mesenchymal-type movement or amoeboid movement. Slow “mesenchymal” movement requires proteolytic extracellular matrix remodeling and the cells show an elongated cellular morphology. Amoeboid movement is faster, the cells have a round

morphology and levels of actomyosin contractility are elevated. Tumor cells can switch between these two modes, demonstrating once again the high degree of plasticity of tumor cells [101].

### **3.2.2.3 Surviving in the circulation**

After leaving the primary tumor and transendothelial migration, circulating tumor cells enter the bloodstream and travel as single cells or clusters until they get arrested in small capillaries of different organs. There are several barriers tumor cells must overcome to survive in the circulation.

First, it has been shown that epithelial and endothelial cells actively undergo apoptosis, if they lose cell-cell contact, cell-matrix contact or the adhesive tissue is inappropriate [105], [106]. This induced apoptosis is called anoikis and is considered to ensure tissue homeostasis. Suppressing anoikis is an important feature of tumor cells, as during several steps of the metastatic cascade tumor cells lose the cell-matrix contact or enter a foreign environment. For example during transendothelial migration in the circulation or the lymphatic system and finally after extravasation in a foreign microenvironment [107]. Integrins in the cell membrane interact with diverse molecules of the ECM and trigger intracellular signaling cascades. Therefore, integrins play a major role in the suppression of anoikis. Activation of integrins protects cells from anoikis [106], as well as activation of downstream mediators including FAK [108], integrin-linked kinases [109], [110] and SRC family kinases [105]. Tumor cells often express a different repertoire of integrins [111], [112] and show high levels of FAK [113], protecting them from anoikis and stimulating cell survival, proliferation, and migration.

Further, anoikis has been linked to EMT. In melanoma cells it has been shown that blocking N-cadherin sensitizes cells to anoikis [93].

Also, tumor cells have to deal with shear forces in the circulation. To survive these physical forces, adhere to endothelial cells and extravasate, melanoma cells share many antigens expressed by endothelial cells. Among them MCAM/MUC18, L1-CAM, ICAM, VCAM, activated leukocyte cell adhesion molecule (ALCAM), neural cell adhesion molecule (NCAM), vascular endothelial (VE)-Cadherin, and Platelet/endothelial cell adhesion molecule (PECAM) [114].

MCAM/MUC18 enhances homotypic adhesion of melanoma cells, leading to clumping and emboli formation in the circulation. Inner cells are protected from physical shear stress and immunosurveillance being advantageous for metastasis formation [2].

### **3.2.2.4 Tumor cell arrest and extravasation**

Whereas circulating tumor cells only spend some seconds freely in the circulation before they get trapped and arrested in small capillaries, they can spend hours or days arrested in the capillaries until extravasation [115]. The capillaries serve to supply the organ with nutrients and

to carry away waste products. Arrested in the capillary beds circulating tumor cell survival is heavily reduced by the experienced biomechanical forces, mainly constriction. Cytoplasm and nucleus are severely deformed, and can lead to tumor cell death [115]. Cell deformation can also activate mechanosensitive pathways that promote metastasis and enhance tumor cell survival. Extrinsic forces can alter chromatin organization and motility, which is connected to the actomyosin cytoskeleton and nuclear lamina and thereby influences gene expression [116]. Biomechanical forces can deform the nucleus, thereby inducing stretching and opening of the chromatin, which facilitates transcription and alters cellular fate [117]. *In vitro* it has been shown that transition through capillary constrictions alters gene expression and induce expression of EMT-related proteins such as Twist 2 and downregulation of E-Cadherin [118]. EMT also plays a role in extravasation from the circulation into the target organ. In general, mechanisms described above that facilitate intravasation into the circulation also play a crucial role in extravasation.

### **3.2.2.5 Survival and adaptation to the microenvironment**

Upon extravasation tumor cells have to adapt to a foreign microenvironment. Endothelial cells of each organ express a unique pattern of adhesion molecules building a unique vascular bed [75]. Circulating tumor cells expressing the corresponding receptor can therefore “address” to certain tissues [76], [119]. Further, arrested tumor cells can only outgrow to macrometastases if the microenvironment of the target organ is compatible with the properties and requirements of the arrested tumor cell [81]. Single tumor cells can reside in a dormant state for a long period of time [120], [121]. Experiments in mice have shown that the majority of tumor cells remains in dormancy and only a small proportion of 0.006% of cells grow out into a tumor [122]. Several mechanisms underlying dormancy have been described.

First, micrometastases can remain small due to a balance of a slow rate of apoptosis and proliferation [123]. Remarkably, the dormant state can be favored by the primary tumor. It was shown that secretion of angiostatin by the primary tumor hindered angiogenesis and the micrometastases only grew out upon removal of the primary tumor [124].

Second, the immune system plays an important role in the outgrowth of metastases and can hold micrometastases in a dormant state of equilibrium [125].

Third, several genes have been identified that suppress metastasis and restrict the outgrowth of macrometastases [126]. Overexpression of these genes has been shown to suppress metastases but not the growth of a primary tumor. For several of these genes, it has been shown that they act on the secondary site through RHO or MAPK signaling [127].

### **3.2.2.6 Angiogenesis**

Adaptation to the microenvironment is not sufficient for the outgrowth of a macrometastasis. Avascular tumors cannot grow larger than 1 mm in size, as this is the limit of passive diffusion of nutrients and oxygen [128]. Therefore, angiogenesis is essential for the outgrowth of macrometastases. Under physiological conditions angiogenesis mainly occurs during wound healing and the female reproductive cycle. Angiogenesis is tightly held in balance by anti-angiogenic factors (for example thrombospondin 1, angiostatin, endostatin and tumstatin) and pro-angiogenic factors, most importantly vascular endothelial growth factor (VEGF)-A, fibroblast growth factor (FGF), platelet derived growth factor (PDGF), and epidermal growth factor (EGF) [129], [130]. During induction of vascularization in the tumor this balance is tipped towards pro-angiogenic factors, the so called “angiogenic switch” [131]. Tumor-cell intrinsic factors, as well as stromal cells are involved in the angiogenic switch [132]. Also, VEGF is a target gene of hypoxia inducible factor (HIF)1 $\alpha$ , induced by hypoxia [133].

Melanoma metastases show a highly angiogenic phenotype. Several inflammatory molecules are involved in melanoma angiogenesis, among them IL8, VEGF-A, bFGF, platelet activating factor and lipoprotein a [2]. Especially the role of IL8 is very dynamic during melanoma progression. Normally, IL8 is expressed by endothelial cells and macrophages to induce chemotaxis. In melanoma, IL8 expression is linked to highly metastatic melanoma and patients serum levels correlate with metastasis and poorer survival [134].

However, in comparison to normal blood vessels, the tumor blood vessels are highly abnormal. Arterioles, capillaries, and venules have a chaotic organization and changes in blood flow direction. Leakiness of vessels and local stops of blood flow can occur. This results in a high tissue pressure in solid tumors and inefficient supply with nutrients. Therefore, anti-angiogenic therapies can increase the efficacy of cytotoxic agents by “normalization” of the tumor vasculature and thereby optimizing tumor perfusion [135].

### **3.2.3 The hepatic vascular niche**

Several unique functional characteristics of the liver support blood-borne liver metastasis. The strong vascularization of the liver in combination with an exceptionally low blood flow rate and a fenestrated endothelium without basement membrane renders the liver susceptible for metastasis and supports the extravasation of circulating tumor cells [136].

#### **3.2.3.1 Formation of a premetastatic niche**

Before metastatic spread occurs, future metastatic sites are already primed for metastatic susceptibility by the primary tumor, the so called pre-metastatic niche is established [137]. Besides the controversial discussion of the clinical relevance of the pre-metastatic niche, tumor-secreted factors and exosomes have been identified to orchestrate the formation of the

pre-metastatic niche [138]. In colorectal cancer, tissue metalloproteinase 1 (TIMP1) has been shown to be involved in the formation of a premetastatic niche and increased TIMP1 levels of patients correlated with liver metastasis. Seubert *et al.* showed that TIMP1 is linked to increased levels of stromal-derived factor 1 alpha, which recruits neutrophils to the liver [139]. Interestingly, TIMP1 expression is also an example of sex disparity in cancer. In male patients, TIMP1 expression was linked to a higher risk of developing liver metastasis in pancreatic cancer, colon carcinoma and melanoma [140]. Further, VEGF-A produced by colorectal cancer cells has been linked to the formation of a premetastatic niche [141].

#### **3.2.4 Exosomes in melanoma metastasis**

Exosomes are small vesicles with a membrane and a size of 30-100 nm. They are formed by inward budding of multivesicular bodies and subsequent fusion of the multivesicular bodies and the plasma membrane [142], [143]. Their release can either be induced or occur spontaneously. Several mechanisms have been described how exosomes support the formation of a pre-metastatic niche. For example, exosomes can influence the behavior of bone marrow dendritic cells (BMDCs) that act as mediator of crosstalk between the tumor and the metastatic niche. Further, changes in gene expression in target organs of metastasis can be induced by exosomes [144]. Additionally, exosomes can modulate the extracellular matrix and prime the lymph node environment to a pro-angiogenic state [145].

Another example of pre-metastatic niche formation by exosomes has been shown in colorectal cancer. Shao *et al.* showed that exosomes are released by the primary tumor that carry a microRNA (miRNA). The miRNA-21-5p binds to toll-like-receptor 7 on macrophages, that in turn release IL-6 inducing the formation of a proinflammatory, pre-metastatic niche [146].

#### **3.2.5 Role of liver resident cells in metastasis.**

Liver resident cells play important roles during metastases. Activation of liver sinusoidal endothelial cells (LSEC) facilitates the adhesion and migration of tumor cells into the space of Disse [147].

Kupffer cells are highly abundant in the liver and part of the innate immune system. Kupffer cells can eliminate incoming tumor cells by release of oxygen metabolites, phagocytosis, release of cytotoxic cytokines and secretion of proteases [148]. However, experiments showed, that the antitumorigenic activity of Kupffer cells was limited to early events of metastasis [149] and that an increase in tumor burden induces a switch towards tumor promoting activity of Kupffer cells [150]. Kupffer cells facilitate tumor cell adhesion by inducing the expression of vascular endothelial cell adhesion molecules on LSEC [151], [152]. Additionally, the production of IL-6, HGF, VEGF, and MMPs by Kupffer cells facilitates tumor cell invasion and promotes proliferation and angiogenesis [153].

Moreover, Kupffer cells can activate hepatic stellate cells by the release of TGF $\beta$ . Activation of hepatic stellate cells results in the deposition of extracellular matrix proteins. Fibronectin deposits have been shown to facilitate the recruitment of bone-marrow derived myeloid cells, via serving as a docking station for integrins expressed on bone-marrow derived myeloid cells [154].

Further, hepatic stellate cells can also directly support tumor growth. In a B16 model of melanoma metastases, secretion of VEGF-A and angiopoietin-1 by hepatic stellate cells has been described to induce angiogenesis [155]–[157]. Also, secretion of HGF and TGF $\beta$  by hepatic stellate cells can promote tumor growth [158].

### **3.2.6 Histopathological growth patterns of hepatic metastases**

Three different growth patterns have been identified of liver metastases of colorectal cancer (CRC), uveal melanoma, and cutaneous melanoma [159]–[163]. The replacement type is characterized by permeation of tumor cells between the hepatocytes without disruption of the normal architecture. Desmoplastic metastases are separated from the liver parenchyma by a band of fibrous tissue and metastases that show a pushing type growth pattern expand quickly and compress the surrounding liver hepatocytes [161], [163]. Replacement, desmoplastic and pushing type metastases show differences regarding their angiogenic properties. Hepatic metastases of the desmoplastic and the pushing type growth pattern strongly rely on *de-novo* synthesis of tumor blood vessels, whereas the replacement type growth pattern co-opts the pre-existing sinusoidal vasculature and is therefore independent of *de-novo* angiogenesis. In malignant melanoma about 50% of hepatic metastasis show a desmoplastic growth pattern and are associated with an improved prognosis as compared to any replacement growth pattern in cutaneous melanoma [164]. In CRC, desmoplastic growth pattern is associated with an increased response to antiangiogenic therapy and strong immune cell infiltration [159], [165]. About 12% of hepatic metastases of malignant melanoma are classified as pushing type and are associated with a rapid mortality [164].

### **3.2.7 Notch signaling in metastasis.**

The notch signaling pathway regulates multiple cellular processes, among them stem cell maintenance, proliferation, differentiation, angiogenesis, and cell death. In human and mice there are four paralogue notch receptors [166] and five notch ligands (delta-like proteins [DLL1, DLL2, DLL3], jagged 1 and jagged 2) [167]. Notch receptors form a heterodimer with a transmembrane unit and an extracellular subunit. Extracellular binding of ligands from neighboring cells results in separation of the heterodimer and proteolytic cleavage of the transmembrane subunit. The notch intracellular domain is released and migrates into the nucleus to activate transcription of target genes [168]. Notch signaling was first linked to cancer in human T-cell acute lymphoblastic leukemia. A translocation of chromosome 9-7 results in a

constitutively active form of NOTCH1 [169]. Indeed, 50% of T-cell acute lymphoblastic leukemia patients have activating NOTCH1 mutations [170].

Since then, Notch signaling has been linked to many different cancer entities in humans, including breast, colorectal, lung, pancreatic and prostate cancers [171]. In a model of neuroblastoma and breast cancer it has been shown that global notch inhibition results in increased liver metastases [172]. In malignant melanoma endothelial expression of NICD correlated with higher rates of metastasis and shorter progression free survival. Further endothelial notch activation led to an increase in lung metastasis [173].

### **3.3 The Liver**

The liver is a unique organ in function and architecture. It is the largest internal organ of the human body [174] and has a variety of different functions including metabolism of fat, glucose and carbohydrates, clearance of the blood from noxious factors, uptake of nutrients, storage of vitamins, glycogens and minerals, production of bile and also immunological functions [175]. The liver receives blood from two different sources. The hepatic artery delivers oxygen-rich blood from the circulation into to the liver and the portal vein supplies nutrient-rich blood from the small intestine that also contains substances secreted by the pancreas, the spleen, and the intestine. The blood drains through the liver tissue and the hepatic cells metabolize, bio transform, and store incoming substances. Finally, the blood drains out the liver in the central vein [174].

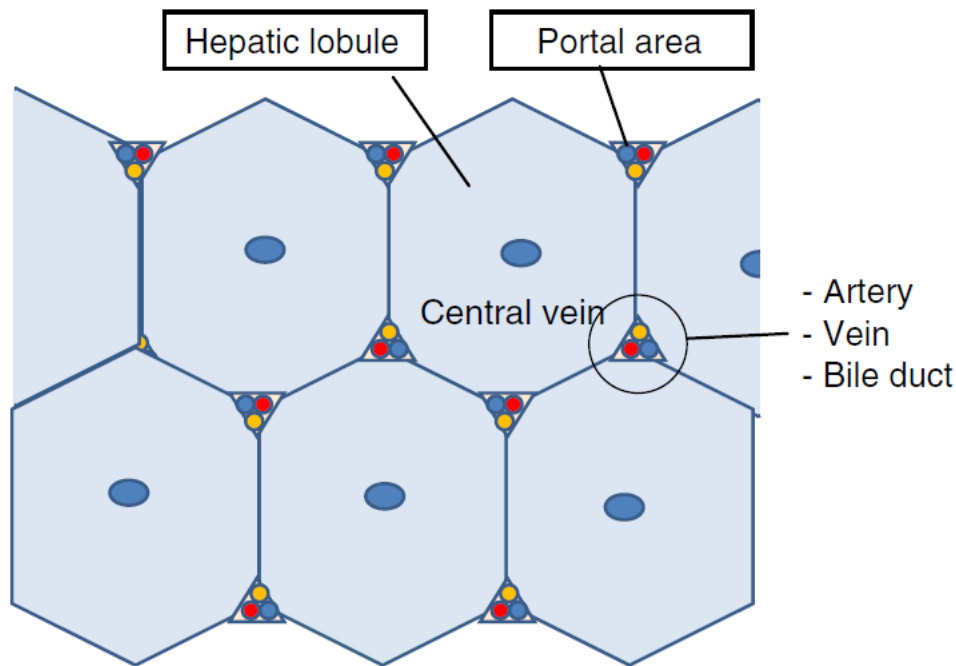


**Figure 3 Hexagonal structure of the hepatic lobules in the liver.** Blood drains from the portal triad formed by the hepatic arteriole, the portal venule and the bile duct, at the corner of the hexagonal structure to the central vein in the center of the hepatic lobule. Figure taken from Ishibashi et al., 2009 [174] with kind permission from *Seminars in Immunopathology*.

The functional unit of the liver is a hepatic lobule, which forms a hexagonal structure. At its center is the central vein. At each corner of the hepatic lobule is the so-called portal triad, consisting of a portal venule, a hepatic arteriole, and bile ducts [176], [177]. Blood flows from the portal triad to the central vein. An important functional characteristic of the liver is the differential expression of genes and functional capabilities of hepatocytes and endothelial cells, depending on their location. Hepatocytes and epithelial cells, located close to the central vein, express a different gene pattern from those located next to the portal triad. This differential expression results in metabolic and endothelial zonation of the liver [178], [179].

### 3.3.1 Hepatocytes

The liver parenchyma is formed by hepatocytes. About 60% of liver cells are hepatocytes and they make up 80% of the liver volume [180]. In humans, hepatocytes have a diameter of 20-30  $\mu\text{m}$  and about 25% of hepatocytes contain 2 nuclei [181]. Most of these nuclei are tetraploid, meaning they contain twice the number of chromosomes [182]. Hepatocytes have a range of different functions including the uptake and storage of nutrients, blood detoxification, and excretion of bile [183]. Like all epithelial cells, hepatocytes possess a polarized plasma membrane with a basolateral domain facing the space of Disse and an apical domain. Each membrane domain is composed of different surface proteins, channels, and receptors. A unique feature of hepatocytes is the possession of several basolateral and apical membrane

domains in close proximity [184]. Additionally, gene expression of hepatocytes is also influenced by hepatocyte location in relation to the central vein, the so-called metabolic zonation.

Hepatocytes close to the central vein express high levels of  $\beta$ -catenin target genes, among them glutamine synthetase [185]. Transcriptional activity of the wnt signaling protein  $\beta$ -catenin shows a gradient in its expression. Pericentral hepatocytes have a high transcriptional activity of  $\beta$ -catenin, whereas periportal hepatocytes show a low transcriptional  $\beta$ -catenin activity [186], [187]. This transcriptional gradient of  $\beta$ -catenin is maintained by the wnt signaling pathway. Metabolic zonation, with specialized metabolic functions of hepatocytes according to their location is maintained not only by wnt signaling but also other pathways are involved. Examples of metabolic specialized functions of peri-central hepatocytes are glucose uptake, lipo- and ketogenesis, bile-acid synthesis and expression of glutamine synthetase and cytochrome P (CYP)-enzymes. Periportal hepatocytes are specialized in  $O_2$  uptake, glucose delivery, urea synthesis and fatty acid oxidation [188].

Hepatocytes also play an important role in the secretion of proteins. Key proteins secreted by hepatocytes include albumin, transferrin,  $\alpha$ -fetoprotein, plasminogen, fibrinogen and clotting factors [183].

### **3.3.2 Hepatic stellate cells**

Under physiological conditions about 10-15% of liver cells are hepatic stellate cells (HSCs) [189]. HSCs have a dendritic “star-like” morphology and are located in the space of Disse between hepatocytes and LSEC. One major function of HSCs is the storage and transport of vitamin A (retinol). About 80% of the total body retinol is stored in HSCs in lipid droplets [190]. Vitamin A and its metabolites are involved in the regulation of various cellular activities, such as cell proliferation, differentiation, tumorigenesis and morphogenesis [190].

HSCs also secrete extracellular matrix proteins, such as Collagen I, Collagen III, Collagen IV, and MMPs, that degrade extracellular matrix proteins, as well as TIMPs. Thereby, HSCs regulate the extracellular matrix turnover in the space of Disse [191].

Further, HSCs are involved in the regulation of sinusoidal blood flow [192]. They express numerous receptors and intracellular mediators linked to cellular contraction [193] and are thought to have a potential role in vasoregulation.

Under physiological conditions HSCs rest in a quiescent state. Upon liver injury or damage HSCs are activated and change their phenotype to highly proliferative, myofibroblast-like cells. The activated state is characterized by loss of vitamin A droplets, well-developed rough surface endoplasmic reticulum and Golgi-apparatus, expression of alpha smooth muscle actin ( $\alpha$ -SMA) and secretion of extracellular matrix proteins [191], [194]. HSC activation is a hallmark

of liver fibrosis. Increased deposition of extracellular matrix proteins results in disruption of the liver architecture and finally in liver cirrhosis [195]. Additionally, activated HSCs are involved in tumorigenesis. In hepatocellular carcinoma, activated HSCs promote tumor growth and tumor angiogenesis [196], [197]. HSCs have been shown to infiltrate the tumor stroma and localize around tumor sinusoids, fibrous septa and capsules [194].

### **3.3.3 Kupffer cells**

Kupffer cells are tissue-resident macrophages in the liver [198]. They are located in the sinusoids, where they phagocytize pathogens entering from the arterial or the venous system. Also, pathogens and immunoreactive agents entering from the gut via the portal vein, as well as other particles, such as dead erythrocytes are cleared from the circulation by Kupffer cells [199]. On the one hand Kupffer cells have a protective function for example against drug-induced liver injury [200] and toxin-induced fibrosis [201], on the other hand dysregulation of Kupffer cells can contribute to chronic liver inflammation [202].

The precursors of Kupffer cells are monocytes derived from the bone marrow. Monocytes enter the liver and other tissues via the circulation, where they mature into tissue-resident macrophages [198].

During development of liver metastases Kupffer cells have been shown to play a bimodal role. Pharmacological depletion of Kupffer cells in the early phase of metastases in a model of colorectal cancer increased the metastatic load. However, depletion of Kupffer cells in the late phase of metastasis decreased metastatic burden in the same model [203]. Further, Kupffer cells have been shown to mediate liver toxicity during treatment with immune checkpoint inhibitors [204].

### **3.3.4 LSEC**

LSEC are highly specialized endothelial cells that line the sinusoids of the liver. They make up 15-20% of liver cells, but account only for 3% of liver mass [136], [205]. LSEC form a barrier between the circulation and hepatocytes and hepatic stellate cells in the space of Disse [206], [207].

#### **3.3.4.1 Origin**

LSEC precursors are endothelial cells that further differentiate into LSEC. Differentiation is characterized by the gradual loss of markers of continuous endothelium, such as CD31 and CD34 and the acquirement of markers of adult sinusoidal cells such as CD4, CD32 and ICAM1 [208], [209]. Further, during differentiation a reduction of perisinusoidal deposits of laminin alpha 4 is observed. In the human development the switch from EC to LSEC occurs between 5 and 12 weeks of gestation and is completed around week 20 of gestation [208]. In mice the morphological switch of EC occurs between E9.5 and E10.5 [210]. The morphological

development of LSEC is a critical step during embryogenesis. Genetic endothelial specific depletion of the master regulator GATA Binding Protein 4 (GATA4) results in liver fibrosis, liver hypoplasia, and embryonic lethality [211].

### 3.3.4.2 Morphology and Location

Morphologically LSEC are highly specialized and different from most other endothelial cells. They form a discontinuous, fenestrated endothelium, lacking a basement membrane and a diaphragm [136]. The open pores, called fenestrae, are arranged in clusters forming a sieve plate and have diameters of 50-150 nm [212], [213]. The fenestrae are lined by microtubules, intermediate filaments, and intracellular microfilaments that allow a high plasticity and a dynamic adaptation to different micromilieus [214], [215].

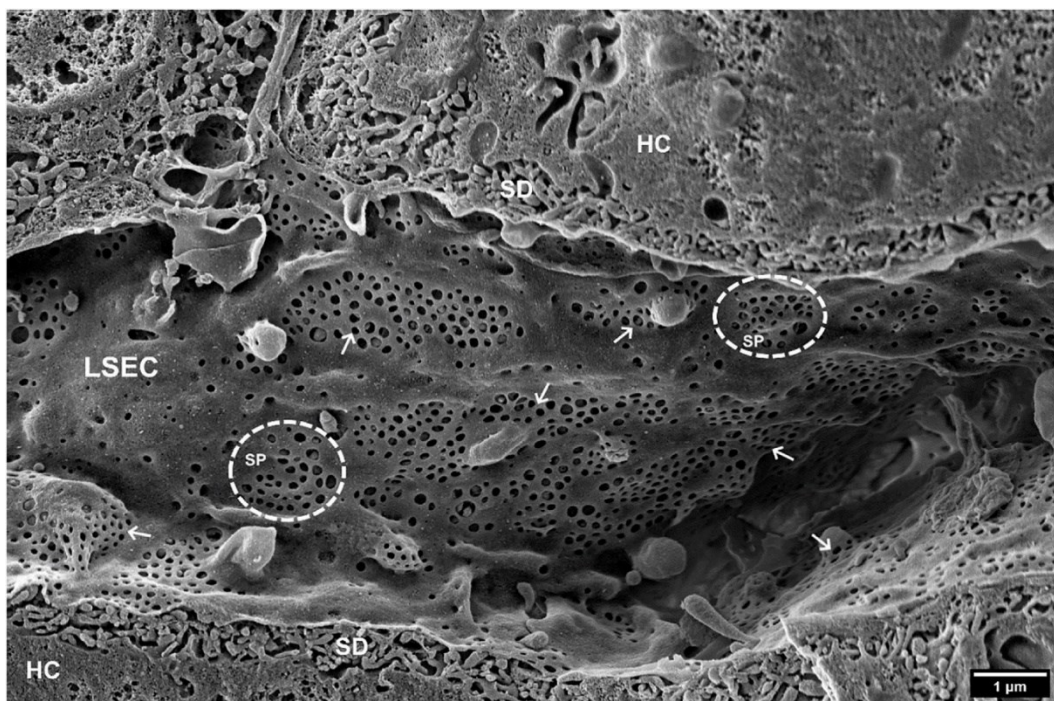


**Figure 4 Morphology of LSEC.** Scanning electron microscopy of LSEC of 4-month-old C57BL6 mice. Fenestrations without diaphragm of LSEC are arranged in clusters, the so-called sieve plates and become visible under the electron microscope. Figure taken from Szafranska et al., 2012 [216]. © 2021 Szafranska, Kruse, Holte, McCourt and Zapotoczny, <https://creativecommons.org/licenses/by/4.0/>

Further, LSEC can be distinguished by their location within the hepatic lobule. Along the axis of the liver lobule from the portal triad to the central vein a gradient of oxygen, shear stress, and redox is generated, accompanied by highly specialized LSEC [217].

Periportal LSEC express Dll4 and U6 snRNA-associated Sm-like protein (LSm 1) and generate a niche for resident LSEC progenitor cells. Upon liver injury resident endothelial progenitor cells in the niche of the portal vein can expand by proliferation [218]. Further, portal LSEC play

an important role in monocyte recruitment via notch signaling and differentiation of Kupffer cells, thereby maintaining liver homeostasis [219].

The major endothelial subpopulation of LSEC are midlobular LSEC. They express a broad range of scavenger receptors, among them stabilin-1, stabilin-2, lymphatic vessel endothelial hyaluronan receptor-1 (Lyve-1), CD206, and vascular endothelial growth factor receptor (VEGFR)3. Their main function is the clearance of the blood via scavenger receptors and antigen presentation [205].

Pericentral LSEC are located at the central vein. The Wnt ligands Wnt2, Wnt 9b and R-Spondin 3 (Rspo3), an enhancer of wnt signaling, are secreted by pericentral LSEC. The established angiocrine Wnt gradient results in metabolic zonation of hepatocytes. Mice deficient of angiocrine Wnt secretion show a loss of hepatic zonation, impairment of liver regeneration, and reduced liver size [220]–[223].

### **3.3.4.3 LSEC functions**

LSEC have a broad range of functions in liver homeostasis including clearance of macromolecules and small particles from the blood, control of leukocyte trafficking, vascular control of hepatocyte function, immunological functions, and vascular control of liver fibrosis and regeneration.

#### **3.3.4.3.1 Endocytic functions of LSEC**

LSEC express a broad range of endocytosis receptors to clear soluble macromolecules and small molecules from the blood. Indeed, LSEC are one of the cells with the highest endocytic capacity of the human body [224]. In combination with a strong lysosomal activity, LSEC are professional pinocytes. The different endocytosis receptors expressed by LSEC include scavenger receptors, mannose receptors and Fc gamma receptor IIb2 [224], [225]. Scavenger receptors mediate endocytosis of a broad range of molecules, among them polyanionic molecules, glycation end products and waste products, such as hyaluronan and chondroitin sulphate. The major scavenger molecules of LSEC are stabilin-1 and stabilin-2. They are redundant in their function, as single knockout mice do not show a phenotype. However, double-knockout of stabilin-1 and stabilin-2 results in a mild liver fibrosis, but in a severe renal glomerular fibrosis [226], indicating the importance of the clearance of noxious factors to protect the kidney. Mannose receptors bind different glycoproteins, microbial glycans and lysosomal enzymes, that are essential for the degradational capacity of LSEC [227]. The only Fc-gamma receptor expressed by LSEC is Fc gamma receptor IIb2 that is involved in the clearance of small, circulating immune complexes [224], [225].

#### **3.3.4.3.2 Leukocyte trafficking**

LSEC are involved in the recruitment of circulating lymphocytes from the periphery to the liver. Lymphocyte arrest and attachment is facilitated in the hepatic sinusoids by low shear stress and a low blood pressure. Instead of selectin-mediated tethering and rolling, atypical adhesion molecules are important for lymphocyte recruitment and can recruit specialized subsets [228]. Surface molecules involved in lymphocyte recruitment involve VCAM1, ICAM1, scavenger receptor class F member 1 (SCARF-1) and stabilin-1. Stabilin-1 has been shown to mediate recruitment of Tregs [206], whereas SCARF-1 mediates adhesion of CD4<sup>+</sup> T-cells [229]. Lymphocyte recruitment is further enhanced by the stimulation of LSEC by tumor necrosis factor alpha (TNF $\alpha$ ) and interferon gamma (INF $\gamma$ ) [230].

#### **3.3.4.3.3 Angiocrine signaling**

LSEC play an important role in maintaining liver homeostasis and liver zonation. Angiocrine signaling molecules secreted by LSEC are involved in multiple processes and functions. For example secretion of Wnt2, Wnt9a and RSPO3 by pericentral LSEC are essential for metabolic zonation of hepatocytes, as mentioned earlier [220]–[223]. Further angiocrine signaling of bone morphogenetic protein (BMP)2 and BMP6 are important for iron homeostasis of hepatocytes [231], [232]. Additionally, liver regeneration upon injury is orchestrated by angiocrine signaling of LSEC. Angiocrine secretion of VEGFR2-DNA-binding protein inhibitor 1 (Id1), Wnt2, and hepatocyte growth factor (HGF) stimulates hepatocyte proliferation and liver regeneration [233].

#### **3.3.4.3.4 Immunological functions of LSEC**

One major immunological function of LSEC is the clearance of circulating antigens. Besides the clearance of lipopolysaccharide (LPS) [234], blood-borne small IgG-Immuno-complexes are removed by receptor mediated endocytosis by LSEC [224], [225].

Further, pattern recognition receptors (PRRs), that recognize pathogen-associated molecular patterns and damage-associated molecular patterns, are expressed by LSEC. Stabilins, mannose receptors, and endocytosis receptors expressed on LSEC can act as PRRs [235], [236]. Further, six different Toll-like receptors that recognize structurally conserved microbial molecules are expressed on LSEC [237], [238].

In adaptive immunity LSEC play a critical role and can function as antigen-presenting cells. As mentioned before, LSEC have a high endocytic capacity and multiple receptors are involved in the uptake of antigens. LSEC constitutively express MHC II molecules that can be further enhanced upon stimulation by TNF $\alpha$  or INF $\gamma$  [239]. However, they only express low levels of co-stimulatory molecules and lack IL12 expression [240]. Therefore, antigen-specific stimulation of CD4<sup>+</sup> T cells by LSEC induces immune tolerance [241].

Also endocytosed-soluble antigens are presented on MHC-I molecules by LSEC to CD8<sup>+</sup> T cells [242]. LSEC have a high scavenging potential and antigen uptake and presentation is even more efficient in LSEC compared to dendritic cells. However, in contrast to professional antigen presenting cells, LSEC present antigens for only a short period of time [243]. As a result of the interaction of the presented antigen on the MHC-I molecule and the CD8<sup>+</sup> T cell receptor, antigen-specific CD8<sup>+</sup> T cells are recruited to the liver [244].

#### **3.3.4.4 LSEC and their role in liver regeneration.**

LSEC have long been recognized as important players of liver regeneration upon injury by the secretion of HGF, Wnt2 and angiopoietin-2. It has been shown, that upon liver injury HGF is increased in endothelial cells, stimulating hepatocyte proliferation [245]. However, newer studies suggest that not LSEC, but rather bone-marrow derived sinusoidal endothelial cell progenitor cells drive liver regeneration. Sinusoidal endothelial cell progenitor cells are recruited from the bone marrow to the liver upon injury and express high levels of HGF [246]. As they share surface marker expression with mature LSEC and also do not differ in size, they are not easy to distinguish and to separate in studies of LSEC functions [246].

#### **3.3.4.5 LSEC dysfunction and liver fibrosis**

LSEC phenotype is critical to maintain their physiological function and liver homeostasis. Upon chronic injury, LSEC can lose their phenotype, a process called capillarization. Sinusoidal capillarization is characterized by morphological changes such as loss of fenestrations and synthesis of a basement membrane [247]. Further, a molecular switch in marker expression is observed. Typical LSEC markers such as Lyve-1, CD32b, stabilin 1 and stabilin 2 are downregulated, whereas expression of markers associated with continuous endothelium, such as CD31 and VCAM1 is upregulated [206], [211]. Dedifferentiated LSEC lose their capacity to keep hepatic stellate cells in a quiescent state [248], [249]. Activation of hepatic stellate cell contributes to the deposition of extracellular matrix molecules and liver fibrosis. Therefore, sinusoidal capillarization precedes liver fibrosis [250], [251].

Chronic liver damage, for example by alcohol abuse or chronic hepatitis C (HCV) infection, leads to endothelial dysfunction and fibrosis. Also non-alcoholic steatohepatitis (NASH) causes liver fibrosis [252]. A hallmark of fibrosis is the excess deposition of extracellular matrix proteins, which distorts the liver architecture [253]. Fibrosis results in the formation of a fibrous scar tissue and at the latter stage of fibrosis, so-called cirrhosis, nodules of regenerating hepatocytes develop. Eventually cirrhosis results in hepatic insufficiency and portal hypertension and often liver transplantation is the last treatment option [254].

#### **3.3.4.6 LSEC and their role in metastasis.**

LSEC form the first barrier that circulating tumor cells encounter in the liver. Tumor cells are physically trapped in fenestrations of LSEC and encounter mechanical stress and deformation [255]. Arrest of larger clumps of tumor cells results in localized ischemia-reperfusion and subsequently release of nitrogen oxide (NO) [256] and reactive oxygen species (ROS) from LSEC and Kupffer cells [257]. About 95% of arrested tumor cells in LSEC undergo apoptosis [258]. However, besides the anti-metastatic activities LSEC also possess pro-metastatic features.

Kupffer cells are stimulated by metastatic cells to release the pro-inflammatory cytokines TNF $\alpha$  and IL-1, which in turn activate LSEC and lead to the upregulation of cellular adhesion molecules, such as ICAM1, VCAM1, E-selectin, and CD31 [259]. Adhesion molecules facilitate tumor cell attachment at LSEC and arrest in the liver, thereby promoting liver metastases [260].

Despite adhesion molecules, also factors secreted by LSEC can be pro-metastatic. One example is the secretion of fibronectin. Fibronectin interacts with the integrin  $\alpha$ 9 $\beta$ 1 on the surface of colorectal cancer cells and induces EMT, which increases the metastatic capability of cells [261].

### **3.4 Models of melanoma metastasis**

Studying complex biological processes such as melanoma biology and metastasis requires *in vivo* studies and is difficult or impossible to be replicated by *in vitro* analyses. Hence, different melanoma models have been developed in recent years and new insights were gained by *in vivo* studies in mouse models. In general, these can be categorized into xenotransplantation models, syngeneic transplantation models and genetically modified mice.

#### **3.4.1 Xenotransplantation models**

In xenotransplantation models human tumor xenografts are transplanted subcutaneously in immunosuppressed mice [262], [263]. In this model, direct interactions between the tumor xenograft and the lymphatic and blood vessels can be studied, especially with respect to drug response and tumor growth [264], [265]. Xenograft models are also used to study melanoma metastasis [266], [267]. Spontaneous metastasis formation in lymph nodes, lung, liver, or brain can be observed in xenotransplantation models, mimicking organotropism of malignant melanoma in human [264], [268], [269]. However, even so having a high clinical relevance and being especially relevant to assess the efficacy of targeted therapies, a huge disadvantage is the immunosuppression of mice. Mice, used for xenotransplantation models, are either deficient of T-cells (nude athymic mice) or T-cells and B-cells (severe combined immune-deficient mice) and therefore unsuited to study the effect of immunotherapy [270]–[272].

### 3.4.2 Syngeneic transplantation model

Syngeneic transplantation models are widely used to study melanoma behavior and metastasis. A major advantage over xenotransplantation models is the use of immunocompetent mice. However, injected cell lines also originate from mice and therefore differ from human tumor biology for example in respect of expression of adhesion molecules and growth factor expression [272]. The most widely used cell line for syngeneic transplantation models is the B16 cell line, derived from C57BL/6J mice that spontaneously develop melanoma upon chemical induction. Several subclones of the B16 cell line have been established, among them B16F1 and B16F10. The B16F1 cell line has a low metastatic potential and is well suited to study primary tumor growth. B16F10 cells, obtained by serial passages, have a high metastatic potential especially for lung metastasis [273], [274]. B16F10 *luc2* cells are widely used in melanoma research and are transfected with the firefly luciferase gene allowing *in vivo* monitoring of tumor growth using bioluminescence.

Besides B16 cell lines, other cell lines for syngeneic transplantation models have been established, harboring different mutations linked to malignant melanoma, such as BRAF and NRAS mutations, and representing different aspects of tumor biology [275], [276]. WT31 cells derive from melanocytes of mice harboring a mutation of NRas and loss of the tumor suppressor INK4a [275]. HcMel12 cells were generated from dimethylbenzanthracene (DMBA)-induced melanomas in HGF-CDK4 mice by serial transplantation. After intracutaneous injection, HcMel12 spontaneously develop lung metastases in immunocompetent C57BL/6 mice [277]. D4M.3A (Dartmouth Murine Mutant Malignant Melanoma) cells were established from Tyr::CreER;Braf<sup>CA</sup>;Pten<sup>lox/lox</sup> mice and represent the biology of BRAF V600E mutant tumors *in vivo*. The tumorigenic potential of the D4M.3A cell line was shown by intradermal injection [278].

### 3.4.3 Genetically engineered mouse models

Mice only rarely develop spontaneous melanoma. Therefore, genetically engineered mouse models are widely used to address different questions of tumor biology. Especially regarding identification of driver mutations, studying melanoma-initiation, identification of diagnostic biomarkers, and development and improvement of melanoma therapies [279].

Generating genetically engineered mouse models first require a tissue-specific promoter to modulate gene expression in melanocytes, exclusively. A widely used tissue-specific promoter is derived from the *tyrosinase (tyr)* gene that plays an important role in melanin synthesis. Noteworthy, Tyr is not only expressed in melanocytes but also in Schwann cells and spinal ganglia [280]. A wide-range of different melanoma-associated oncogenes have been expressed under the Tyr-promoter and other tissue-specific promoters, resulting in numerous genetically engineered mice.

Activating mutations of NRAS are often observed in human melanoma. Expression of mutant NRAS<sup>Q61R</sup> under the Tyr promoter in mice results in cutaneous melanoma, however at a low penetrance of 29% and a long latency of more than a year. Development of melanoma in these mice can be accelerated by crossing these mice into a *Ink4a/Arf4*-null background. At a latency of six months 94% of mice developed cutaneous melanoma and 36% showed metastases in the lung or liver [281].

BRAF V600E mutation is the single most common mutation in human melanoma. Expression of BRAF V600E under the Tyr promoter results in developmental defects and lethality before birth or shortly after birth in mice [282]. Activation of BRAF V600E expression in adult mice, leads to the development of benign melanocytic lesions, but not in melanomas [283], [284]. Combining BRAF V600E expression with loss of *Ink4A/ARF1* or loss of *Cdkn2a* increases melanomagenesis and latency [285], [286]. Also, UV-irradiation increased melanoma genesis of BRAF<sup>V600E</sup> expressing mouse models.

Another genetically engineered mouse model used in melanoma research are RET mice. Expression of the proto-oncogene receptor tyrosine kinase (Ret) under the metallothioneine promoter results in the spontaneous development of skin tumors, that also develop metastases at distant organs [287], [288].

### **3.5 Aim of the Thesis**

As liver metastasis remains a major challenge in the treatment of metastatic cancer and is further associated with a poor prognosis in malignant melanoma the aim of my thesis is to decipher endothelial mechanisms of liver metastasis in malignant melanoma.

To analyze hepatic melanoma metastasis our group established a model of liver colonization by injecting different murine melanoma cell lines into the spleen or the tail vein. Therefore, five different murine melanoma cell lines, harboring different driver mutations were selected to represent the heterogeneity of malignant melanoma.

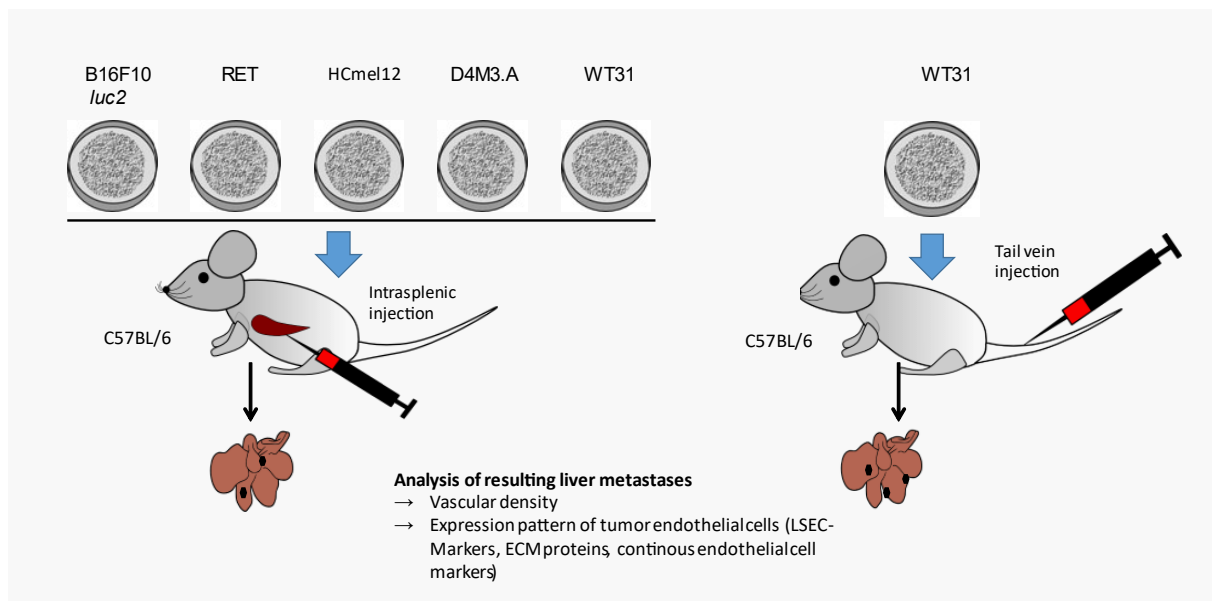


**Figure 5 Scheme of the melanoma model.** Melanoma cells of five different cell lines are injected into the spleen or in the tail vein. Resulting liver metastases are analysed in respect of vascular density and expression pattern of tumor endothelial cells.

In the first part of my thesis, I focused on tumor-intrinsic mechanisms of hepatic metastases. Three melanoma cell lines with high or intermediate metastatic efficiency were analyzed histomorphologically and the tumor endothelium was studied. Besides vascular density, I thoroughly studied the protein expression pattern of tumor endothelial cells, and cell lines were compared by RNA sequencing.

In the second part of my thesis, I focused on endothelial mechanisms of hepatic metastases. The established models of liver colonization were used to analyze the effects of hepatic endothelial overexpression of NICD on liver metastases. To achieve a liver-specific endothelial overexpression of NICD (NICD<sup>OE-HEC</sup>) a Clec4g-cre driver mouse was combined with a Rosa26NICD mouse, resulting in an overexpression of NICD in Clec4g-positive cells, which mainly compromise the liver endothelium.

To study liver metastasis in the NICD<sup>OE-HEC</sup> mice, the B16F10 *luc2* model of intrasplenic injection and the WT31 model of tail vein injection were chosen. Additionally, another tumor entity was included in the study by injection of the colon carcinoma cell line MC38 in the spleen. Liver colonization experiments showed a reduced metastatic susceptibility in NICD<sup>OE-HEC</sup> mice. I thoroughly studied and characterized the NICD<sup>OE-HEC</sup> mice to decipher the molecular mechanisms underlying the protection of hepatic metastasis.

## 4. Material and methods

### 4.1. Material

#### 4.1.1. Chemicals, solvents, and reagents

<b>Chemical/Reagent</b>	<b>Manufacturer</b>	<b>Order no.</b>
2-Propanol	Sigma-Aldrich	33539-M
4',6-Diamidino-2-phenylindol (DAPI)	Thermo Fisher Scientific	D1306
4 % formaldehyde solution ROTI Histofix	Carl Roth	P087.3
Advanced Dulbecco`s Modified Eagle Medium (DMEM)/F12	Thermo Fisher Scientific	12634010
Agarose	Sigma-Aldrich	A9539
$\beta$ -Mercaptoethanol	Sigma-Aldrich	60-24-2
Bovine Serum Albumin (BSA)	VWR	J642-1ML
Carprofen (Rimadyl®)	Zoetis	RXRIM-INJ
Cell Dissociation Solution	Millipore	S-014-B
Dako Antibody Diluent	Agilent Technologies	K346430-2
Dako fluorescence mounting medium	Agilent Technologies	S302380-2
DMEM Glutamax	Life Technologies	11574516
Deoxynucleotide (dNTP) Mix 10mM	Invitrogen	18109017
D-luciferin 1-(4,5-dimethoxy-2- nitrophenyl)ethyl ester (Luciferin)	BioVision	2779
Ethanol	Carl Roth	5054.3
Ethylenediaminetetraacetic acid (EDTA)	Invitrogen	15575-038
Eukitt®	Sigma-Aldrich	03989
Fetal Bovine Serum (FBS)	Life technologies	10270106
Gene Ruler DNA Ladder mix, 100 – 10000bp	Thermo Fisher Scientific	SM0333

Glucose	Gibco	15023-021
Glycin	Carl Roth	HN07.1
Heat Induced Epitope Retrieval (HIER)	Zytomed Systems	ZUC028-500
Citrate Buffer pH 6.0, 10x		
4-(2-hydroxyethyl)-1-piperazineethanesulfonic acid (HEPES) buffer solution	Sigma-Aldrich	83264
Isoflurane	WDT	21311
Laemmli buffer, 2x	Bio-Rad	1610747
L-Alanine	Carl Roth	3076.1
L-aspartic acid	Carl Roth	1690.1
L-glutamine	Sigma-Aldrich	G8540
L-glutamic acid	Carl Roth	1743.1
L-serine	Carl Roth	1714.1
L-Threonine	Carl Roth	1738.1
Loading Dye, 6x	Thermo Fisher Scientific	R0611
Magnesium chloride (MgCl <sub>2</sub> )	Carl Roth	KK36.1
<b>Maxima Reverse Transcriptase, 200 U/μl</b>	Thermo Fisher Scientific	EP0741
Natrium chloride (NaCl) (0.9%)	Fresenius	808765
Natriumpyruvat	Thermo Fisher Scientific	11530396
Non-essential Amino Acids (NEAA) (100x)	Sigma-Aldrich	M7145
Nonident P40 (NP-40) Substitute	Fluka	74385
Normal donkey serum	Dianova	017-000-121
Oligo(dT)18 Primer	Life Technologies	SO132
Paraformaldehyde (PFA)	Carl Roth	0335.3
Penicillin/Streptomycin, 10.000 U/ml	Thermo Fisher Scientific	15140122
Phosphate-buffered saline (PBS)	Life Technologies	14190169
PBS buffer (1x, Dulbecco`s)-powder	PanReac AppliChem	A0964

Phosphate-buffer saline +/- (PBS +/-)	Thermo Fisher Scientific	14040117
Roswell Park Memorial Institute (RPMI) 1640 Medium	Thermo Fisher Scientific	11530586
RPMI Glutamax	Thermo Fisher Scientific	61870044
Standard Rodent Diet	Ssniff	V1534-000
Sucrose	Sigma Aldrich	16104
Tris-hydrogen chloride (HCl) Ultra Pure, 1M pH8	Life Technologies	15568025
Trypan blue solution	Sigma Aldrich	T8154
Trypsin-EDTA, 10x	Sigma-Aldrich	59418C
Tween 20	Sigma-Aldrich	P7949
Ultra Pure Water Dnase/Rnase Free	Life technologies	10977-049

#### 4.1.2. Buffers and media/recipes

<b>Buffer/medium</b>	<b>composition</b>
4% PFA pH 7.2	40 g PFA powder 100 mL 10 x PBS 900 mL dH <sub>2</sub> O
30% Sucrose	3 g Sucrose 10 mL 1x PBS
WT31, B16F10 <i>luc2</i> and RET medium	500 mL RPMI Glutamax 10% FBS 1% P/S

D4M3.A medium	500 mL Advanced DMEM F12 5% FBS 1% P/S 1% L-Glutamine
HCmel12 medium	500 mL RPMI 1640 50 µL HEPES (1M) 3.75 µL β-Mercaptoethanol 10% FBS 1% L-glutamine (2mM) 1% P/S 1% Natrium Pyruvate 1% NEAA (0.1mM)
MC38 medium	500 mL DMEM Glutamax 10% FBS 1% P/S

#### 4.1.3. Kits

<b>Kit</b>	<b>Manufacturer</b>	<b>Order no.</b>
KAPA HotStart Mouse Genotyping Kit	Sigma-Aldrich	KK7352
innuprep DNA Mini Kit	Analytik Jena	845-KS-10410
innuPREP RNA Mini Kit 2.0	Analytik Jena	845-KS-20400
QIAprep Spin Miniprep Kit	QIAGEN	27104
TURBO DNA-free Kit	Thermo Fisher Scientific	AM1907

#### 4.1.4. Unconjugated antibodies

Table 1. Unconjugated antibodies

Specificity	Clone	Host	Manufacturer	Order no.	Dilution
Arginase 1	polyclonal	goat	Santa Cruz	sc-18351	1:100
Caveolin-1	polyclonal	rabbit	BD	610060	1:50
CD31	SZ31	Rat	Dianova	DIA-310	1:50
CD32b	polyclonal	Goat	R&D Systems	AF-1460	1:75
Collagen I	polyclonal	Rabbit	Acris antibodies	R1038	1:200
Collagen III	polyclonal	Rabbit	Acris antibodies	R1040	1:200
Collagen IV	polyclonal	Rabbit	Novus biologicals	NB120-6586	1:200
CYP2E1	polyclonal	Rabbit	Merck Millipore	AB1252	1:2000
Desmin	polyclonal	Rabbit	Abcam	ab15200	1:500
Endomucin	V.7C7	Rat	Life Technologies	14-5851-85	1:100
Fibronectin	polyclonal	rabbit	Abcam	ab23750	1:100
Gata 4	polyclonal	Rabbit	Abcam	ab84593	1:50
GFP	polyclonal	chicken	Abcam	ab13970	1:800
Glutamine synthetase	polyclonal	rabbit	Sigma-Aldrich	G2781	1:1000
ICAM-1	polyclonal	Rabbit	Proteintech	10020-1-AP	1:100
Lama4	polyclonal	goat	R&D Systems	AF3837	1:100
LYVE-1	polyclonal	Goat	R&D Systems	AF2125	1:100
Podocalyxin	polyclonal	goat	R&D Systems	AF1556	1:100
Rhbg	polyclonal	goat	Thermo Fisher Scientific	PA5 19369	1:50
Stabilin-2	Pep15	Rabbit	[226]		1:700
TRP2	polyclonal	rabbit	Abcam	ab74073	1:1000
VCAM-1/CD106	polyclonal	Goat	R&D Systems	AF643	1:100
VE-Cadherin	polyclonal	Goat	R&D Systems	AF3837	1:50

#### 4.1.5. Conjugated antibodies

Table 2. Conjugated antibodies

Specificity	Conjugate	Clone	Manufacturer	Order no.	Application	Dilution
Goat IgG	AF488	polyclonal	Dianova	705-545-147	IF	1:400
Goat IgG	AF647	polyclonal	Dianova	705-605-147	IF	1:400
Goat IgG	Cy3	polyclonal	Dianova	705-165-147	IF	1:400
Rabbit IgG	AF488	polyclonal	Dianova	711-545-152	IF	1:400
Rabbit IgG	AF647	polyclonal	Dianova	711-605-152	IF	1:400
Rabbit IgG	Cy3	polyclonal	Dianova	711-165-152	IF	1:400
Rat IgG	AF488	polyclonal	Dianova	712-545-153	IF	1:400
Rat IgG	AF647	polyclonal	Dianova	712-605-153	IF	1:400
Rat IgG	Cy3	polyclonal	Dianova	712-165-153	IF	1:400

#### 4.1.6. Primers for Genotyping

Oligonucleotides were ordered lyophilized from Metabion international AG.

Table 3. Primes for genotyping

PrimerID	Gene	Sequence 5' - 3'
PC1	Mm Clec4g-iCre_Fw	AAGCTGAACAACAGGAAATGGTTC
PC2	Mm Clec4g-iCre_Rv	GGAGATGTCCTTCACTCTGATTCT
PE1	Mm_RosaEvi_common_fw	CTCGCTCTGAGTTGTTATCAG
PE2	Mm_RosaEvi_flox_rv	GACGACAGTATCGGCCTCAGGAAG
PE3	Mm_RosaEvi_wt_rv	CCAGATGACTACCTATCCTCC
PY1	Mm ROSA26YFP_Common	AAAGTCGCTCTGAGTTGTTAT
PY2	Mm ROSA26YFP_Mutant	AAGACCGCGAAGAGTTTGTC
PY3	Mm ROSA26YFP_Wildtype	GGAGCGGGAGAAATGGATATG

#### 4.1.7 Consumables

<b>Consumable</b>	<b>Manufacturer</b>	<b>Order no.</b>
15 mL Cellstar Tubes	Greiner Bio-One	18827
50mL Cellstar Tubes	Greiner Bio-One	2272616
Cell culture Flask, T75	Greiner Bio-One	658175
Cell culture Flask, T175	Greiner Bio-One	660175
Cryo tubes, 2ml	Greiner Bio-One	122263
Cryomold, 15 x15 x 15 cm	Weckert	4566
Dako Pen	Agilent technologies	S200230
Disposable scalpel	Carl Roth	T998.1
Erlenmeyer flask	Carl Roth	X749.1
Microscopy slides Super Frost Plus	Langenbrinck	03-0060
Microtome blades, S35	pfm medical	207500000
Microvette ® 500 LH	Sarstedt	20.1345
Needle, 26G ½	BD	303800
Needle, 30G ½	BD	304000
Paraffin embedding cassettes	neoLab Migge	60001580
Parafilm ® M	Merck	P7793
PCR stripes, 0.2 mL	Sarstedt	72.991.992
Pipette filter tips, 10 µL	Biozym	VT0200
Pipette filter tips, 100µL	Biozym	VT0230
Pipette filter tips, 200 µL	Biozym	VT0240
Pipette tips, 10 µL	Biozym	VT0104
Pipette tips, 200 µL	Biozym	VT0144
Pipette tips, 1250 µL	Biozym	VT0174
Polystyrene Round-bottom Tubes, 5 mL	Falcon	352052
Reaction Tubes Safe-Lock, 1.5 mL	Eppendorf	30120086

Reaction Tubes Safe-Lock Biopur, 1.5 mL	Eppendorf	30120094
Reaction Tubes Safe-lock, 2 mL	Eppendorf	30120094
Reaction Tubes Safe-Lock, 5mL	Eppendorf	30119401
Serological Pipette, 5mL	Greiner Bio-One	606180
Serological Pipette, 10 mL	Greiner Bio-One	607180
Serological Pipette, 25 mL	Greiner Bio-One	760180
Syringe, 1 mL	B.Braun	9161502
Syringe, 20 mL	B.Braun	4606205V
Tissue-Tek® optimum cutting temperature (O.C.T.) compound	Weckert	600001
Vicryl 6.0	Ethicon	JV492H

#### 4.1.8. Technical equipment

Device	Manufacturer
Balance analytical	Sartorius
Balance PT210	Sartorius
Cell culture incubator HERAccl® 150i	Thermo Fisher Scientific
Centrifuge 5417 R	Eppendorf
Centrifuge 5810 R	Eppendorf
Cooling plate 4100	pfm medical
Counting chamber Neubauer improved	Brand
Cryostat CM3050 S	Leica
Eclipse Ni-E motorized upright microscope	Nikon Instruments
DS-Qi2 high-definition monochrome camera	
DS-Ri2 high-definition color camera	
Filterset AHF F36-513 DAPI HC	
Filterset AHF F36-720 Sp. Green HC mFISH	
Filterset AHF F36-740 Sp. Orange HC mFISH	

Filterset Semrock BrightLine Cy5-4040C single-band	
Electrophoresis chamber Mini-PROTEAN Tetra System	Bio-Rad
Fridge profiline	Liebherr
Gas anesthesia system XGI-8	Caliper Life Sciences
Gel electrophoresis system Mupid® One	ADVANCE CO., LTD.
Heating block Thermo Mixer C	Eppendorf
Heating Immersion Circulator	Julabo
Imaging System Intas ChemoStar Touch	Intas Science Imaging
Imaging System Intas GelStick IMAGER	Intas Science Imaging
Incubator	Binder
Intensilight Epifluorescence Illuminator	Nikon Instruments
Inverse microscope Axio Vert.A1	Zeiss
IVIS200	Caliper Life Sciences
Leica Confocal Microscope TCS SP5 DS	Leica Microsystems
Diode laser (405 nm/50 mW)	
Ar-laser (458 nm/5 mW; 475 nm/5 mW; 488 nm/20 mW; 514 nm/20 mW)	
HeNe 543 nm/1 mW	
DPSS 561n	
HCX PL APO CS 20.0x0.70 IMM DRY	
HCX PL APO CS 40.0x1.30 OIL UV	
NanoPhotometer NP80	IMPLEN
Peristaltic pump	Ismatec
Plan Apo $\lambda$ 4x NA 0.2	Nikon Instruments
Plan Apo $\lambda$ 10x NA 0.45	Nikon Instruments
Plan Apo $\lambda$ 20x NA 0.75	Nikon Instruments
Plan Apo $\lambda$ 40x NA 0.95	Nikon Instruments
qTOWER 3 G touch	Analytik Jena

Refrigerator (-20 °C) profiline	Liebherr
Refrigerator (-80 °C)	PHC Europe BV
Rotary microtome 3006EM	pfm medical
Safety cabinet Herasafe KS class II	Thermo Fisher Scientific
Shaker DRS-12	neoLab Migge
Thermal Cycler T100™	Bio-Rad
Thermoblock ThermoMixer C	Eppendorf
Vortex-Genie™ 2	Scientific Industries
Water bath TW8	Julabo
Water bath pura22	Julabo
Water bath 1000	pfm medical
Zeiss Axio Vert.A1 Microscope	Zeiss
Objective LD A-Plan 10x/0,25 M27	

#### 4.1.9 Software

Software	Version	Manufacturer
Fiji ImageJ	2.0.0	National Institutes of Health
GraphPad Prism	9.5	GraphPad Software
Inkscape	1.0.2-2	Inkscape Community
Leica Application Suite	2.7.3.9723	Leica
NIS-Elements Advanced Research (Ar)	5.02	Nikon Instruments

#### 4.1.10 Mouse strains

Table 4. Mouse strains

Name	Official name	Supplier	Publication
B6N Wildtype	C57BL/6N	Janvier Labs	
Clec4g-iCre	C57BL/6N-Tg(Clec4g-icre)1.1 <sup>Sgoe</sup>	Our lab	[289]

NICD <sup>OE-HEC</sup>	Clec4g-Cre <sup>tg/wt</sup> ; Rosa26 <sup>N1ICD-IRES-GFP</sup>	Our lab	[289]
ROSA26 NICD	Rosa26locus Gt(ROSA)26Sor <sup>tm1(Notch1)Dam/J</sup>	Our lab	[290]
Stab2-Cre <sup>tg/wt</sup>	Stabilin-2 <sup>tg1.2cre</sup>	Our lab	[211]
WLS <sup>fl/fl</sup>	B6-Gpr177 <sup>tm1 1775.302Arte</sup> ; TaconicArtemis	Our lab	[291]
WLS <sup>HEC-KO</sup>	Stab2-Cre <sup>tg/wt</sup> ; Wls <sup>fl/fl</sup>	Our lab	[221]

#### 4.1.11 Cell lines

Table 5. Cell lines

Name	Species	Description
B16F10 <i>luc2</i>	Mouse	Melanoma cell line, Perkin Elmer
D4M3.A	Mouse	melanoma cell line isolated from Tyr::CreER;Braf <sup>fCA</sup> ;Pten <sup>lox/lox</sup> mice
HCmel12	Mouse	Melanoma cell line isolated from HGF-CDK4(R24C) mice
MC38	Mouse	Colorectal carcinoma cell line
RET	Mouse	Melanoma cell line isolated from metallothionein-1 (MT)/RET transgenic mice
WT31	Mouse	Melanoma cell line isolated from Tyr::Nras <sup>Q61K<sup>c</sup></sup> ;INK4a <sup>-/-</sup> mice

## 4.2 Methods

### 4.2.1 Cell culture

#### 4.2.1.1 Cell lines

All analyzed cell lines were of murine origin. WT31 cells were isolated from Tyr::Nras<sup>Q61K<sup>c</sup></sup>; INK4a<sup>-/-</sup> mice [292] and were kindly provided by O. Sansom (Beatson Institute for Cancer Research, Scotland). The murine melanoma cell line B16F10 *luc2* is commercially available

and was purchased from Perkin Elmer (MA, USA). RET1 melanoma cells derive from metallothionein-1/RET transgenic mice [287] and were a generous gift from V. Umansky (German Cancer Research Center (DKFZ), Heidelberg, Germany). HcMel12 melanoma cells were isolated from a primary melanoma in HGF-CDK4(R24C) mice [277] and were kindly provided by T. Tüting (University of Magdeburg, Germany). The murine melanoma cell line D4M.3A derive from Tyr::CreER;Braf<sup>CA</sup>;Pten<sup>lox/lox</sup> mice [278] and a kind gift from C. E. Brinckerhoff (Geisel School of Medicine at Dartmouth, NH, USA). All cell lines were regularly tested mycoplasma free by polymerase chain reaction (PCR).

#### **4.2.1.2 Thawing of cells**

Cryotube was thawed in a 37 °C water bath and cells were transferred immediately into a 50 mL Falcon tube with 10 mL respective cell culture medium. Cells were centrifuged for 5 min at 3200 rpm, medium was aspirated. The cell pellet was resuspended in 1 mL medium and transferred in a T75 cell culture flask containing 10 mL respective cell culture medium. Cells were incubated overnight at 37 °C, 5% CO<sub>2</sub>. Cell culture media was removed, cells were washed once with 10 mL PBS and 10 mL fresh cell culture media was added. Incubation at 37 °C, 5% CO<sub>2</sub> was continued.

#### **4.2.1.3 Freezing of cells**

Cells were cultured in cell culture flask (T175) to reach a density of 80%. Cell culture medium was removed and cells were washed once with PBS, by adding 10 mL PBS. PBS was removed and 2 mL Trypsin-EDTA was added. Cells were incubated for 2-5 min at 37 °C, 5% CO<sub>2</sub>. After detachment of cells, 10 mL cell culture media was added to stop the reaction. Cell suspension was transferred in a 50 mL Falcon tube and centrifuged for 5 min, 3200 rpm by room temperature. Cells were resuspended in 10 mL medium and a 20 µL aliquot was taken for counting the cells using a Neubauer Counting Chamber. Cells were centrifuged for 5 min, 3200 rpm and the media was completely removed. Cells were resuspended in FBS/Glycerol in the appropriate volume. Cells were frozen in appropriate container at -80 °C and then transferred into liquid nitrogen for long-term storage.

#### **4.2.1.4 Splitting**

For splitting of cells, cell culture media was removed, and cells were washed once with 10 mL PBS. PBS was removed completely and either 1 mL Trypsin-EDTA was added to a T75 flask or 2 mL Trypsin-EDTA was added to a T175 flask. Cells were incubated at 37 °C, 5% CO<sub>2</sub> for 2-5 min or until detached. 10 mL respective cell culture medium was added to the flasks and cell suspension was transferred into new flasks. Incubation was continued at 37 °C, 5% CO<sub>2</sub>.

#### **4.2.1.5 Seeding of cells**

For seeding of cells they were washed with 10 mL PBS. PBS was removed completely and 1 mL Trypsin-EDTA was added. Cells were incubated at 37 °C, 5% CO<sub>2</sub> for 5 min. 10 mL respective cell culture media was added, and cells were transferred into a 50 mL Falcon tube. 20 µL were removed from the cell suspension for counting and cells were centrifuged at 3200 rpm for 5 min. Cells were counted under the light microscope using a Neubauer counting chamber. The cell pellet was resuspended in the appropriate volume of cell culture media and the respective number of cells was seeded in a T175 cell culture flask and incubated overnight at 37 °C, 5% CO<sub>2</sub>.

#### **4.2.1.6 Harvesting cells**

Cells were harvested at a confluency of ~ 50%. Medium was removed and cells were washed with PBS. PBS was removed and 2 mL Cell Dissociation Buffer was added. Cells were incubated at 37 °C, 5% CO<sub>2</sub> for 10 min. After dissociation cells were thoroughly resuspended in 10 mL PBS and transferred in a 50 mL Falcon tube. 20 µL were taken from the cell suspension for counting with the Neubauer Counting Chamber. Cells were centrifuged for 5 min at 3200 rpm and cell pellet was redissolved in the appropriate volume of PBS +/- depending on cell concentration.

### **4.2.2 Preparation of murine melanoma cell lines for *in vivo* experiments**

For tumor experiments cells were thawed always at the same passage and cell culturing followed a strict protocol for each cell line.

#### **4.2.2.1 B16F10 *luc2***

One cryotube, containing 1 million B16F10 *luc2* cells (p12) was thawed and cells were transferred in a T75 cell culture flask. B16F10 *luc2* cells were maintained in RPMI 1640 Glutamax media with 10% (v/v) fetal calf serum (FCS) and 100 U/mL penicillin/streptomycin at 37 °C, 5% CO<sub>2</sub>. After incubation overnight at 37 °C, 5% CO<sub>2</sub> media was exchanged. On day 3 cells were seeded with a density of 2-2.5 million cells in a T175 flask and incubated overnight at 37 °C, 5% CO<sub>2</sub>. On day 4 cells were harvested for tumor experiments, at 50% confluency.

#### **4.2.2.2 WT31**

One cryotube containing 2 million WT31 cells (p9) was thawed and transferred into a T175 cell culture flask containing 20 mL RPMI 1640 Glutamax media with 10% (v/v) FCS and 100 U/mL penicillin/streptomycin. Cells were incubated overnight at 37 °C, 5% CO<sub>2</sub> to adhere to the cell culture flask, then media was exchanged. Cells were incubated for another 24 h at 37 °C, 5% CO<sub>2</sub>. On day 3, cells were split 1:3 in a T175 flasks and incubated at 37 °C, 5% CO<sub>2</sub> for another 3 days. On day 7 cells were split again 1:3 and seeded in 3 T175 flasks to yield high cell numbers for the tumor experiment. Cells were incubated at 37 °C, 5% CO<sub>2</sub>. On day 9 cells

were seeded for the tumor experiment at a density of 4-4.5 million cells. After incubation overnight cells reached a confluency of 50% and were harvested for the tumor experiment.

#### **4.2.2.3 RET**

One cryotube containing 1 million RET cells (p9) was thawed and transferred into a T75 cell culture flask containing 10 mL RPMI 1640 media with 10% (v/v) FCS and 100 U/mL penicillin/streptomycin. After incubation overnight at 37 °C, 5% CO<sub>2</sub> media was exchanged. On day 3, cells were seeded with a density of 2-2.5 million cells in a T175 flask and incubated overnight at 37 °C, 5% CO<sub>2</sub>. On day 4 cells, were harvested for tumor experiments at 50% confluency.

#### **4.2.2.4 D4M3.A**

One cryotube containing 1 million D4M3.A cells (p7) was thawed and transferred into a T75 cell culture flask. D4M3.A cells were maintained in Advanced DMEM/F-12 with 5% (v/v) FCS, 100 U/mL penicillin/streptomycin and 1 x glutamine. After incubation overnight at 37 °C, 5% CO<sub>2</sub> media was exchanged. On day 3 cells were seeded with a density of 2-2.5 million cells in a T175 flask and incubated overnight at 37 °C, 5% CO<sub>2</sub>. On day 4, cells were harvested at 50% confluency.

#### **4.2.2.5 HCmel12**

One cryotube containing 1 million HCmel12 cells was thawed and transferred into a T75 cell culture flask. HCmel12 cells were cultured in RPMI with 10% (v/v) FCS, 1 M HEPES, β-Mercaptoethanol, 1% L-glutamine, 100 U/mL penicillin/streptomycin, 1 mM Natrium Pyruvate and 0.1 mM NEAA. After incubation overnight at 37 °C, 5% CO<sub>2</sub> media was exchanged. Cells were split 1:3 on day 5 and seeded on day 7 with a density of 4.5 million cells in a T175 flask and incubated overnight at 37 °C, 5% CO<sub>2</sub>. On day 8 cells were harvested at 50% confluency.

#### **4.2.2.6 MC38**

One cryotube containing 2 million MC38 cells was thawed and transferred into a T75 cell culture flask containing 10 ml DMEM Glutamax with 10% (v/v) FCS and 100 U/mL penicillin/streptomycin. After incubation overnight at 37 °C, 5% CO<sub>2</sub> media was exchanged. On day 3 cells were split 1:5. On day 6 cells were seeded for the colonization experiment with a density of 4 million cells in a T175 flask and incubated overnight at 37 °C, 5% CO<sub>2</sub>. On day 7 cells were harvested for tumor experiments at 50% confluency.

### **4.2.3 Animal experiments**

#### **4.2.3.1 Animal housing and breeding**

Mice were housed in the animal facility of the Zentrum für Medizinische Forschung (ZMF) in Mannheim under specific pathogen free conditions in single ventilated cages (Sealsafe plus

DGM™, Techniplast, Italy; Bedding H0234-20, Ssniff, Germany) in a room with a 12h/12h light/dark cycle. Animals were fed *ad libitum* with a standard rodent diet and had free access to water.

C57Bl/6N mice were purchased by Janvier for *in vivo* experiments and were used at least at 10 weeks of age for metastasis experiments.

The animal ethic committee of Baden Württemberg (Regierungspräsidium Karlsruhe) approved all animal experiments, and the animals received humane care in compliance with the Guide for the Care and Use of Laboratory Animals published by the National Academy of Sciences.

#### **4.2.3.2 Generation of liver-specific endothelial Notch1 overexpression mice**

For generation of NICD<sup>OE-HEC</sup> mice (Clec4g-Cre<sup>tg/wt</sup>; Rosa26<sup>N1ICD-IRES-GFP</sup> mice) a male Clec4g-iCre driver mouse (C57BL/6N-Tg(Clec4g-iCre)1.1<sup>Sgoe</sup>) on C57BL/6N background was crossed to female Rosa26<sup>N1ICD-IRES-GFP</sup> mice. The Rosa26<sup>N1ICD-IRES-GFP</sup> mouse line bears a fragment of the Notch 1 gene and a green fluorescent protein (GFP) inserted into the Rosa26 locus (Gt(ROSA)26Sortm1(Notch1)Dam/J; [JAX008159] [290]. At P28 genotyping of offspring was performed using primer pairs PC1 and PC2 for Cre, and PY1, PY2 and PY3 for Rosa26<sup>N1ICD IRES-GFP</sup>.

All animals were on a C57BL/6 background and at least 10 weeks of age for *in vivo* experiments. Age-matched siblings were chosen as controls.

#### **4.2.3.3 Generation of Wls<sup>HEC-KO</sup> mice**

For generation of Wls<sup>HEC-KO</sup> mice (Stab2-Cre<sup>tg/wt</sup>; Wls<sup>fl/fl</sup>) in a first step Stab2-Cre<sup>tg/wt</sup> mice were crossed with Wls<sup>fl/fl</sup> mice [B6-Gpr177<sup>tm1 1775.302Arte</sup>; TaconicArtemis], that have a loxP-sequence flanking exon 3 of the Wls-Gene. To generate heterogenous Wls<sup>fl/fl</sup> mice, the resulting mice from the first crossing Stab2-Cre<sup>tg/wt</sup>; Wls<sup>tg/wt</sup> were crossed again with Wls<sup>fl/fl</sup> mice resulting in Wls<sup>HEC-KO</sup> mice. Offspring was genotyped for Cre-Expression using primer pairs PC1 and PC2 and Wls<sup>fl/fl</sup> was confirmed by genotyping with primer pairs PE1, PE2 and PE3.

#### **4.2.3.4 Liver colonization assays**

For liver colonization experiments female mice of at least 10 weeks of age were used.

##### **4.2.3.4.1 Intralial injection of cells**

Carprofen was injected intraperitoneally as analgetic. Mice were anaesthetized with isoflurane and on the left side a laparotomy was performed. The spleen was prepared and put out of the peritoneum with the help of a soft cotton stick. Melanoma cells or colon carcinoma cells were slowly injected into the spleen at the indicated doses in a volume of 60 µL. 15 min after intralial injection a splenectomy was performed to prevent the formation of a tumor at the

injection site. For the splenectomy blood vessels were ligated and the spleen was removed. The peritoneum and the skin were closed by suture with Vicryl 6.0. 0.9% NaCl was applied subcutaneously for rehydration and animals were monitored carefully after the procedure.

Intralienal injection of B16F10 *luc2* cells and MC38 cells in NICD<sup>OE-HEC</sup> mice and WLS<sup>HEC-KO</sup> mice were performed by Sebastian Wohlfeil. Intralienal injection of C57BL/6 mice with B16F10 *luc2*, WT31 and Ret cells were performed by Dr. Sebastian Wohlfeil, Céline Weller, Christof Dormann and Bianca Dietsch.

#### **4.2.3.4.2 Intravenous injection of WT31 cells**

Mice were anaesthetized with Isoflurane and WT31 melanoma cells were slowly injected into the tail vein at the indicated doses in a volume of 100-200 µL per injection.

Tail vein injections were performed by Dr. Sebastian Wohlfeil.

#### **4.2.3.5 Bioluminescence Imaging**

For bioluminescence imaging luciferin (30 mg/mL) was injected intraperitoneally. For *in vivo* imaging, animals were imaged using an IVIS 200 charge-coupled device imaging system with an exposure time of 45 secs. For *ex vivo* BLI of the liver or lung mice were sacrificed 10 mins after luciferin injection, and organs were excised and placed in a petri dish. Using the IVIS 200 system (exposure time 45 sec) *ex vivo* imaging of organs was performed.

#### **4.2.3.6 Dissection of mouse organs, cryopreservation and paraffin embedding**

Mice were sacrificed by cervical dislocation at indicated time points after liver colonization experiment or at age 10-12 weeks for basal characterization of NICD<sup>OE-HEC</sup> mice. Tail clipping was performed for genotype reconfirmation. Selected organs were carefully excised, weighted, photographed, and cut into several pieces for histological analysis.

For paraffin embedding liver, lung, brain, spleen, and heart were fixed in phosphate-buffered 4% formaldehyde solution at room temperature for one to seven days. After dehydration of the tissue, fixed tissue was paraffin embedded in embedding cassettes according to standard protocols.

For histological analysis by cryosection, tissue was embedded in Tissue Tek® O.C.T™ compound in cryomolds, snap-frozen in liquid nitrogen and stored at -80 °C.

For nEGFP co-immunofluorescence staining, livers were perfused and fixed in 4% PFA overnight. After 24 h incubation in 30% sucrose in PBS livers were embedded in Tissue Tek® O.C.T™ compound, snap frozen in liquid nitrogen and stored at -80 °C. Perfusion of mice was performed by Dr. Sebastian Wohlfeil.

#### 4.2.3.7 Blood parameters

Blood samples were taken from the retrobulbar vein plexus under isoflurane anesthesia after 4 hours of fasting during the day cycle. Plasma was separated in the Microvette ® 500 LH by centrifugation (7000 g, 7 min, 20 °C) and analyzed for the following parameters: Triglycerides, Cholesterol, Bilirubin, alanine transaminase (ALT), aspartate aminotransferase (AST), glutamate dehydrogenase (GLDH), cholinesterase (CHE), and total protein. Analysis was performed by the technicians at the core facility of the ZMF using a Cobas c311 analyzer (F. Hoffmann-La Roche) and according to the manufacturers protocol. Blood sugar was measured using a point-of-care testing device (StatStrip™ Xpress™, Nova Biomedical, USA).

Blood samples of the retrobulbar vein plexus were jointly taken with Hiltrud Schönhaber.

#### 4.2.4 Molecular biology methods

##### 4.2.4.1 Genotyping

For genotyping DNA was extracted from ear tissue and strain-specificity was visualized by PCR reaction. DNA was extracted from tissue by lysis with 10x KAPA Express Buffer and 1 U/μL KAPA Express Extract Enzyme at 75 °C for 10 min. Samples were denaturalized for 5 min at 95 °C. Extracted DNA was diluted 1:10 in 10 mM Tris-HCL, pH 8.

##### 4.2.4.2 Polymerase chain reaction (PCR)

For polymerase chain reaction (PCR) a PCR mix with the following components was prepared:

###### **iCre and Evi KO:**

PCR-grade water	3 μL
2x KAPA2g Mix	5 μL
10 μM Forward Primer	0.5 μL
10 μM Reverse Primer	0.5 μL
DNA	1 μL

###### **Rosa26 locus:**

PCR-grade water	2,5 μL
2x KAPA2g Mix	5 μL
10 μM Primer 1	0.5 μL
10 μM Primer 2	0.5 μL

10 $\mu$ M Primer 3	0.5 $\mu$ L
DNA	1 $\mu$ L

PCR was performed using a thermocycler and the following protocol:

95 °C 3 min  
95 °C 15 sec }  
60 °C 15 sec } 35 x  
72 °C 15 sec }  
72 °C 1 min  
12 °C  $\infty$

Subsequently, PCR products were analyzed by agarose gel electrophoresis.

#### **4.2.4.3 Agarose gel electrophoresis**

For agarose gel electrophoresis 2  $\mu$ L 6x loading dye was added to PCR products. PCR products and Gene Ruler DNA ladder mix were loaded on a 2% agarose gel containing 10% Nancy-520 and gel electrophoresis was performed for 30 min at 100 V. The agarose gel was imaged, and the DNA was visualized with Intas Gel Stick Imager.

#### **4.2.4.4 RNA isolation**

For RNA isolation, cell lines were prepared according to the protocols for cell preparation for liver colonization assays. Cells were harvested at 50% confluency by adding cell dissociation buffer. Cells were centrifuged and the pellet was used for RNA isolation. RNA isolation was performed using innuPREP RNA Mini Kit 2.0 according to the manufacturer's protocol. RNA was eluted in 20  $\mu$ L RNase free water and treated with TURBO DNA-free Kit (AM1907, Invitrogen USA). RNA concentration was measured with NanoPhotometer NP80 and stored at -80 °C.

#### **4.2.4.5 RNA sequencing**

For RNA sequencing RNA quality was assessed by the Affymetrix core facility of the UMM using a 2100 Bioanalyzer. 2  $\mu$ g RNA was sent to BGI (Hongkong, China) and used for RNA sequencing with an Illumina HiSeq 4000 sequencing system according to the manufacturer's protocol. Raw and normalized gene expression profiling data were deposited in NCBI's gene expression Omnibus and were available through GEO Series accession number GSE185539. Statistical analysis with R and preparation of graphs of RNA sequencing was done by Dr. Carsten Sticht and Dr. Sebastian Wohlfeil.

## **4.2.5 Histological methods**

### **4.2.5.1 Hematoxylin & Eosin (H&E) Staining**

Hematoxylin and Eosin (H&E) stainings were performed on paraffin sections using an automatic stainer by the technicians at the core facility of the ZMF following a standard protocol.

#### H&E Staining Standard Protocol

Xylol	3x 2 min
100% Ethanol	1 min
96% Ethanol	1 min
80% Ethanol	1 min
70% Ethanol	1 min
Running tap water	1 min
Hematoxylin	4 min
Running tap water	10 min
Eosin	2 min
Tap water	30 sec
80% Ethanol	30 sec
96% Ethanol	1 min
100% Ethanol	2x 1 min
Xylol	2x 1 min

After staining slides were mounted with Eukitt.

### **4.2.5.2 Immunofluorescence staining of cryosections**

Embedded frozen tissue was cut into 8 µm cryosections using the cryostat and air dried for 1 hour. Before staining the tissue was surrounded with a hydrophobic ring using the Dako pen. Cryosections were fixed with 4% PFA in PBS for 10 min at room temperature. PFA was removed by washing for 5 min in PBS. Sections were blocked for 30 min with blocking buffer (5% normal donkey serum in PBS) at RT. After blocking, Slides were incubated with primary antibody at indicated concentration in 1% normal donkey serum in PBS overnight, at 4 °C in a humidity chamber.

Slides were washed three times in PBS for at least 5 min, before adding secondary antibody. Secondary antibodies and DAPI were diluted at indicated concentrations in 1% normal donkey serum in PBS and protected from light. Secondary antibody dilution was added to slides and incubated for 45 min at room temperature in a humidity chamber protected from light. After incubation slides were washed 3 times in PBS for at least 5 min. Before mounting with DAKO fluorescence mounting medium slides were rinsed in H<sub>2</sub>O.

Slides were air-dried overnight at room temperature in the dark and stored at 4 °C.

#### **4.2.5.3 Immunofluorescence staining of paraffin-embedded sections.**

Paraffin-embedded tissue was cut at 3 µm thick sections using the microtome. Slides were dried overnight at 60 °C. Sections were rinsed in 100% Xylene for three times 5 min, in ethanol 100% 2 times for 3 min, 3 min in ethanol 90%, 3 min in ethanol 80%, 3 min in ethanol 70% and 3 min in PBS. Antigen retrieval was performed in prewarmed HIER Citrate Buffer (pH=6) at 95 °C for 30 min. Slides were cooled down for 20 min before transferred in PBS. Dako pen was used to draw a hydrophobic barrier around the tissue and slides were washed in PBS. Primary antibody was diluted at the respective concentration in Dako antibody diluent and 200 µL were added per section. Primary antibody was incubated overnight at 4 °C. Slides were washed three times for 5 min in PBS. Secondary antibody and DAPI was diluted in Dako antibody diluent at indicated concentrations and incubated on the slides for 1 h. Slides were washed three times for 5 min in PBS. Before mounting with DAKO fluorescent mounting medium slides were shortly rinsed in H<sub>2</sub>O. Slides were air dried overnight and stored at 4 °C.

### **4.2.6 Image acquisition and analysis**

#### **4.2.6.1 Brightfield images**

Brightfield images were taken with Zeiss Axio Vert. A1 using a 10x/0,25 LD A-Plan objective. Data were not compressed during acquisition. Images were processed using Image J software.

#### **4.2.6.2 Image acquisition and processing of routine histology stainings**

Images of H&E stainings were acquired by Nikon Eclipse Ni-E Microscope using a 10x/0.45 plan apochromat objective. Data were not compressed during acquisition. Images were processed using NIS-Elements software.

#### **4.2.6.3 Confocal microscopy**

Fluorescent stainings were imaged with a TCS SP5 DS laser scanning spectral confocal microscope using a HCX PL APO CS 20.0x0.70 IMM DRY or HCX PL APO CS 40.0x1.30 OIL UV objective. Excitation wavelengths were set to 488, 543 and 633 nm, respectively. Emission maxima for Alexa Fluor 488, Cy3 and Alexa Fluor 647 conjugates were detected at 518, 570

and 673 nm respectively. For each sample at least three representative areas were chosen, and images were acquired in a sequential mode. Image processing was performed by Image J software.

#### **4.2.6.4 Image analysis with Image J**

Marker expression was quantified using Image J. Color thresholds were set in relation to the fluorescent area applying manual and auto thresholding. The lower threshold was adjusted to represent the positive signal and the total positive area was measured. For each animal at least three representative images were analyzed and the mean positive area was calculated. The mean positive area of sections of Knockout animals was normalized to the mean positive area of control animals on the same slide.

To quantify signal inside and outside the metastatic area, the metastatic area was marked manually using DAPI or tyrosinase related protein 2 (TRP2) as a reference of the metastatic area. As described before thresholding was applied and the areas positive for marker expression inside and outside the metastatic area were calculated and measured as area fraction. To measure the double positive area of two overlapping fluorescent signals, single channel images were subtracted from each other after applying thresholding and area inside the metastasis was measured. To measure the total vessel area inside the metastatic area, single channel images of endothelial markers were added to each other upon setting the threshold, and the total intratumoral vessel area was measured. Last, the percentage of a certain marker expression was set in relation to the total intratumoral vessel area.

#### **4.2.7 Statistical analysis**

Statistical analyses and graphical displays were performed with GraphPad Prism9.5 software. If data met the criteria of normality an unpaired, two-tailed t-test was applied for statistical analysis. Otherwise, or when indicated a Mann Whitney U test was used. Differences between data sets with  $p \leq 0.05$  were considered statistically significant.

## 5. Results

### 5.1 Murine Melanoma cell lines differ in their hepatic metastatic efficiency.

Malignant melanoma is a heterogenic disease differing in the underlying driver mutations, but also in clinical and phenotypic features. So far, tumor intrinsic factors driving hepatic colonization of malignant melanoma have not been analyzed in detail. Also models of liver metastasis of malignant melanoma are rare. Therefore, five different murine melanoma cell lines, with different underlying driver mutations (Figure 6 A-E), were compared in a model of intrasplenic injection in their efficiency to form macroscopically visible metastases in the liver.

For liver colonization experiments, cells were harvested in the exponential growth phase at 50% - 60% confluence (Figure 6 A-E). Interestingly, WT31 cells were the most pigmented ones, visible by a deep black cell pellet in cell culture, whereas the other four cell lines showed a bright cell pellet.

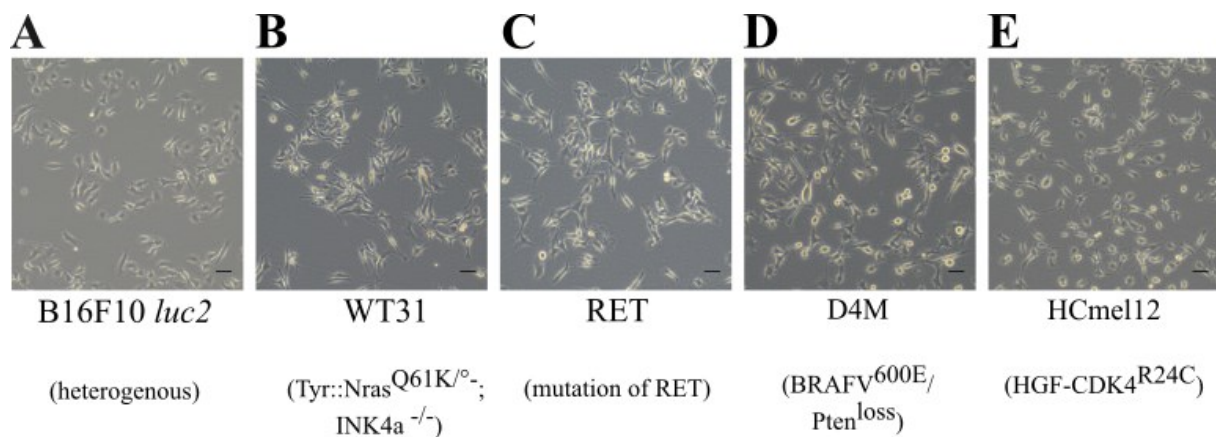


**Figure 6 Melanoma cell lines.** Representative brightfield images of the five different murine melanoma cell lines in exponential growth phase in cell culture. A) B16F10 *luc2* B) WT31 C) RET D) D4M and E) HCmel12. Scale bar = 100  $\mu$ m, n = 5

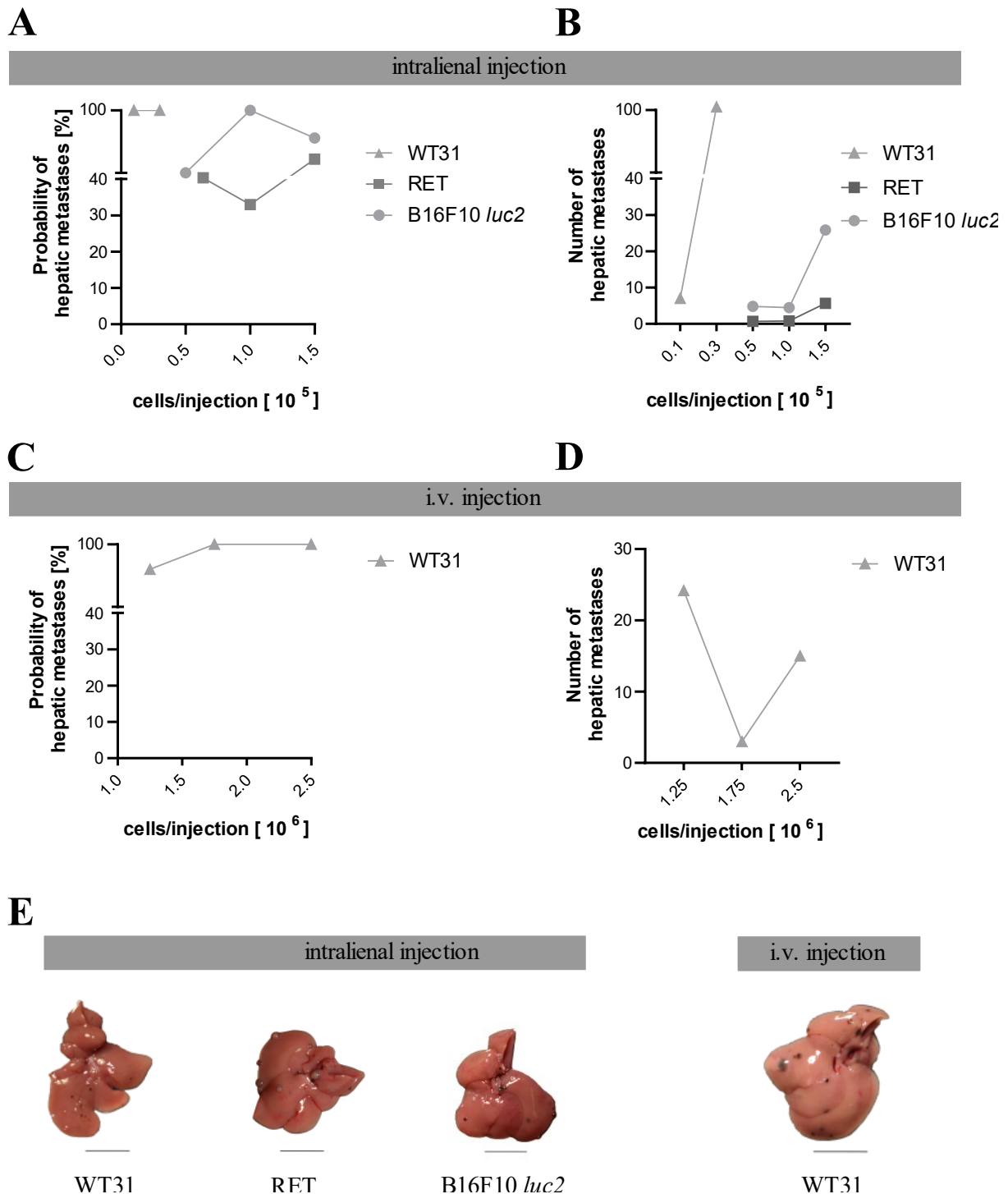


**Figure 7 Metastatic efficiency and number of hepatic metastases of melanoma cell lines.** A) RET and B16F10 *luc2* cells were injected into the spleen at doses of 50000, 100000 and 150000 cells/injection. WT31 cells were injected into the spleen at doses of 10000 and 30000 cells/injection. Injections were performed by Bianca Dietsch, Christof Dormann, Céline Weller, and Dr. Sebastian Wohlfeil. Animals were sacrificed at day 14 or 21. A pooled analysis of the two timepoints is presented. Livers were screened for macroscopically visible metastases. Percentage of animals with macroscopically visible hepatic nodules are shown. B) Hepatic nodules were counted and mean numbers of hepatic nodules/animal at the indicated doses of injection is shown. C) WT31 cells were injected into the tail vein at doses of 1.5 million, 1.75 million and 2.5 million cells/injection. Intravenous injections were

*performed by Dr. Sebastian Wohlfeil. At the highest doses 100% of the analyzed animals showed hepatic nodules. N ≥ 6. D) Macroscopically visible hepatic nodules were counted after i. v. injection of WT31 cells at the indicated doses. Mean numbers of hepatic nodules/animals are shown. E) Representative images of livers upon intralial injection or i. v. injection with macroscopically visible metastatic nodules. Scale bar = 1cm. Data published [293] and modified. <https://creativecommons.org/licenses/by/4.0/>*

After intrasplenic injection, the five different murine melanoma cell lines showed a high variability in the efficiency of colonizing the liver. WT31 cells showed the highest efficiency of liver colonization and intrasplenic injection of WT31 cells led to the formation of liver metastases in 100% of analyzed animals even at low concentrations of 10.000 and 30.000 cells/animal. B16F10 *luc2* cells and RET cells showed an intermediate efficiency of liver colonization. Injection of B16F10 *luc2* cells led to the formation of macroscopically visible liver metastases in all analyzed animals at an intermediate dose of 100.000 B16F10 *luc2* cells/animal. Injection of RET cells resulted in liver metastasis in 50% of animals upon injection of the highest dose of 150.000 cells/animal. Hcmel12 cells and D4M3.A cells did only yield metastasis upon very high doses of injection (data not shown, [293]).

Intralial injections of B16F10 *luc2* cells were performed by Dr. Sebastian Wohlfeil. Intralial injections of WT31 cells were performed by Dr. Sebastian Wohlfeil and Bianca Dietsch. Intralial injections of RET cells were performed by Dr. Sebastian Wohlfeil, Céline Weller, Bianca Dietsch and Christof Dormann. I prepared cell lines and animals for surgery and assisted during the surgery.

Cell lines not only differed in their metastatic efficiency but also in numbers of hepatic metastasis. Macroscopically, black or grey round tumor nodules were observed on the liver surface of mice injected with WT31, B16F10 *luc2* or RET cells. Visible tumor nodules of WT31, B16F10 *luc2* and RET derived hepatic metastases were counted by hand and quantified. The high metastatic melanoma cell line WT31 yielded highest numbers of metastatic foci/liver with a mean of 100 metastatic foci/liver upon injection of 30.000 cells. The mean number of metastatic foci for B16F10 *luc2* cells was 25 foci/liver and the mean number of metastatic foci for RET cells was 8 metastatic foci/liver upon injection of the highest dose of 150.000 cells/animal.

Further, WT31 cells have been reported to yield liver metastasis upon injection into the tail vein [275]. Therefore, WT31 cells were injected into the tail vein at doses of 1.25, 1.75 and 2.5 million cells/injection. At the highest doses of 1.75 and 2.5 million cells 100% of animals showed metastatic foci in the liver. Usually, several metastatic foci were observed per animal, with a mean of 16 metastatic lesions per animal upon injection of 2.5 million cells into the tail vein. Besides hepatic colonization, metastatic foci were observed at other organs. 100% of

analyzed animals showed metastases in the lung upon tail vein injection. Additionally, in decreasing frequency macroscopically visible metastases were detected in kidney, bones, adipose tissue, spleen, ovary, and brain (table 6).

**Table 6. Metastatic sites upon WT31 tail vein injection.** 2.5 million of WT31 cells were injected into the tail vein. After 19 days animals were sacrificed and scanned for hepatic and extrahepatic metastases. 100% of animals showed metastases of lung and liver. Other sites of metastasis with decreasing frequency were kidney, bones, adipose tissue, spleen, ovary and brain. N = 12

<b>Metastatic sites</b>	<b>Percentage of animals with macroscopically visible metastases</b>
<b>Lung</b>	100
<b>Liver</b>	100
<b>Kidney</b>	85.71
<b>Bones</b>	28.57
<b>Adipose tissue</b>	14.29
<b>Spleen</b>	14.29
<b>Ovary</b>	14.29
<b>Brain</b>	12.5

Besides their differences in the underlying driver mutations, murine melanoma cell lines differ in their ability to colonize the liver and grow out to form macroscopically visible hepatic metastases. The analyzed murine melanoma cell lines can be categorized into three groups according to their metastatic efficiency. WT31 cells have a high metastatic capacity leading to hepatic metastases upon tail vein injection. B16F10 *luc2* and RET cells have an intermediate metastatic capacity and D4M.3A and HCmel12 have a low metastatic capacity, not yielding hepatic metastases at the indicated doses in this study.

## **5.2 Histomorphological analysis of hepatic metastases of WT31, B16F10 *luc2* and RET cells.**

Next, the histopathological growth pattern of the hepatic metastasis of WT31, B16F10 *luc2* and RET cells was analyzed by H&E staining (Figure 8 A-C). In all three cell lines a pushing type growth pattern with fast and suppressing growth without a desmoplastic rim was identified. Melanoma cells grow in a bulk and the hepatic tissue is pushed away, resulting in a brick-like formation of hepatocytes.

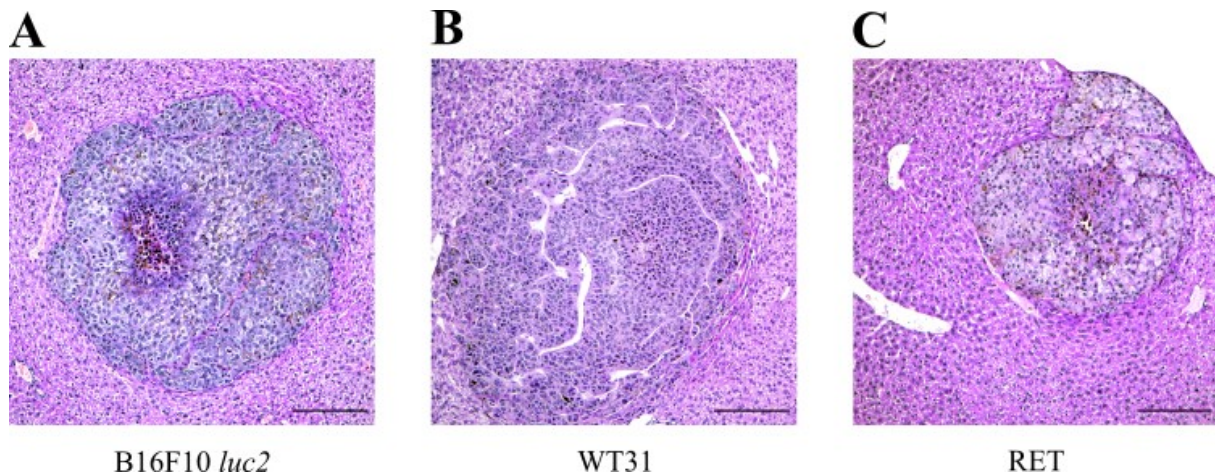


**Figure 8 Histopathological analysis of hepatic metastases.** H&E staining of hepatic metastases of A) B16F10 *luc2*, B) WT31 and C) RET cells were analyzed by H&E-Stainings. Histomorphological all three cell lines show a pushing type growth pattern. Scale bar = 200  $\mu$ m; n  $\geq$  5. Data published [293] and modified. <https://creativecommons.org/licenses/by/4.0/>

### 5.3 Hepatic metastases differ in their vascular density but share a common endothelial expression profile on intratumoral blood vessels.

Metastases of the pushing type growth pattern rely on neo-angiogenesis for supply with nutrients and oxygen [162]. Therefore, I analyzed the vascularization density and protein expression of intratumoral blood vessels of the hepatic metastasis of B16F10 *luc2*, RET and WT31 metastases.

Vascular density was analyzed by immunofluorescence staining of endomucin, Lyve-1 and TRP2. Endomucin is a marker expressed by continuous endothelium, whereas Lyve-1 is a classical LSEC marker. TRP2 is an enzyme of melanin biosynthesis and highly expressed in melanocytes and was used as a marker of melanoma cells. Total vessel area in the metastases defined as positive immunofluorescence signal of Lyve-1, endomucin or co-expression of the two markers was quantified and normalized to the metastatic area. The metastatic area was marked by hand using TRP2 to clearly identify the metastatic border.

Hepatic metastases derived from WT31 cells showed significantly more intratumoral vascularization (11.8% total vessel area in the metastases) than RET (6.7% total vessel area in the metastases) and B16F10 *luc2* (4.9% total vessel area in the metastases) metastases, which were only poorly vascularized (Figure 9 A).

Further, intratumoral blood vessels were almost exclusively positive for endomucin and Lyve-1 was only weakly expressed or absent in the intratumoral vasculature. Therefore, the expression of Lyve-1, endomucin and co-expression of Lyve-1 and endomucin in intratumoral

blood vessels was quantified. Between the three cell lines, slight differences in the expression pattern were observed. In B16F10 *luc2* and WT31 derived metastases almost 80% of intratumoral blood vessels expressed exclusively endomucin and only a small fraction of 10% (B16F10 *luc2*) to 18% (WT31) was exclusively positive for Lyve-1 expression. In RET metastases a larger fraction of double-positive intratumoral blood vessels (29%) was detected, whereas 53% of intratumoral blood vessels were exclusively positive for endomucin and a small fraction of blood vessels (18%) showed single expression of Lyve-1 (Figure 9 C).

As expression of endomucin is associated with continuous endothelium, I hypothesized that intratumoral blood vessels show phenotypic characteristics of a continuous endothelium. To prove this hypothesis, intratumoral endothelium was further analyzed by immunofluorescence stainings of tissue sections.

Next, the endothelial markers CD32b and CD31 were stained. CD32b is highly expressed on pericentral LSEC, whereas CD31 is a marker of continuous endothelium [294]. Quantification showed that in all three cell lines intratumoral blood vessels expressed almost exclusively CD31 (90% B16F10 *luc2*, 90% RET and 96% WT31 single expression of CD31 on intratumoral blood vessels), whereas expression of CD32b (<10% of intratumoral blood vessels) was almost absent, supporting the hypothesis (Figure 9 B and D).

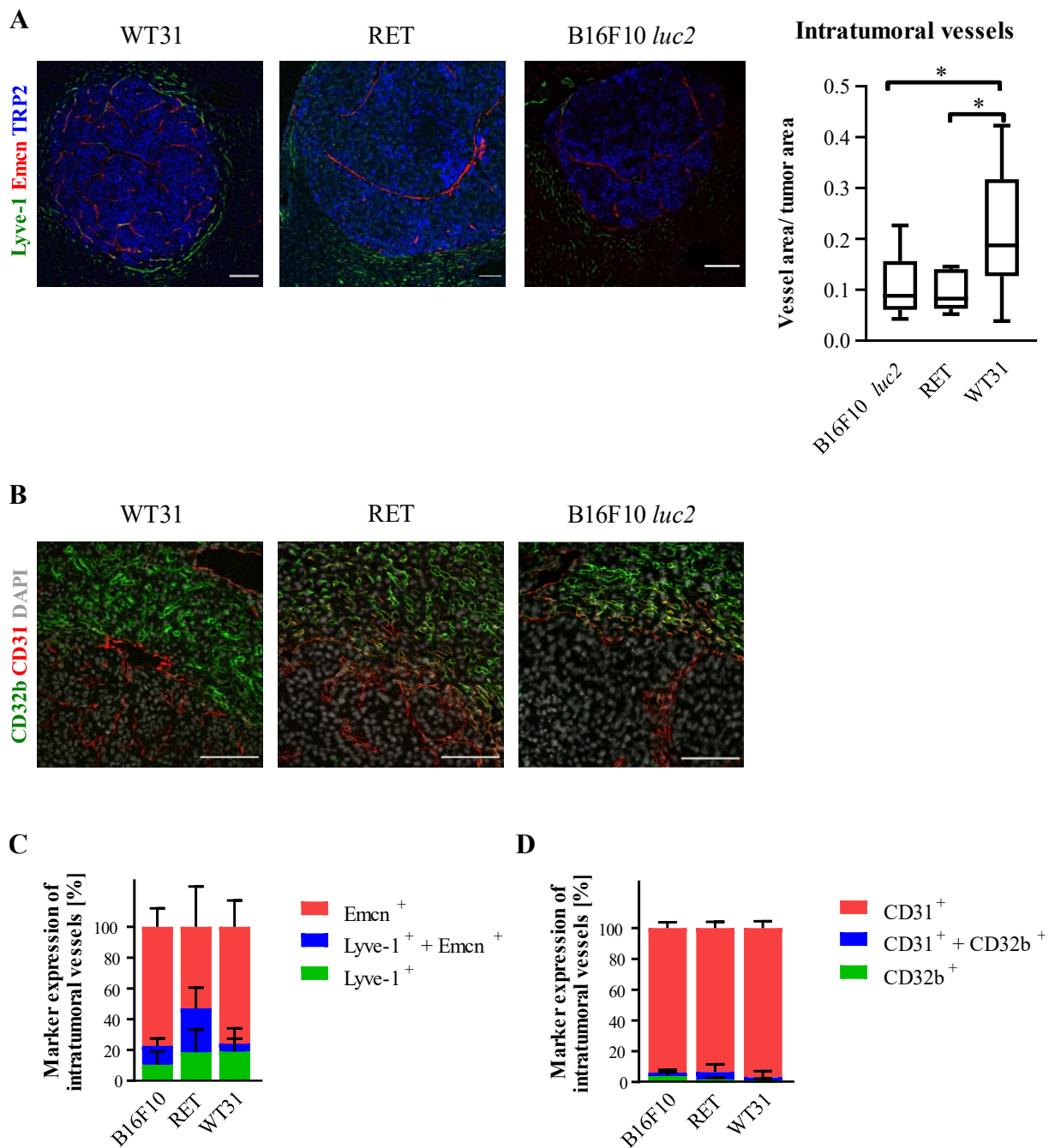


**Figure 9 Immunofluorescence staining of intratumoral blood vessels.** A) Endothelial cells were stained by Lyve-1 and Emcn. Melanoma cells of hepatic metastases were stained by TRP2. Intratumoral vessel area, defined as endomucin-positive, Lyve-1-positive or double-positive area was calculated and normalized to metastatic area marked by TRP2 positive area. Scale bar = 100  $\mu$ m. B) Immunofluorescence stainings of CD32b, CD31 and DAPI of hepatic sections with metastasis of WT31, RET and B16F10 *luc2* cells. Scale bar = 100  $\mu$ m. C) Quantification of Emcn-positive, Lyve-1-positive and Lyve-1 + Emcn-positive intratumoral blood vessels. D) Quantification of CD31-positive, CD32b-positive and CD31+CD32b-positive intratumoral blood vessels. Data published [293] and modified. <https://creativecommons.org/licenses/by/4.0/>

To further characterize the intratumoral endothelium immunofluorescence stainings of stabilin 2 and VE-Cadherin were performed. Stabilin 2 is a scavenger receptor highly expressed by LSEC. Intratumoral blood vessels, showed a weak expression of stabilin 2 and mainly in blood vessels located at the outer border of the metastases (Figure 10 A).

VE-Cadherin is highly expressed in adherens junctions of epithelial cells and a marker of vascular integrity. Intratumoral blood vessels showed a strong expression of VE-Cadherin (Figure 10 B) indicating increased stability of adherens junctions in intratumoral blood vessels.

Another hallmark of LSEC is the possession of fenestrations. Caveolin-1 is a structural protein of LSEC fenestrations. It has been shown that during CCL-4 induced defenestration and sinusoidal capillarization caveolin-1 is degraded [295]. Caveolin-1 was co-stained with podocalyxin, which is broadly expressed on vascular endothelium. In tumor endothelial cells of WT31 and B16F10 *luc2* cells expression of caveolin-1 was almost absent, whereas in metastases derived from RET cells caveolin-1 expression was observed in tumor endothelial cells at the tumor edge (Figure 10 C).

Next, pericyte coverage was analyzed by immunofluorescence staining of Desmin, which is expressed by hepatic stellate cells, that are located in the space of Disse. There were no differences in Desmin-positive peri-endothelial cells indicating a similar coverage of the tumor endothelium by pericytes in the three analyzed cell lines (Figure 10 D).

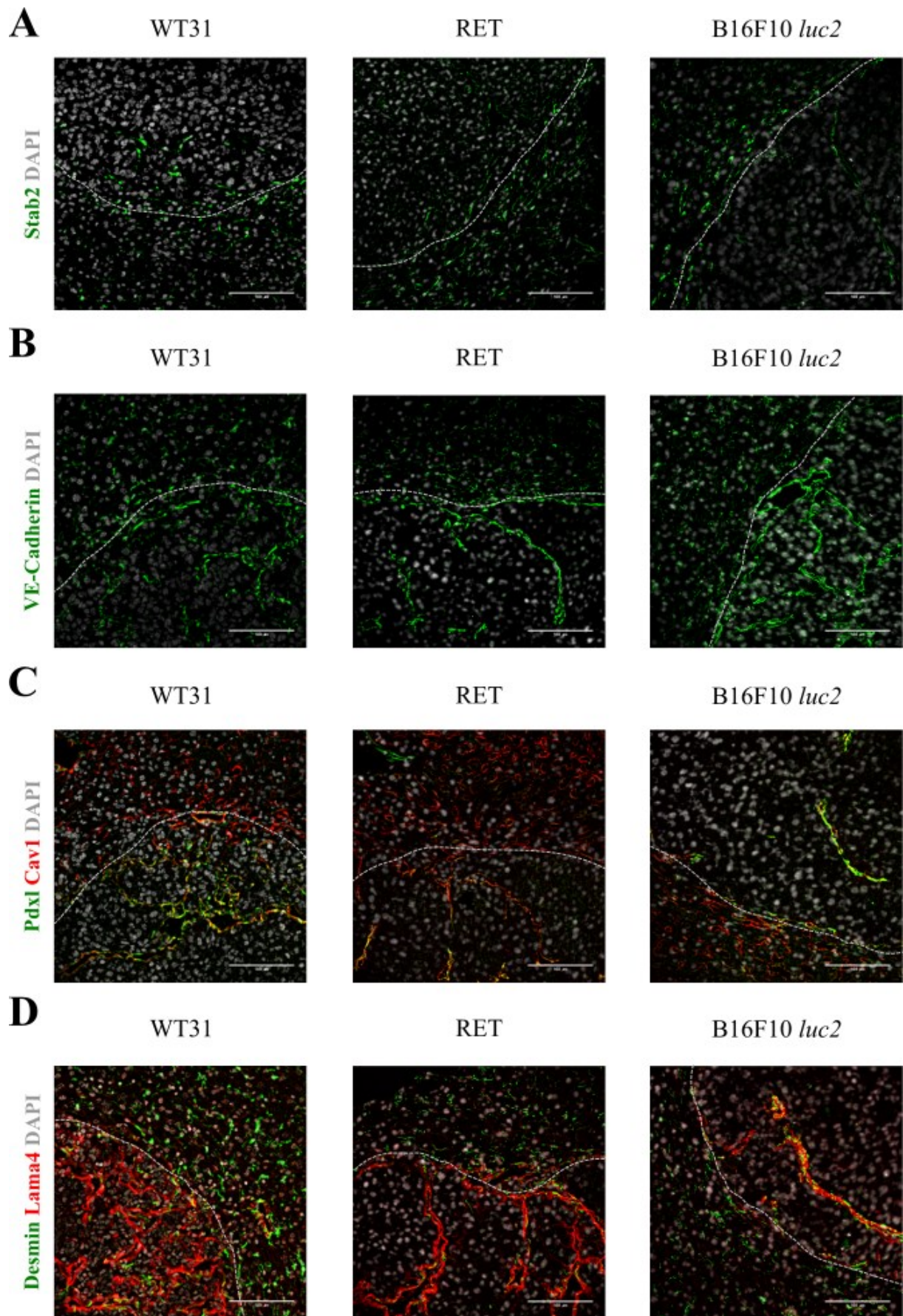


**Figure 10 Immunofluorescence stainings.** A) Immunofluorescence staining of LSEC-specific marker STAB-2 in liver tissue and intratumoral blood vessels of WT31, RET and B16F10 *luc2* derived

*metastases. Scale bar = 100  $\mu$ m. B) Immunofluorescence staining of VE-Cadherin expressed in adherens junctions. Scale bar = 100  $\mu$ m. C) Immunofluorescence staining of Podocalyxin (Pdxl) and Caveolin-1 (Cav1) of hepatic metastases of WT31, RET and B16F10 luc2 cells. Scale bar = 100  $\mu$ m. D) Immunofluorescence staining of Desmin and LAMA4 of hepatic metastases. Scale bar = 100  $\mu$ m.*

Another characteristic of continuous endothelium and dedifferentiation is the subendothelial deposition of extracellular matrix proteins. Therefore, immunofluorescence stainings of extracellular matrix proteins on hepatic metastases of the three cell lines were performed. In all analyzed hepatic metastases of the three different cell lines extracellular matrix proteins surrounding the intratumoral endothelium were markedly increased, as shown by staining of LAMA4 (Figure 10 D), Collagen I (Figure 11 A), Collagen III (Figure 11 B), Collagen IV (Figure 11 C) and Fibronectin (Figure 11 D). Subendothelial deposition of extracellular matrix proteins indicates the formation of a basement membrane.

Interestingly, in hepatic metastases derived from WT31 cells deposition of Collagen IV outside the perivascular space was detected (Figure 11 C). Collagen IV staining appeared sleeve-like indicating the formation of so-called empty sleeves. During blood vessel formation and morphogenesis Collagen IV is deposited early at the basement membrane. Empty sleeves of Collagen IV basement membrane, that are devoid of endothelial cells are a marker of vessel instability and may be a result of high, but inefficient angiogenic activity.

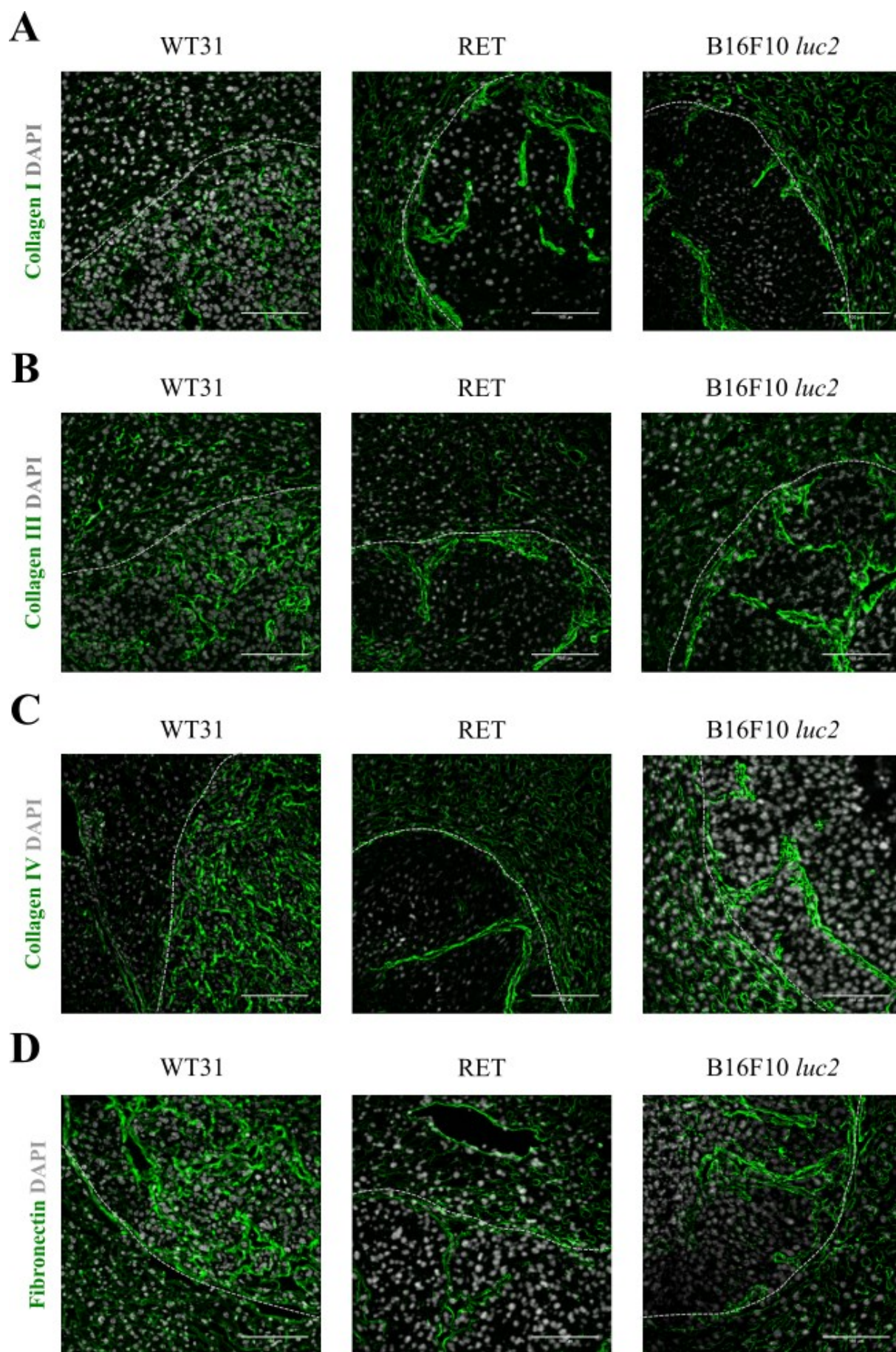


**Figure 11 Immunofluorescence staining of extracellular matrix proteins.** A) Immunofluorescence staining of Collagen I. Scale bar = 100  $\mu\text{m}$ . B) Immunofluorescence staining of Collagen III. Scale bar = 100  $\mu\text{m}$ . C) Immunofluorescence staining of Collagen IV. Scale bar = 100  $\mu\text{m}$ . D) Immunofluorescence staining of Fibronectin. Scale bar = 100  $\mu\text{m}$ . Nuclei stained by DAPI. Data of B published [293] and modified. <https://creativecommons.org/licenses/by/4.0/>

Overall, these observations support the hypothesis that intratumoral blood vessels share characteristics of continuous endothelium without fenestrations and the formation of a basement membrane. Expression of markers of fully differentiated LSEC were almost absent in tumor endothelial cells or only observed at endothelial cells close to the metastatic edge. Remarkably, all three types of hepatic metastases of malignant melanoma shared common characteristics of intratumoral endothelial cells and showed the same phenotype of the tumor vasculature.

#### **5.4 RNA sequencing of melanoma cell lines**

For further molecular and mechanistic insight into pathways and processes that influence the metastatic efficiency of melanoma metastasis to the liver, all five melanoma cell lines were analyzed by RNA sequencing. Melanoma cells were prepared *in vitro* following the same protocol that was used for cell preparation for tumor experiments. Cells were harvested at 50-60% confluence and RNA was isolated.

Therefore, RNA sequencing analysis reflects the original cell state, that cells obtained before being injected into the animals. For further analysis, the five murine melanoma cell lines were divided into two groups. WT31, RET and B16F10 *luc2* cells were grouped as melanoma cell lines with a high or intermediate metastatic efficiency (referred to as HIM-melanoma) and compared to cell lines with low metastatic efficiency, comprising D4M3.A and HCmel12 cells (referred to as LM-melanoma). In a first step of analysis, significant genes with the same direction of regulation among HIM-melanoma cell lines were identified. Thereby commonly regulated genes and pathways among HIM-melanoma cell lines were selected. This gene set was first compared to the LM-melanoma cell line D4M3.A, identifying a set of 6386 significantly regulated genes. Secondly, this analysis was repeated with the LM-melanoma cell line HCmel12 as reference and 4249 significantly regulated genes in relation to commonly regulated genes of HIM-melanoma were identified (Figure 12 A). The two gene sets of 6386 genes with D4M3.A as reference cell line and 4249 genes with HCmel12 as reference cell line were matched and 1995 commonly regulated genes of HIM-melanoma in comparison to LM-melanoma were identified (Figure 12 B). RNA sequencing analysis was performed by Dr. Sebastian Wohlfeil and Dr. Carsten Sticht.

This resulting gene set was further analyzed by an over-representation analysis (ORA) of gene ontology biological processes (GOBP) or HALLMARK pathways (Figure 12 C and D).

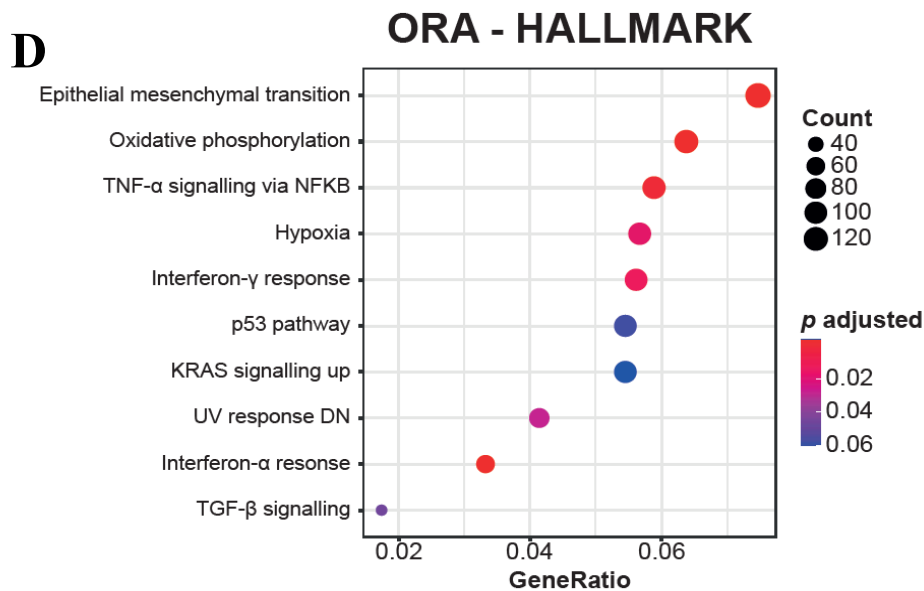
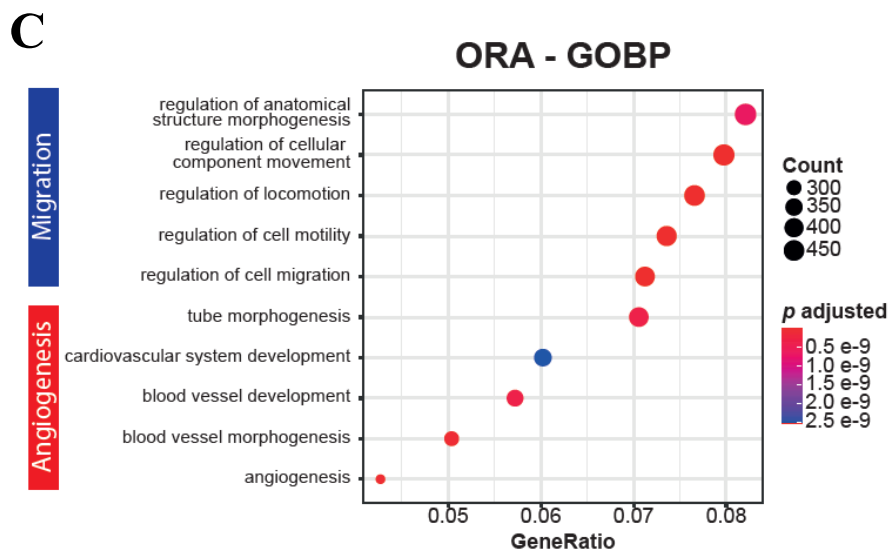
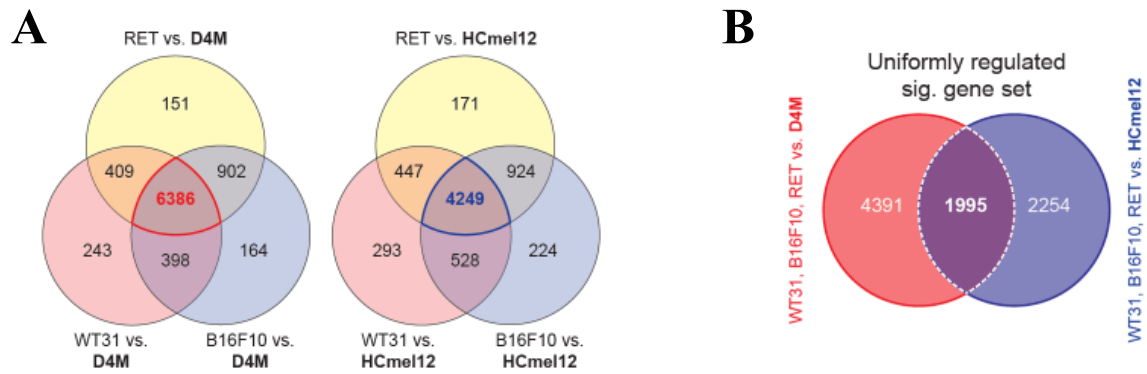


**Figure 12 RNA sequencing analysis.** RNA was isolated from sub-confluent cells and analyzed by RNA-sequencing.  $N = 5$  for each cell line. A) Venn diagram of uniformly regulated significant genes of RET (yellow), WT31 (red) or B16F10 luc2 (blue) in comparison to D4M3.A and Venn diagram of

*commonly regulated significant genes of RET (yellow), WT31 (red) or B16F10 (blue) in comparison to HcMel12 melanoma. B) Venn diagram of the identified gene sets of commonly regulated significant genes of B16F10 luc2, RET and WT31 in relation to D4M3.A (red) and commonly regulated significant genes of B16F10 luc2, RET and WT31 in relation to HcMel12 (blue). Overlay of these 2 gene sets results in a set of 1995 significant genes which are uniformly regulated in HIM-Melanoma in comparison to LM-Melanoma. C) Overall representation analysis of the previously identified gene set of gene ontology biological processes (GOBP). Number of regulated genes by count, gene ratio and adjusted p-value of corresponding pathways displayed by dot plot. D) Overall representation analysis of the previously identified gene set of HALLMARK pathways. Number of regulated genes by count, gene ratio and adjusted p-value of corresponding pathways displayed by dot plot. RNA sequencing analysis was performed by Dr. Carsten Sticht and Dr. Sebastian Wohlfeil. Data published [293]. <https://creativecommons.org/licenses/by/4.0/>*

GOBP analysis revealed that the processes involved in cell migration or angiogenesis were significantly regulated. Further, gene enrichment analysis of HALLMARK pathways identified among others significant regulation of EMT, oxidative phosphorylation, and TNF $\alpha$ -signaling.

## **5.5 Summary**

In the first part of my PhD project, the metastatic efficiency of five murine melanoma cell lines, that differed in their genetic background was compared. Three of the five analyzed cell lines showed a high or intermediate metastatic efficiency and were subject to further analysis. Histological analysis showed a pushing type growth pattern of hepatic metastases. Hepatic metastasis of the three analyzed cell lines differed in vascular density, but the tumor vasculature shared a common expression profile of endothelial markers. In general, intratumoral blood vessels showed strong expression of markers associated with continuous endothelium and in line with that peri-endothelial deposition of extracellular matrix proteins was observed, indicating the formation of a basement membrane. More molecular insight was gained by RNA sequencing and comparison of HIM-melanoma cell lines with LM- melanoma cell lines. Especially, processes of cell migration and angiogenesis were significantly regulated.

## **5.6 Hepatic melanoma metastasis in genetically modified mice overexpressing the notch1 intracellular domain in LSEC.**

Next, the established and characterized models of hepatic melanoma metastasis were used to study the role of notch signaling in hepatic metastases. It has been shown that lung metastasis is promoted by endothelial overexpression of notch [173], whereas non selective, global notch inhibition promoted liver metastases [172]. Therefore, hepatic metastasis was studied in a model of EC subtype-specific overexpression of notch signaling.

## 5.7 Generation of NICD<sup>OE-HEC</sup> mice

To study the influence of endothelial notch signaling in an organ-specific manner Clec4g-CRE<sup>tg/wt</sup> mice were crossed to Rosa26<sup>N1ICD\_IRES\_GFP</sup> mice. Clec4g is a gene expressed by hepatic EC but absent in vascular endothelial cells of most other organs. Reporter activity of Clec4g-CRE has been shown to start from day E13.5 in hepatic endothelial cells [289]. Clec4g was used as a promoter to drive cre expression and combined with Rosa26<sup>N1ICD\_IRES\_GFP</sup> mice that express a constitutively active Notch1 intracellular domain. The resulting NICD<sup>OE-HEC</sup> mice were viable, and genotypes were distributed as expected by mendelian laws (Figure 13 A). Expression of nuclear enhanced GFP was confirmed in HEC by immunofluorescence staining, whereas all other cells in the liver were negative (Figure 13 B), leading to the conclusion that the intracellular domain of notch1 is overexpressed in hepatic endothelial cells.

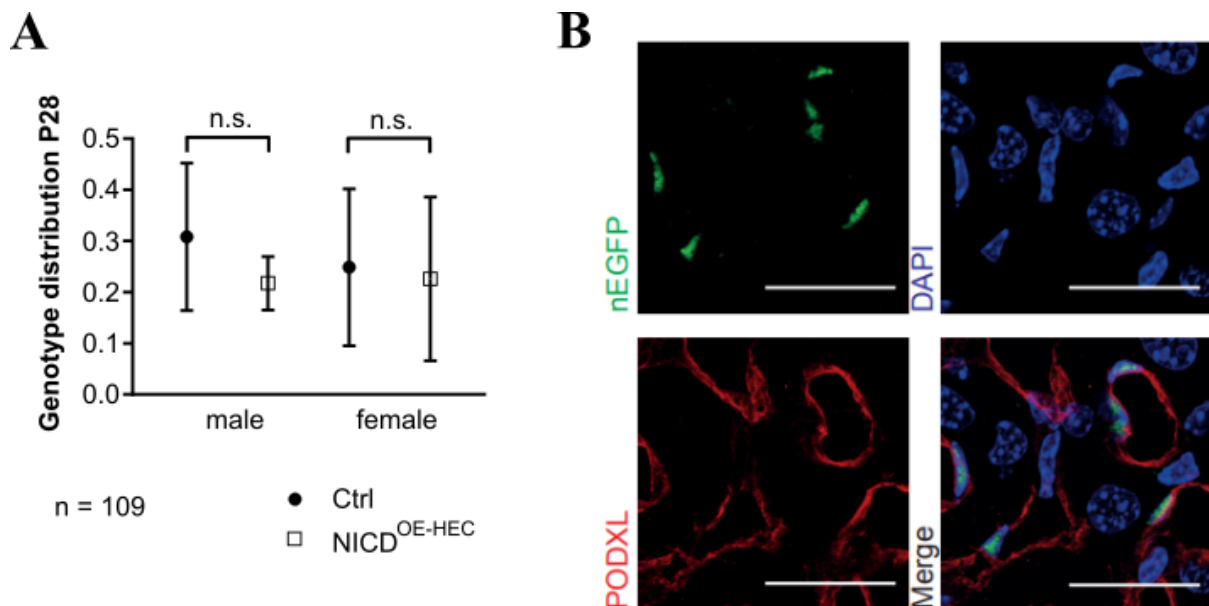


**Figure 13** Generation of Clec4g-Cre<sup>tg/wt</sup>;Rosa26<sup>N1ICD-IRES-GFP</sup> (NICD<sup>OE-HEC</sup>) and verification of endothelial Cre activity. A) Genotype distribution of offspring (male and female) of Clec4g-Cre<sup>tg/wt</sup> x Rosa26<sup>N1ICD-IRES-GFP</sup> at P28 is displayed. Ctrl and NICD<sup>OE-HEC</sup> mice are distributed according to mendelian laws. N = 109. B) Immunofluorescence staining of nEGFP and Podocalyxin (PODXL) in the liver. nEGFP staining is restricted to podocalyxin-positive cells and co-localizes with nuclei (DAPI) leading to the conclusion that Cre-activity is restricted to endothelial cells in the liver. Scale bar = 25 μm; n = 5. Data published [289] and modified.

## 5.8 Hepatic endothelial activation of NICD protects from liver metastasis.

To study the influence of notch signaling on hepatic metastases B16F10 *luc2* cells were injected in the spleen. Spleen injection was performed by Dr. Sebastian Wohlfeil. The number of hepatic metastases was counted after 14 days and the metastatic burden was measured by bioluminescence imaging. NICD<sup>OE-HEC</sup> animals showed a significant reduction of liver metastases in comparison to control mice (Figure 14 A). Indeed, none of the injected

NICD<sup>OE-HEC</sup> animals showed macroscopically visible metastatic nodules in the liver. In line with that, bioluminescence measurement showed a significant reduction of metastatic burden in NICD<sup>OE-HEC</sup> mice (Figure 14 A). Surprisingly, NICD<sup>OE-HEC</sup> animals showed metastatic nodules in the lungs, whereas control animals had no tumors in the lungs. The significant increase in metastatic nodules in the lung of NICD<sup>OE-HEC</sup> animals was also confirmed by bioluminescence measurement (Figure 14 B).

To validate these results, WT31 cells were injected into the tail vein of WT and NICD<sup>OE-HEC</sup> animals at a dose of 2.5 million cells per animal. Intravenous injections were performed by Dr. Sebastian Wohlfeil. Macroscopically visible metastatic nodules in the liver were counted after 19 days and a significant reduction of hepatic metastases in NICD<sup>OE-HEC</sup> mice was observed (Figure 14 C).

Besides melanoma, also colon carcinoma shows metastatic tropism of the liver [153]. To analyze if the observed effect was melanoma-specific, experiments were repeated with a second tumor entity. The colon carcinoma cell line Mc38 was injected into the spleen by Dr. Sebastian Wohlfeil at a dose of 150.000 cells per animal to induce hepatic metastases. Again, metastatic nodules were counted after 21 days and a significant reduction of hepatic metastases in NICD<sup>OE-HEC</sup> mice was observed (Figure 14 D).

Overall, overexpression of NICD in the hepatic endothelium protects from hepatic metastases, not only in two models of malignant melanoma, but also in one model of colorectal carcinoma.

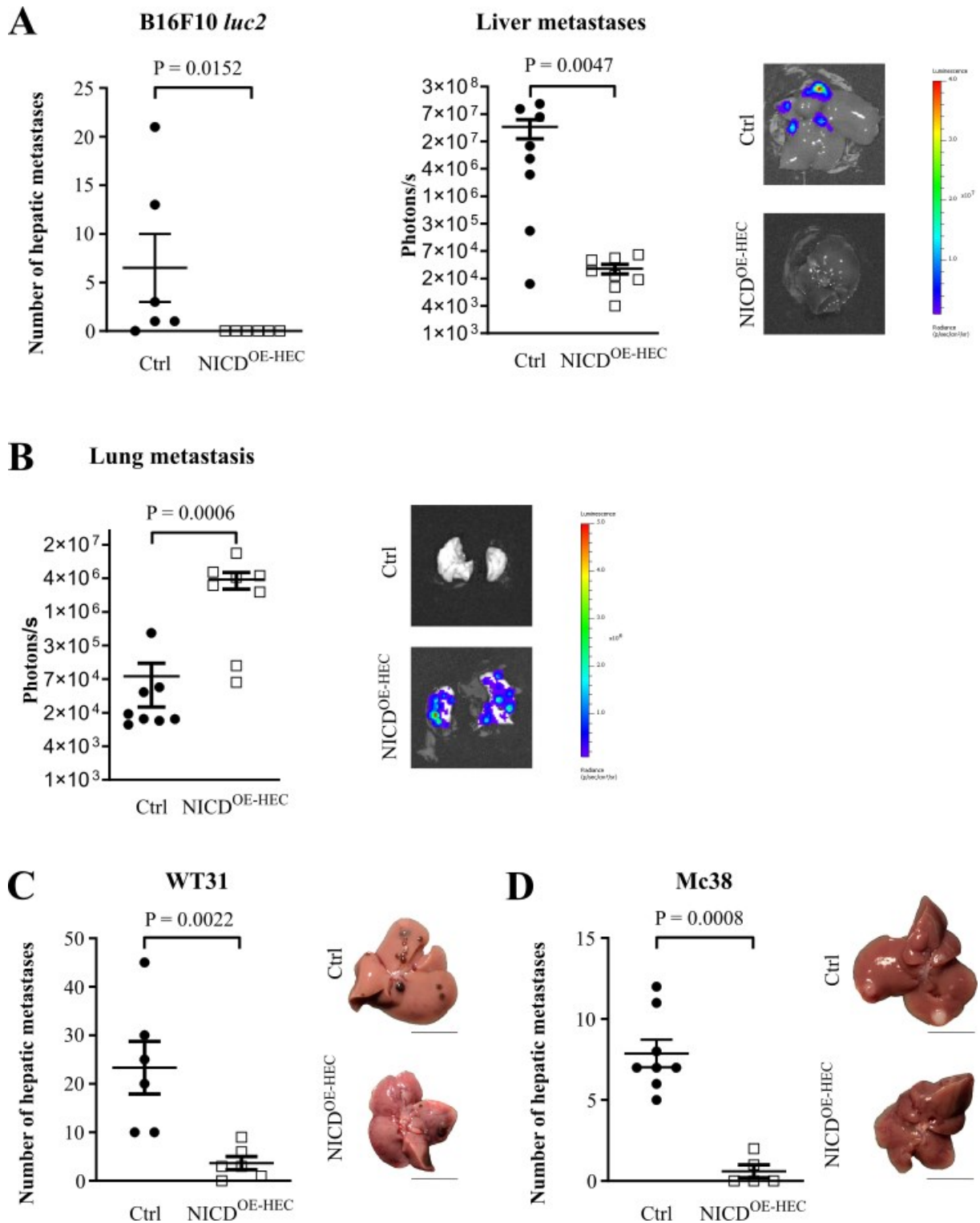


**Figure 14 Hepatic endothelial notch activation protects from metastasis.** A) 150000 B16F10 *luc2* cells were injected into the spleen. Mice were sacrificed after 14 days and macroscopical visible hepatic metastases were counted (left-hand side) and quantified ex vivo by bioluminescence (right-hand side). NICD<sup>OE-HEC</sup> mice showed significantly less hepatic metastases.  $N = 6$  per group;  $p = 0.0152$  (macroscopic count) and  $p = 0.0047$  (bioluminescence quantification). B) Quantification with bioluminescence of lung metastasis ex vivo. NICD<sup>OE-HEC</sup> mice showed significantly more metastases in the lung 14 days upon injection of B16F10 *luc2* cells.  $N = 6$  per group;  $p = 0.0006$ . C) Macroscopic count

of hepatic metastases upon injection of 2.5 million WT31 cells into the tail vein. Mice were sacrificed after 19 days, livers isolated and macroscopically visible metastases were counted.  $NICD^{OE-HEC}$  mice had significantly less hepatic metastases in comparison to control animals.  $N = 6$  per group,  $P = 0.0022$ . Macroscopic photographs of livers *ex vivo*. Scale bar = 1 cm. D) Macroscopic count of hepatic metastases 21 days after injection of 150000 Mc38 cells into the spleen and representative photographs of livers *ex vivo*.  $NICD^{OE-HEC}$  mice showed significantly less hepatic metastases.  $N = 8$  (ctrl) vs 5 ( $NICD^{OE-HEC}$ ),  $p = 0.0008$ , scale bar = 1 cm. Liver colonization experiments were jointly done with Dr. Sebastian Wohlfeil. Data published [289] and modified.

## 5.9 Phenotypic characterization of adult $NICD^{OE-HEC}$ mice

To understand the mechanism of protection from liver metastasis I studied  $NICD^{OE-HEC}$  mice in more detail. Phenotypically mutant mice appeared normal and total body weight was not altered (Figure 15 A). Internal organs were assessed by a macroscopic screening. Brain, kidney, and lungs of  $NICD^{OE-HEC}$  mice did not show obvious alterations (Figure 15 E). However, livers of  $NICD^{OE-HEC}$  mice showed slightly dilated vessels on the surface (Figure 15 C) and liver/body weight ratio was significantly reduced in mutant mice (Figure 15 B). Further,  $NICD^{OE-HEC}$  mice showed a moderate increase in spleen/body weight ratio and lung/body weight ratio (Figure 15 D) and a significant increase in heart/body weight ratio (Figure 15 F).

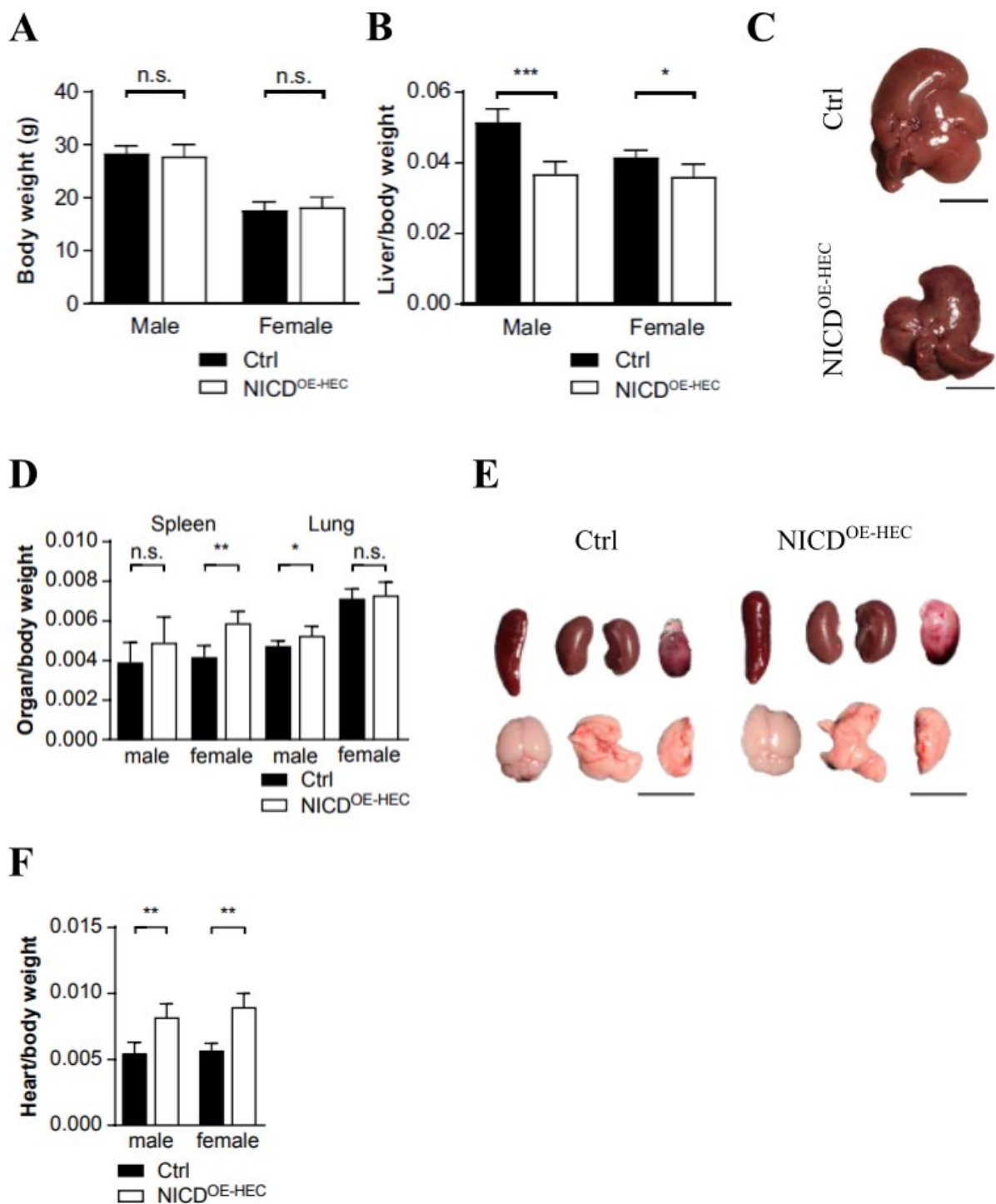


**Figure 15 Characterization of adult NICD<sup>OE-HEC</sup> mice.** A) Total body weight of male and female NICD<sup>OE-HEC</sup> and Ctrl mice. There was no difference between NICD<sup>OE-HEC</sup> and control mice in body weight. Male:  $n = 8$  per group, female:  $n = 13$  per group. B) Liver/body weight ratio was significantly reduced in male and female NICD<sup>OE-HEC</sup> mice. Male:  $n = 8$  per group, female:  $n = 13$  per group. C) Representative photographs of livers ex vivo of Ctrl and NICD<sup>OE-HEC</sup> mice. Scale bar = 1 cm,  $n \geq 5$ . D) Spleen/body weight was not altered in male mice but significantly increased in female NICD<sup>OE-HEC</sup> mice. Male:  $n = 8$  per group, female:  $n = 5$  per group. Lung/body weight ratio was increased in male NICD<sup>OE-HEC</sup> mice but not altered in female NICD<sup>OE-HEC</sup> mice. Male:  $n \geq 5$ /group, female:  $n \geq 5$  per group. E) Photographs of spleen, kidney, heart, brain, and lung of NICD<sup>OE-HEC</sup> and Ctrl mice. Scale bar = 1 cm,  $n \geq 5$ . F) Heart/body

weight ratio was significantly increased in male and female  $NICD^{OE-HEC}$  mice. Male:  $n = 4$  per group, female:  $n = 5$  per group. Data published [289] and modified.

The organ function of  $NICD^{OE-HEC}$  mice was further assessed by clinical chemistry. Hepatic enzymes AST, ALT, and GLDH were not altered in the blood of  $NICD^{OE-HEC}$  mice, indicating normal liver function (Figure 16 A-C). However, cholinesterase synthesis was altered in  $NICD^{OE-HEC}$  mice and CHE was significantly increased in blood of  $NICD^{OE-HEC}$  mice (Figure 16 D), whereas blood cholesterol was significantly reduced in  $NICD^{OE-HEC}$  mice (Figure 16 E).

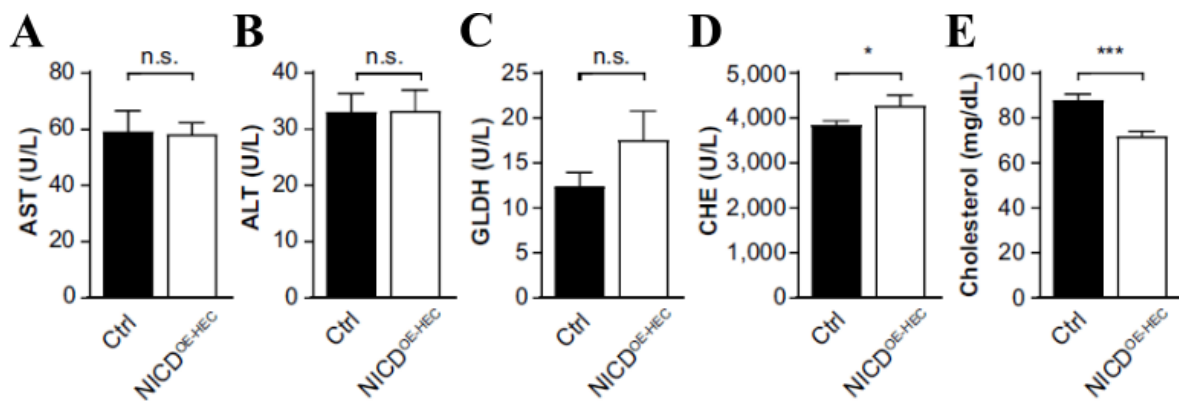


**Figure 16 Plasma analysis of 8-week-old mice after 4 hours of fasting.** A-C) Hepatic enzymes AST, ALT and GLDH were not altered in  $NICD^{OE-HEC}$  mice.  $N = 14-18$  animals per group, mean values represented. D) Cholinesterase (CHE) was significantly increased in  $NICD^{OE-HEC}$  mice.  $N = 14-18$  animals per group, mean values represented. E) Plasma cholesterol levels were significantly reduced in  $NICD^{OE-HEC}$  mice.  $N = 14-18$  animals per group, mean values represented. Experiments were jointly done with Hiltrud Schönhaber and the help of lab technicians of the ZMF. Data published [289] and modified.

### 5.10 Characterization of the hepatic endothelium of $NICD^{OE-HEC}$ mice

The first line of defense that the tumor cells encounter upon entering the capillary bed of the liver is formed by the hepatic endothelium. Therefore, the liver endothelium of  $NICD^{OE-HEC}$  mice was studied in more detail.

To characterize the liver endothelium, immunofluorescence stainings of the classical LSEC markers Lyve-1, stabilin 2 and CD32b and immunofluorescence staining of markers of continuous endothelium, namely CD31 and Emcn (Figure 17 A-B) were performed. Additionally, the endothelial marker podocalyxin (Pdxl) was used to stain the liver endothelium (Figure 17 A). Quantification of immunofluorescence staining showed that the expression of the markers associated with continuous endothelium (CD31 and Emcn) was significantly

increased in the livers of  $NICD^{OE-HEC}$  mice (Figure 17 C). Markers expressed in fully differentiated LSEC, such as Stablin2 and CD32b showed a reduced expression in  $NICD^{OE-HEC}$  livers, whereas Lyve-1 expression, another classical LSEC marker, was increased in  $NICD^{OE-HEC}$  livers (Figure 17 C). The pan-endothelial marker Pdxl was not altered in  $NICD^{OE-HEC}$  mice (Figure 17 C).

These results indicate that  $NICD^{OE-HEC}$  livers show a form of dedifferentiation of the hepatic endothelium.

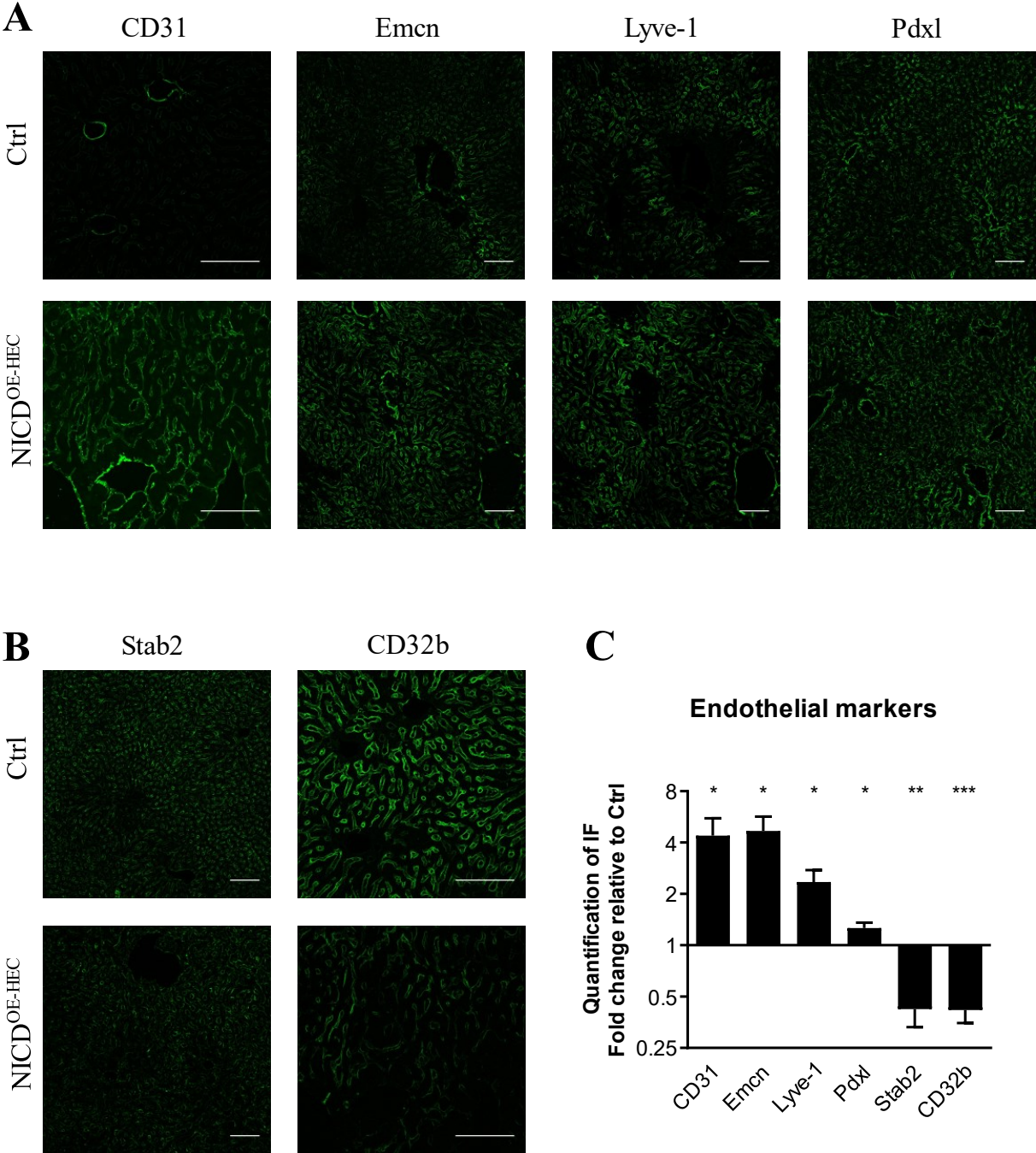


**Figure 17 Analysis of endothelial zonation of  $NICD^{OE-HEC}$  mice.** A) Immunofluorescence staining of endothelial proteins, CD31, Emcn, Lyve-1, and Pdxl of liver tissue of  $NICD^{OE-HEC}$  and Ctrl mice.

Scale bar = 100 $\mu$ m, n = 5. B) Immunofluorescence staining of Stab2 and CD32b of liver tissue of NICD<sup>OE-HEC</sup> and Ctrl mice. Scale bar = 100  $\mu$ m, n = 5. C) Quantification of immunofluorescence of NICD<sup>OE-HEC</sup>. Y-Axis represents logarithmic fold change in relation to ctrl (ctrl set to 1). CD31 (p = 0.0434), Emcn (p = 0.0080), Lyve-1 (p = 0.0295) and Pdx1 (p = 0.498) expression is increased in NICD<sup>OE-HEC</sup> mice. Expression of Stab2 (p = 0.0031) and CD32b (p < 0.0001) is reduced in NICD<sup>OE-HEC</sup> mice. \*, p < 0.05, \*\*, p < 0.01; \*\*\*, p < 0.001, one-sample t test used for statistical analysis. Data published [289] and modified.

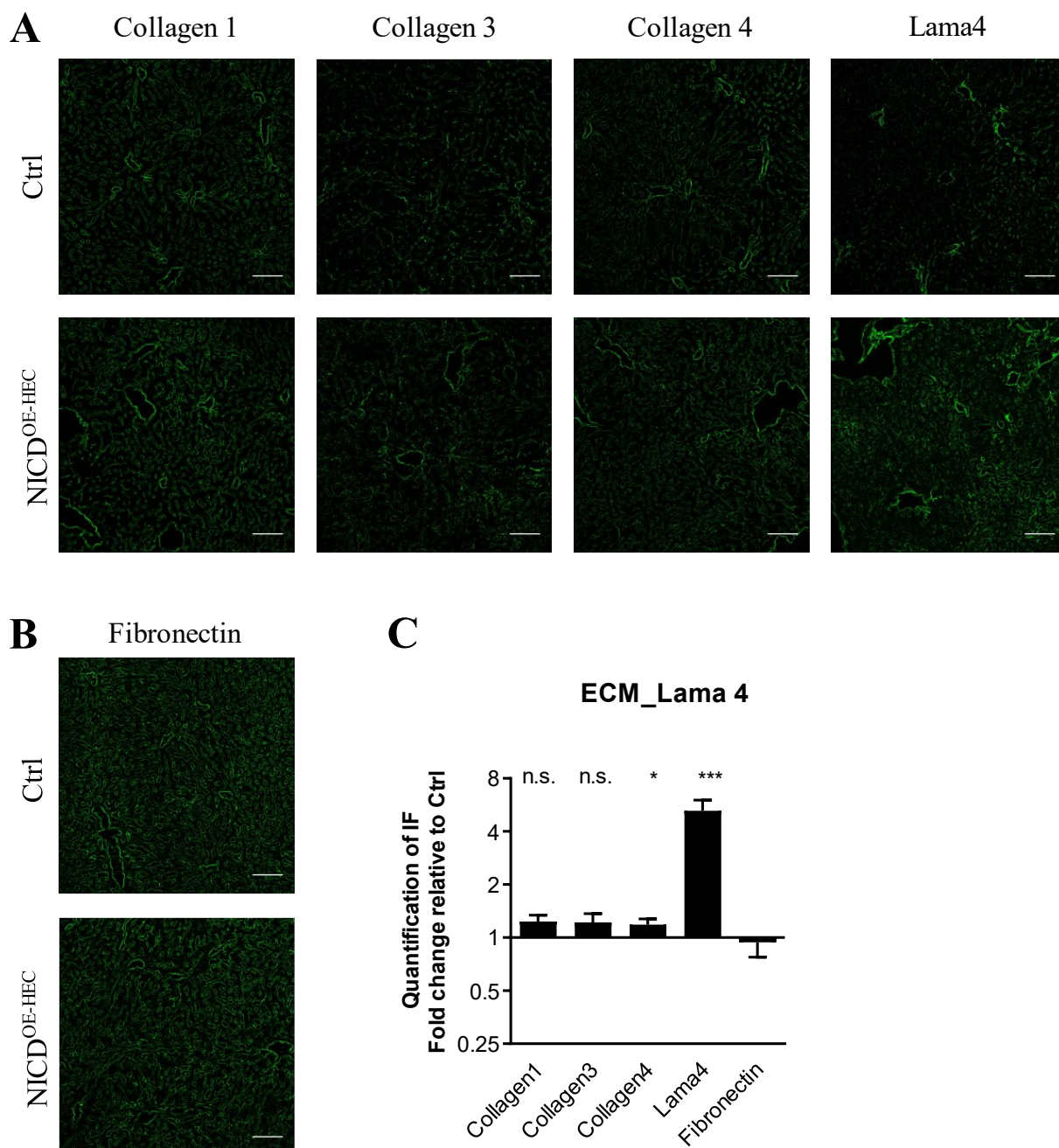


**Figure 18 Immunofluorescence staining of extracellular matrix proteins.** A) Immunofluorescence staining of Collagen I, Collagen III, Collagen IV and Lama4 in frozen liver sections of NICD<sup>OE-HEC</sup> mice and controls. Scale bars = 100  $\mu$ m, n = 5. B) Immunofluorescence staining of Fibronectin on frozen liver tissue of NICD<sup>OE-HEC</sup> and ctrl mice. Scale bars = 100  $\mu$ m, n = 5. C) Quantification of immunofluorescence of NICD<sup>OE-HEC</sup> mice. Y-Axis represents logarithmic fold change in relation to ctrl (ctrl set to 1). Expression of Collagen I, Collagen III, Collagen IV and Fibronectin is not altered in NICD<sup>OE-HEC</sup> mice. Lama4 ( $p = 0.0056$ ) expression is increased in NICD<sup>OE-HEC</sup> mice. \*,  $p < 0.05$ ; \*\*,  $p < 0.01$ ; \*\*\*,  $p < 0.001$ , one-sample  $t$  test used for statistical analysis. Data published [289] and modified.

Another hallmark associated with dedifferentiation of LSEC is the deposition of extracellular matrix proteins. Therefore, immunofluorescence staining of extracellular matrix proteins such as Collagen I, Collagen III, Collagen IV, Lama4, and Fibronectin in the livers of NICD<sup>OE-HEC</sup> and control mice were performed (Figure 18 A-B).

Quantification showed that Lama4 expression was increased in livers of NICD<sup>OE-HEC</sup> mice, whereas the expression of the extracellular matrix proteins Collagen I, Collagen III, Collagen IV and Fibronectin was not altered (Figure 18 C).

Increased deposition of extracellular matrix proteins is often associated with an activation of hepatic stellate cells. Therefore, hepatic stellate cells were analyzed by immunofluorescence staining of Desmin (Figure 19 A). In NICD<sup>OE-HEC</sup> mice Desmin expression was not significantly altered in comparison to control animals (Figure 19 B), indicating that hepatic stellate cells were not activated.

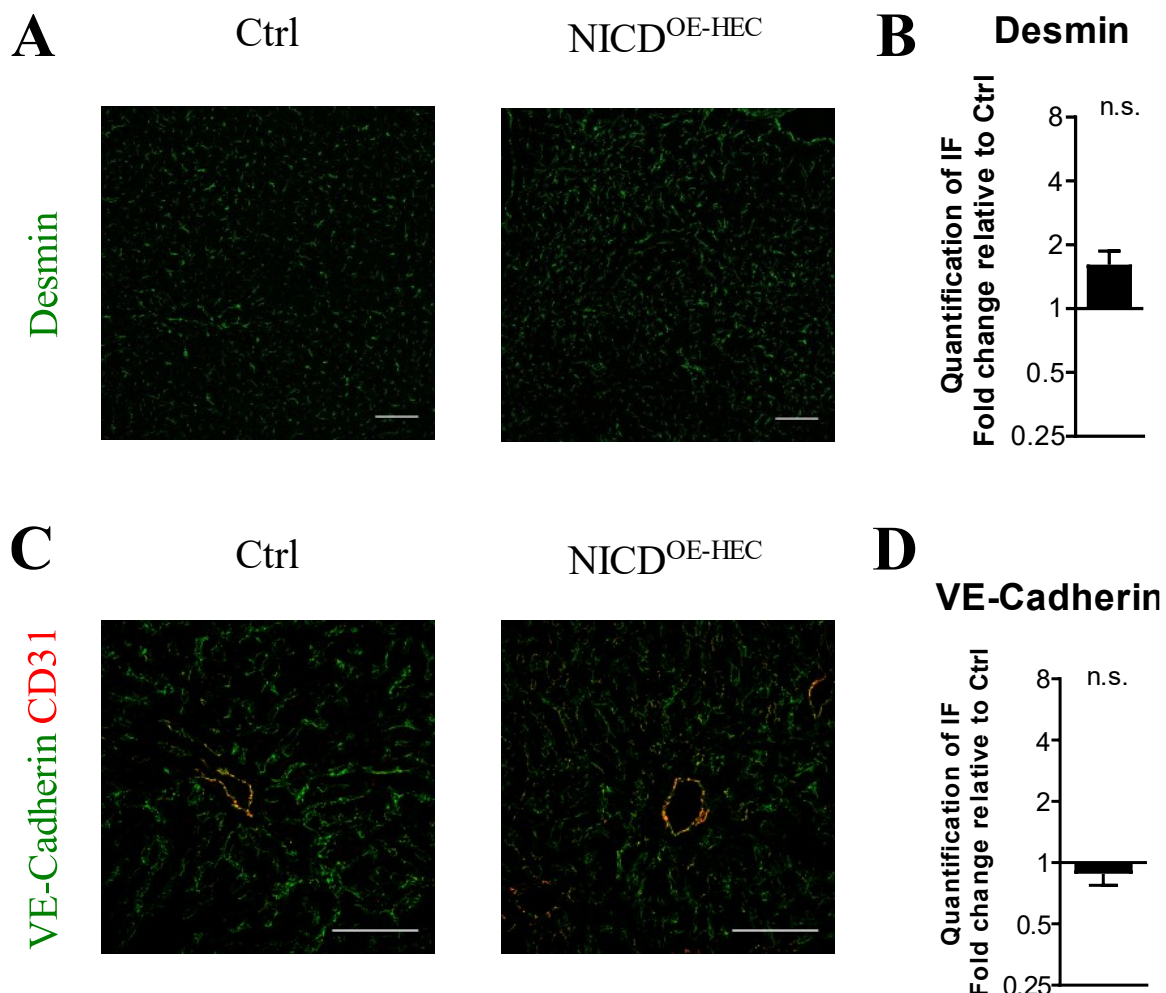


**Figure 19 Immunofluorescence staining of hepatic stellate cells and VE-Cadherin.** A) Immunofluorescence staining of Desmin in liver tissue sections of Ctrl and NICD<sup>OE-HEC</sup> mice. Scale bar = 100  $\mu$ m, n = 5. B) Quantification of Immunofluorescence staining of desmin. Y-Axis shows fold change relative to ctrl on a logarithmic scale (ctrl set to 1). Desmin expression is not significantly

increased in  $NICD^{OE-HEC}$  mice ( $P = 0.0741$ ) C) Immunofluorescence staining of VE-Cadherin on liver tissue of Ctrl and  $NICD^{OE-HEC}$  mice. Scale bar = 100  $\mu m$ ,  $n = 5$ . D) Quantification of immunofluorescence staining of VE-Cadherin shows no difference in  $NICD^{OE-HEC}$  and Ctrl mice. Y-Axis shows fold change relative to ctrl on a logarithmic scale (ctrl set to 1). One-sample  $t$  test used for statistical analysis. Data published [289] and modified.

Finally, endothelial integrity was analyzed by immunofluorescence staining of VE-Cadherin (Figure 19 C). Quantification of immunofluorescence staining of VE-Cadherin showed that VE-Cadherin expression was not altered in  $NICD^{OE-HEC}$  mice (Figure 19 D).

Overall, an atypical dedifferentiation of LSEC in livers of  $NICD^{OE-HEC}$  mice was observed. This atypical dedifferentiation was marked by the increase of markers associated with continuous endothelium, such as CD31 and Emcn and a decrease of LSEC-associated markers, such as Stab2 and CD32b. Interestingly, Lyve-1 expression was not downregulated, as expected in classical dedifferentiation. In contrast Lyve-1 expression was upregulated in livers of  $NICE^{OE-HEC}$  mice.

However, the observed dedifferentiation of the liver endothelium in  $NICD^{OE-HEC}$  mice is accompanied by an increase in Lama4 expression, whereas hepatic stellate cells are not activated and endothelial integrity through adherens junctions, as marked by the expression of VE-Cadherin is not affected.

### **5.11 Metabolic zonation is impaired in $NICD^{OE-HEC}$ mice.**

As notch1 is downstream of Wnt/ $\beta$ -catenin signaling and notch1 negatively regulates wnt/ $\beta$ -catenin signaling [296], the metabolic zonation of hepatocytes of  $NICD^{OE-HEC}$  mice was assessed. The establishment and maintenance of metabolic zonation strongly depends on canonical wnt signaling and establishment of  $\beta$ -catenin gradients. Glutamine synthetase (Glul), the ammonium transporter Rh B glycoprotein (RhBg) and Cytochrome P450 2E1 (CYP2E1) are expressed in pericentral hepatocytes exclusively, whereas Arginase 1 (Arg1) is expressed by midcentral and periportal hepatocytes.

Therefore, immunofluorescence staining of Glul, Rhbg, CYP2E1 and Arg1 on livers of  $NICD^{OE-HEC}$  and Ctrl mice was performed (Figure 20 A).

In  $NICD^{OE-HEC}$  mice a significant reduction in the expression of pericentral genes (Glul, RhBg, CYP2E1) and a significant increase in the expression of Arg1 (Figure 20 B) was observed, indicating disturbed metabolic zonation of the liver and impairment of canonical wnt signaling in  $NICD^{OE-HEC}$  mice.

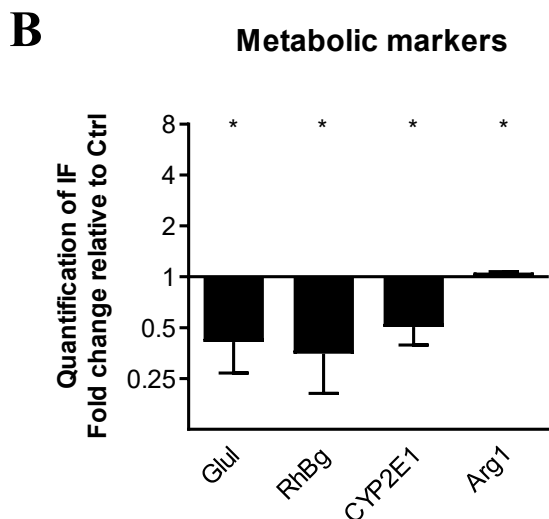
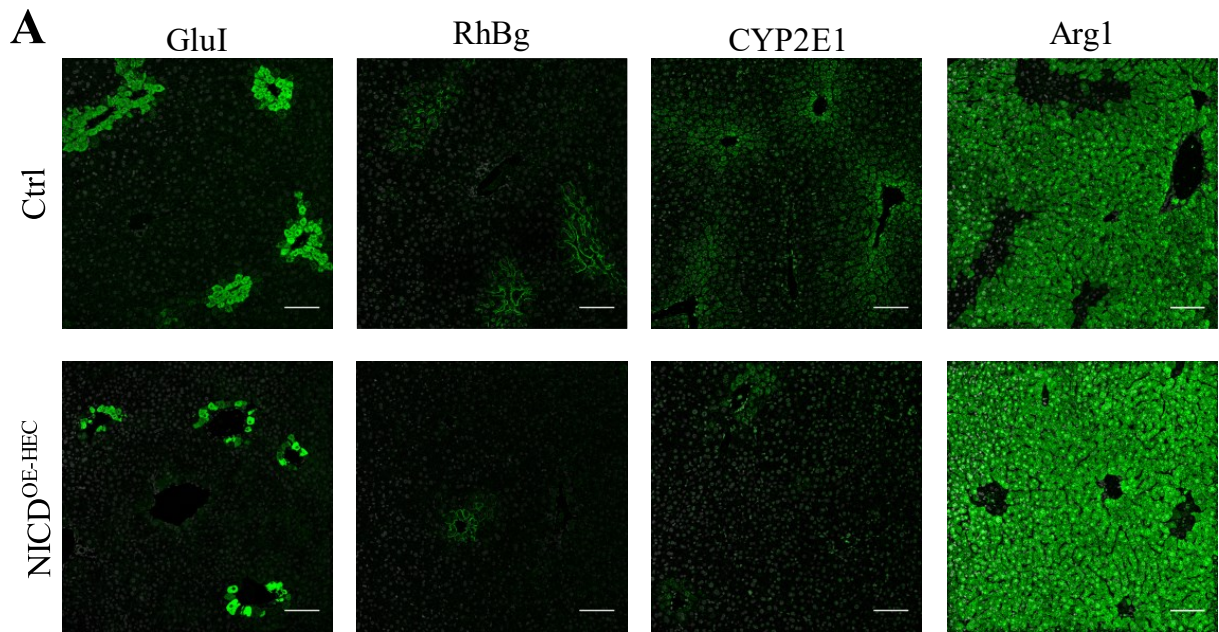


**Figure 20 Metabolic zonation of NICD<sup>OE-HEC</sup> mice.** A) Immunofluorescence staining for Glul, RhBg, CYP2E1 and Arg1 on liver tissue of NICD<sup>OE-HEC</sup> and Ctrl mice. Scale bars = 100  $\mu$ m, n = 5. B) Quantification of metabolic markers. Y-Axis shows fold change relative to ctrl on a logarithmic scale (ctrl set to 1). Glul ( $p = 0.0249$ ), RhBg ( $p = 0.0116$ ) and CYP2E1 ( $p = 0.0202$ ) expression is decreased in NICD<sup>OE-HEC</sup> mice, whereas expression of Arg 1 ( $p = 0.0203$ ) was reduced in NICD<sup>OE-HEC</sup> mice. One-sample  $t$  test used for statistical analysis. Data published [289] and modified.

### 5.12 Metastatic susceptibility is not altered in WLS<sup>HEC-KO</sup> mice.

Impairment of metabolic zonation and alterations of the angiocrine wnt/ $\beta$ -catenin axis might alter metastatic susceptibility of NICD<sup>OE-HEC</sup> mice. To validate this hypothesis metastatic

susceptibility of the liver was studied in  $Wls^{HEC-KO}$  mice.  $Wls^{HEC-KO}$  mice have an endothelial deficiency of the wnt cargo receptor  $Wls$  and show abolished secretion of Wnt ligands in the liver endothelium. Similar to the  $NICD^{OE-HEC}$  mice, metabolic zonation and liver/body weight ratio is altered in  $Wls^{HEC-KO}$  mice [221].

Liver metastasis was studied by the injection of WT31 cells into the tail vein of  $Wls^{HEC-KO}$  mice and quantification of hepatic metastases. Intravenous injection was performed by Dr. Sebastian Wohlfeil. In numbers of hepatic metastases, no difference was observed between control animals and  $Wls^{HEC-KO}$  animals (Figure 21 A-B). This indicates that a deficiency of angiocrine Wnt ligand secretion from HEC and its sequelae such as impaired metabolic zonation and reduced liver size, did not mediate reduced metastatic susceptibility in  $NICD^{OE-HEC}$  mice.

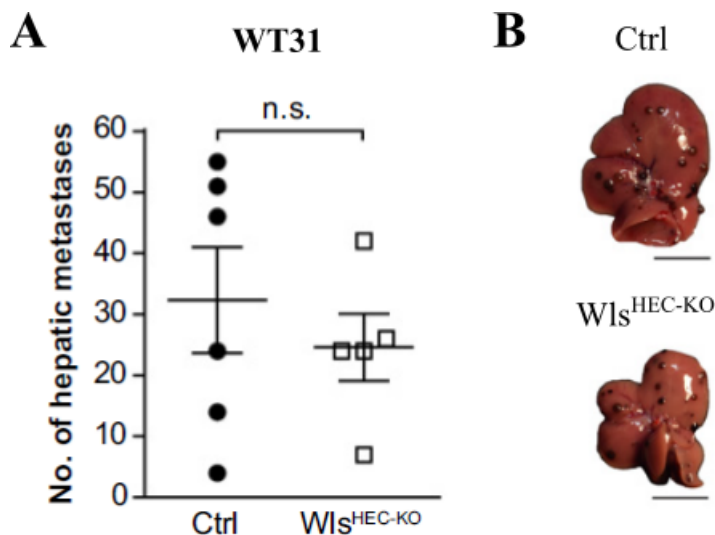


**Figure 21 Metastatic susceptibility of  $Wls^{HEC-KO}$  mice.** A) 2.5 million WT31 melanoma cells were injected into the tail vein of Ctrl and  $Wls^{HEC-KO}$  mice by Dr. Sebastian Wohlfeil. Mice were sacrificed after 19 days and macroscopically visible liver metastases were counted ex vivo. Number of hepatic metastatic foci was not altered in  $Wls^{HEC-KO}$  mice.  $N = 6$  (Ctrl) and  $n = 5$  ( $Wls^{HEC-KO}$ ). B) Representative photographs of livers ex vivo with metastatic foci of Ctrl and  $Wls^{HEC-KO}$  mice. Scale bar = 1cm. Data published [289] and modified.

### 5.13 Expression of adhesion molecules in $NICD^{OE-HEC}$ mice.

Changes in endothelial zonation and metabolic zonation on its own cannot explain the observed phenotype. However, lung colonization in the B16F10 *luc2* model of intrasplenic injection indicated that initial tumor cell adhesion and retention was impaired in  $NICD^{OE-HEC}$  mice.

Therefore, protein expression of some candidates of adhesion molecules, including VCAM1 and ICAM1 were analyzed by immunofluorescence stainings (Figure 22 A). Especially ICAM1 has been well described to mediate adhesion of circulating tumor cells in the liver and has been linked to notch signaling [297].

Quantification of immunofluorescence staining showed an increase in VCAM1 expression in livers of NICD<sup>OE-HEC</sup> mice, but ICAM1 expression was significantly reduced in NICD<sup>OE-HEC</sup> mice (Figure 22 C).

Therefore, reduced expression of ICAM1 in the livers of NICD<sup>OE-HEC</sup> mice might result in reduced adhesion and retention of tumor cells and thereby explain the observed reduced metastatic susceptibility of NICD<sup>OE-HEC</sup> mice.

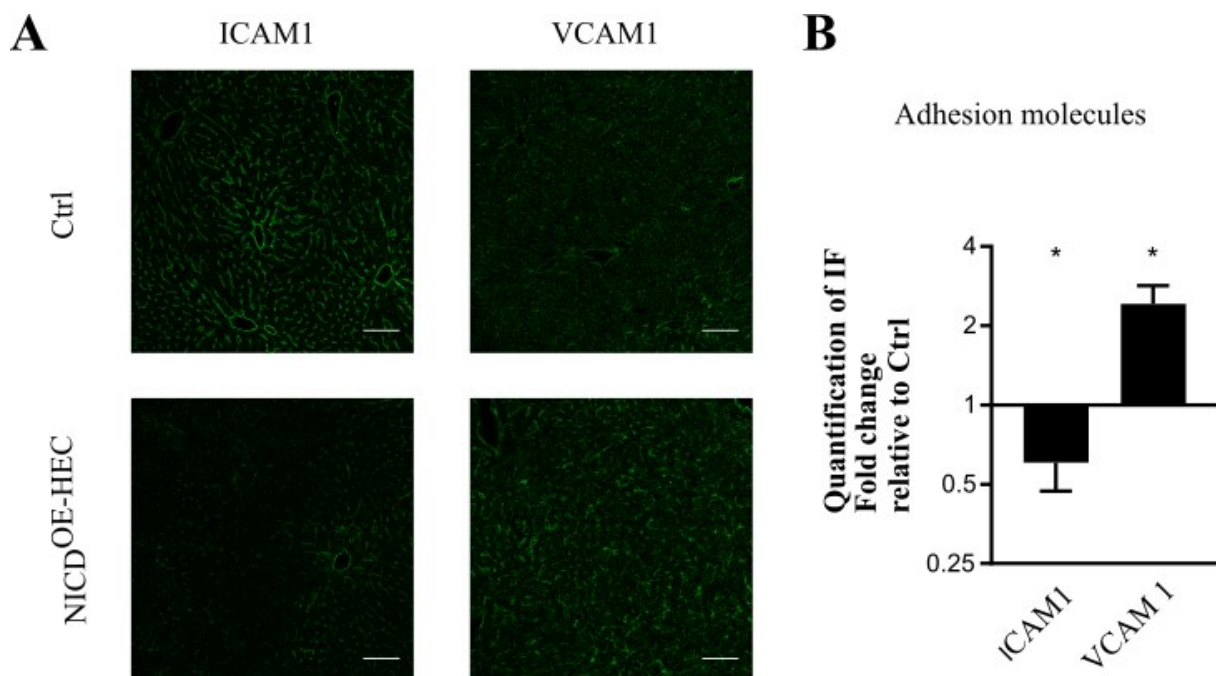


**Figure 22 Immunofluorescence staining of adhesion molecules.** A) Immunofluorescence staining of ICAM1 and VCAM1 on liver tissue of Ctrl and NICD<sup>OE-HEC</sup> mice. Scale bars = 100  $\mu$ m, n = 5. B) Quantification of immunofluorescence intensity of ICAM1 and VCAM1 in livers of Ctrl and NICD<sup>OE-HEC</sup> mice. Y-Axis shows fold change relative to ctrl on a logarithmic scale (ctrl set to 1). ICAM1 expression was significantly reduced in livers of NICD<sup>OE-HEC</sup> mice ( $p = 0.0407$ ), whereas expression of VCAM1 was increased in livers of NICD<sup>OE-HEC</sup> mice ( $p = 0.0289$ ). N = 5. Data published [289] and modified.

## 5.14 Summary

Overexpression of endothelial notch signaling significantly protected from hepatic metastases of malignant melanoma. Further, metastasis of colon carcinoma was significantly reduced in

NICD<sup>OE-HEC</sup> mice. Adult NICD<sup>OE-HEC</sup> mice showed a reduced liver/body weight ratio and dilated vessels on the liver surface. However, clinical chemistry showed no alterations of hepatic enzymes in the blood, despite an increase in blood cholesterol levels and a decrease of cholinesterase. Hepatic endothelium of NICD<sup>OE-HEC</sup> mice showed an atypical dedifferentiation with an increased expression of markers of continuous endothelium and a decreased expression of LSEC markers. Controversially, Lyve-1 expression, which is also a classical LSEC marker was not decreased but increased. Endothelial dedifferentiation was accompanied by deposition of Collagen IV and Lama4. Despite endothelial dedifferentiation also metabolic zonation was altered in NICD<sup>OE-HEC</sup> mice, which is linked to deficiency of wnt signaling. Liver metastasis experiments with WLS<sup>HEC-KO</sup> mice could not link impaired metabolic zonation, reduced liver size and abolished Wnt-signaling to reduced metastatic susceptibility of NICD<sup>OE-HEC</sup> mice. Instead, a significant reduction of the adhesion molecule ICAM1 in livers of NICD<sup>OE-HEC</sup> mice was detected. Overall, the reduced retention of melanoma and colon carcinoma cells in the liver, might be mediated by reduction of ICAM1 expression.

## 5. Discussion

Despite the progress in cancer therapies, hepatic metastasis is still a negative prognostic factor and potentially fatal in tumor progression. Moreover, melanoma patients with hepatic metastasis show a poor response to immunotherapy [69] and targeted therapies [72]. Therefore, studying liver metastasis in preclinical models to identify mechanisms determining organ-specific metastasis are urgently needed.

### 6.1 Mouse models of malignant melanoma

There is only a limited number of genetic mouse models of spontaneous malignant melanoma available and especially hepatic metastasis occur at a very low frequency [279], [298]. To detect statistically significant differences in hepatic metastases high animal numbers would be needed due to the low frequency of hepatic metastasis in models of spontaneous malignant melanoma and is therefore not feasible. Injection of various tumor cells into the spleen, among them melanoma cells, has been shown to result in liver metastases and is an established method to study hepatic colonization [299].

In this study the highest metastatic efficiency of liver colonization was observed by WT31 melanoma cells after intrasplenic injection. Additionally, WT31 melanoma cells also consistently established hepatic metastasis after intravenous injection. Besides hepatic metastases, metastatic nodules were observed in the lung and frequently in other organs, resembling the typical metastatic pattern of cutaneous melanoma. Intravenous and intrasplenic injections are two different techniques that provide reliable results to study hepatic colonization with or without simultaneous colonization of other organs. The WT31 cell line harbors a human NRAS mutation [300]. Mutations of BRAF and NRAS are associated with an increased risk of liver metastasis in humans [301]. However, these driver mutations occur at very high frequencies in malignant melanoma and the association was rather weak. Neither it has been shown that one of these mutations is a major driver of hepatic metastasis. Organotropic metastasis is clearly influenced by the mutational landscape. For example, Kirsten rat sarcoma virus (KRAS) driver mutations were associated with organ-specific brain colonization in malignant melanoma [302]. Tumor-intrinsic properties and the hematogenous route of metastatic spread also influence the metastatic pattern. In a model of NRAS-mutated melanoma, serial passaging over the liver upon intravenous injection resulted in reduced retention in the lung and tumor-intrinsic alterations in pathways linked to cell adhesion [339]. The mutational landscape of malignant melanoma associated with liver metastases remains unclear and has not been analyzed in detail. Hepatotropism of cutaneous melanoma is most likely influenced by several factors, also including non-genetic and epigenetic determinants.

## **6.2 Capillarization of intratumoral blood vessels**

Histopathologically, the analyzed liver metastases in the three models of melanoma showed a pushing type growth pattern. A hallmark of angiogenesis in pushing type liver metastases is the cooperation of smooth muscle actin-positive cells and fusion of partly capillarized sinusoids [303]. Supporting the hypothesis of Paku, in all three analyzed melanoma models supportive connective tissue in the hepatic metastases was visible and a capillarized phenotype of the tumor blood vessels was observed by a strong expression of markers associated with continuous endothelium. Expression of LSEC-specific markers, such as Lyve-1 and CD32b, was almost absent or limited to the intratumoral blood vessels at the metastatic edge. Vascular remodeling is a critical step in tumorigenesis in hepatocellular carcinoma. Alterations in the number and size, as well in maturation of endothelium, occurs early during tumorigenesis [304]. In human and mice transdifferentiation of LSEC to a capillarized phenotype has been described in hepatocellular carcinoma [305]. In line with that, Lyve-1 expression was reported to be absent in the vasculature of hepatocellular carcinomas and liver metastasis of colon carcinoma [306].

## **6.3 Angiogenic processes in liver metastasis**

Metastatic efficiency correlated with the size of metastatic nodules and vascular density, supporting the importance of angiogenic processes in metastatic outgrowth. Without blood supply tumor size is limited to 1-2 mm, the maximal distance oxygen can perfuse [128]. Therefore, once tumor cells are established in their target organ, outgrowth of macro-metastases relies on neo-angiogenesis.

Not only angiogenesis itself, but also vessel maturation is important for sufficient tumor blood supply [307]. In WT31 derived hepatic metastases, so called empty sleeves were observed. Vessel maturation is regulated by vessel pruning and regression. Empty sleeves, as observed in WT31 hepatic metastases by staining of CD31 and Collagen IV are a strong sign of high, but inefficient angiogenic activity accompanied by vessel pruning and regression.

## **6.4 Tumor-intrinsic mechanisms of melanoma metastasis**

To delineate tumor-intrinsic molecular differences the five genetically different murine melanoma cell lines were compared by RNA sequencing. The strongest differences were observed in pathways involved in cell migration, angiogenesis, EMT, oxidative phosphorylation, and TNF $\alpha$  signaling. Cell migration and adhesion are the first steps in colonization of a distant organ. Integrins have been associated with tumor angiogenesis, cell migration, proliferation, and metastasis. Expressed on the melanoma cells surface, integrins play a role in organotropism and promote metastasis [308]–[310]. Integrin  $\alpha$ 4 expression has been associated with increased lymph node metastasis in B16 melanoma [309] but has also been reported to increase tumorigenicity and lymph node metastasis in other malignancies,

including colon cancer, lung cancer, and pancreatic ductal carcinoma [311]. Remarkably, RNA sequencing showed a strong integrin  $\alpha 4$  expression in WT31 cell line, which might contribute to the high metastatic potential of WT31 cells. Further, Integrin  $\alpha 2$  has been associated with enhanced hepatic colonization [308]. However, in this study integrin  $\alpha 2$  was inconsistently expressed among LM- and HIM-melanoma cell lines.

Cell migration and cell adhesion are major determinants of metastatic tropism and are controlled by complex gene sets. It has been shown that gene sets involved in cell adhesion can be predictive for lymph node metastasis [312]. Identifying crucial gene sets of liver metastases in melanoma patients can help to select patients at risk earlier and hence improve their prognosis.

Another differentially regulated process between HIM- and LM-melanoma is angiogenesis. In general angiogenesis facilitates hepatic metastases [313]. In CRC it has been shown that the stromal subtype, with an angiogenic signature showed enhanced liver metastasis [314]. Molecular analysis of liver metastasis and their corresponding primary tumors further supported the critical role of angiogenesis in hepatic metastases of CRC [315].

Anti-angiogenic treatment for example with the anti-VEGF antibody bevacizumab or the multi-kinase-inhibitor Sorafenib disrupts the tumor vasculature [165], [316]. For the investigated model of B16F10 *luc2* liver metastases and WT31 liver metastases it was shown that treatment with Sorafenib results in a pseudocystic degeneration of hepatic metastases [293]. However, clinical trials with anti-angiogenic agents in the treatment of advanced melanoma showed no promising results and were terminated in the early phases [317]. Further, subcutaneous B16 melanoma shows no necrosis or pseudocystic degeneration upon treatment with Sorafenib [318]. Most likely, the microenvironment plays an important role in treatment response and selecting subgroups of patients with hepatic metastases with defined tumor vascularization patterns might be more promising in future clinical trials. In anti-angiogenic treatment of desmoplastic colorectal carcinoma, as well as in anti-angiogenic treatment of B16F10 *luc2* and WT31 melanoma a small rim of viable cells remained upon treatment [293], [319]. Therefore, combination or sequential treatment of anti-angiogenic drugs with standard of care treatment regimens might be necessary to achieve a complete remission in patients with hepatic metastases. In general, anti-angiogenic treatment and its effects on hepatic metastases of malignant melanoma have not been studied in detail so far. Nonetheless, first data shows promising result for future studies.

## **6.5 Tumor-extrinsic mechanisms of hepatic metastasis**

Besides tumor-intrinsic mechanisms the organ microenvironment plays an important role in organ-specific metastasis. Endothelial overexpression of notch signaling protected from

hepatic metastases in the described models of WT31 and B16F10 *luc2* melanoma metastasis, as well as in a model of colorectal carcinoma metastasis. In the past, modulation of notch signaling has been proposed as a therapeutic target in different cancer entities. In hepatocellular carcinoma dysregulated notch signaling has been linked to cancer development [320]. Further, in malignant melanoma notch inhibition suppresses tumor cell growth and treatment efficacy of targeted therapies is enhanced [321]. Endothelial notch signaling has been reported to increase pulmonary metastases in malignant melanoma and lung cancer [173]. However, regarding the liver, global notch inhibition was reported to increase hepatic metastasis [172]. In this study, notch was inhibited pharmacologically resulting in a global, and not cell-type specific depletion of notch signaling. Importantly global notch inhibition might protect from lung metastasis of malignant melanoma [173], but as a disadvantageous side effect the risk of liver metastasis would be enhanced. Therefore, targeting notch signaling as a cancer therapeutic will require more knowledge about organ-specific effects of notch signaling on cancer metastasis.

#### **6.5.1 Clec4g, as an endothelial subtype-specific promoter**

In this study, Clec4g was used as an endothelial subtype-specific driver. Clec4g promoter activity starts on E13.5. Onset of promoter activity is critical for targeting the notch-signaling pathway. Constitutive endothelial activation of notch signaling by expressing NICD under a tie-2 promoter [322] or a stab2 promoter [289], as well as conditional overexpression of Dll4 results in embryonic lethality [323]. Stressing the importance of notch signaling balance during embryonic development also endothelial specific depletion of Notch1 under a tie-2 promoter led to embryonic lethality with vascular defects in yolk sac, placenta and defective blood vessel maturation in the embryo [324].

The endothelial distribution pattern of Clec4g promoter activity is mainly limited to liver endothelial cells, whereas other cell types in the liver, including Kupffer cells and stellate cells are negative. Besides liver endothelial cells, reporter activity is also observed in some endothelial cells of the heart, whereas endothelial cells of lung, kidney, spleen, and bone marrow are negative [289].

#### **6.5.2 Metabolic and endothelial zonation of NICD<sup>OE-HEC</sup> mice**

To elucidate mechanisms of organotropic metastasis, NICD<sup>OE-HEC</sup> mice were analyzed in more detail. Adult NICD<sup>OE-HEC</sup> mice showed slightly dilated vessels on the liver surface and the liver/body weight ratio was reduced. Liver/body weight ratio has been shown to be controlled by angiocrine Wnt signaling. Further, angiocrine wnt signaling has been described to control metabolic liver zonation [221]. Therefore, angiocrine functions of livers of NICD<sup>OE-HEC</sup> mice were analyzed. Metabolic zonation was impaired in NICD<sup>OE-HEC</sup> mice, indicating impairment of angiocrine wnt functions. Duan and colleagues showed that short-term, endothelial notch

activation in a tamoxifen inducible model reduced hepatic angiocrine wnt functions [325], which is in line with my findings. However, in contrast to our model, the inducible model showed no effects on organ size and metabolic zonation. Hepatic angiocrine wnt functions were only relevant upon challenging the liver [325]. This milder phenotype can be most likely explained by mosaic-like transgene activation in inducible models of Cre-expression.

Metabolic alterations observed in NICD<sup>OE-HEC</sup> mice were similar to metabolic alterations described in Wls<sup>HEC-KO</sup> mice [221]. However, deficiency in angiocrine wnt secretion did not affect hepatic metastasis. Therefore, one can conclude that organotropic metastasis is controlled by endothelial notch signaling independently from angiocrine wnt secretion and protection from hepatic metastases cannot be explained by altered metabolic zonation.

Despite impaired metabolic zonation an atypical sinusoidal capillarization in NICD<sup>OE-HEC</sup> mice was observed. The term “capillarization” describes a process, where LSEC lose their specialized phenotype and acquire features of normal capillaries [247]. Typical hallmarks of sinusoidal capillarization are the enhanced expression of markers associated with continuous endothelium, the loss of fenestrations and the formation of a basement membrane. Sinusoidal dedifferentiation precedes inflammation and is commonly observed in fibrotic/cirrhotic liver diseases [251].

The notch target protein Recombination Signal Binding Protein for Immunoglobulin Kappa J Region (RBP-J) has been shown to play an essential role in LSEC homeostasis and regeneration. Conditional deletion of RBP-J in endothelial cells led to LSEC proliferation and obstruction of sinusoidal vasculature, including deposition of fibrin-like material in the sinusoids, increase of endothelial fenestrations, and edema of the space of Disse [326]. During liver regeneration reduced LSEC proliferation and a destroyed sinusoidal structure was observed [326]. Another study showed that conditional knockout of Notch1 led to a reduction of endothelial fenestrae, portal hypertension and over time to hepatic angiosarcoma [327]. An inducible, global endothelial-specific deletion of either RBPJ or Notch-1 led to dilated sinusoids and abnormal vascular architecture, underlining the important role of epithelial notch signaling in development and maintenance of hepatic function and vascular architecture [328].

In our model, an enhanced expression of CD31, Emcn and Lama4 was observed but also an increased endothelial expression of Lyve-1, which is atypical for sinusoidal capillarization. Further, expression of VE-Cadherin was not altered indicating that endothelial integrity was not altered in NICD<sup>OE-HEC</sup> mice.

The LSEC phenotype is maintained by two VEGF-dependent pathways. VEGF secretion from hepatocytes [209] and hepatic stellate cells is essential to maintain LSEC fenestrations, via the NO-dependent VEGF-eNOS-soluble guanylyl cyclase (sGC)-cyclic guanosine

monophosphate (cGMP)-protein kinase pathway and a NO-independent signaling pathway [329]. Alterations of eNOS-sGC-cGMP signaling is a major cause of LSEC capillarization [249]. Also activation of notch signaling in LSEC alters eNOS-sGC signaling and has been shown to result in the loss of LSEC fenestrations [325]. Further, it has been shown that expression of Wnt2a and Wnt9b depends on eNOS-sGC signaling.

### **6.5.3 Role of adhesion molecules in organotropic metastasis**

Besides, its effects on angiocrine wnt signaling and LSEC zonation notch signaling has been shown to regulate the expression of various adhesion molecules among them VCAM1 and ICAM1 [173], [330]. In my model of endothelial overexpression of NICD, endothelial VCAM1 expression was not altered in the liver, but downregulation of ICAM1 was identified as an organ-specific hallmark of endothelial notch activation.

ICAM1 has been reported to be a key player in tumor cell attachment and metastases in a number of different organs, including lung, liver and blood [331], [332]. Besides its role in tumor cell attachment, increased ICAM1 expression induces pro-metastatic signaling pathways involving IL-6 and IL-8. IL-6 and IL-8 are pro-inflammatory cytokines that increase vascular permeability and hence further facilitate tumor cell adhesion, resulting in a pro-metastatic positive feedback loop [255]. Additionally, *in vivo* ICAM1 mediates the infiltration of colorectal cancer cells into tumor mass and is involved in the formation of liver metastases [333]. In colorectal cancer, clinical outcome can be linked to expression levels of ICAM1, VCAM1 and E-Selectin [334].

Functionally, the protective function of endothelial overexpression of NICD in models of hepatic metastases of B16F10 *luc2*, WT31 and MC38 could be due to reduced adhesion of tumor cells in the liver sinusoids mediated by ICAM1. This hypothesis is further supported by reduced adhesion and retention of tumor cells in the liver upon treatment with an anti-ICAM1 antibody [289].

The interaction of tumor cells with ICAM1 on liver sinusoids could either be mediated by the binding of inducible ligands of ICAM1 on tumor cells [335] or involve linker molecules such as fibrin [336]. In colorectal cancer, the ICAM1 ligand LFA-1 on cancer cells has been shown to play a critical role in tumor cell retention and liver metastasis [337].

## **6.6 Summary and Outlook**

In summary, tumor-intrinsic mechanisms and the tumor microenvironment play an important role in the determination of hepatic metastasis. Tumor intrinsic factors, such as the tumor vasculature show a remarkably similar pattern among different melanoma cell lines. Further processes involved in cell migration and angiogenesis were identified as key players in hepatic

metastases. To target angiogenesis in hepatic metastases further investigation of anti-angiogenic treatment options in combination with standard of care treatment are needed.

Regarding the tumor microenvironment notch signaling has been shown to affect metastasis in an organ-specific manner, depending on pre-established, organotypic vascular niches and endothelial differentiation. To further elucidate the effect of the microenvironment on hepatic metastases more studies are needed. One example would be the modulation of notch signaling in an organ-, context- and cell-type-specific manner using nanoparticles. Thereby different steps of the metastatic cascade could be targeted to define the therapeutic window of notch therapy. Also, the effect of sinusoidal capillarization on metastases needs further evaluation. Genetically modified mice that show a similar phenotype of sinusoidal capillarization, as for example LSEC-specific depletion of GATA4 [338] might be a valuable tool to study the effects of capillarization and liver fibrosis on hepatic metastasis.

## References

- [1] R. M. Slominski, M. A. Zmijewski, and A. T. Slominski, "The role of melanin pigment in melanoma," *Experimental Dermatology*. 2015, doi: 10.1111/exd.12618.
- [2] R. R. Braeuer *et al.*, "Why is melanoma so metastatic?," *Pigment Cell and Melanoma Research*. 2014, doi: 10.1111/pcmr.12172.
- [3] A. E. Chang, L. H. Karnell, and H. R. Menck, "The national cancer data base report on cutaneous and noncutaneous melanoma: A summary of 84,836 cases from the past decade," *Cancer*, 1998, doi: 10.1002/(SICI)1097-0142(19981015)83:8<1664::AID-CNCR23>3.0.CO;2-G.
- [4] D. S. Rigel, "Epidemiology of Melanoma," *Semin. Cutan. Med. Surg.*, 2010, doi: 10.1016/j.sder.2010.10.005.
- [5] R. L. Siegel, K. D. Miller, and A. Jemal, "Cancer statistics, 2018," *CA. Cancer J. Clin.*, 2018, doi: 10.3322/caac.21442.
- [6] R. Siegel, D. Naishadham, and A. Jemal, "Cancer statistics, 2012," *CA. Cancer J. Clin.*, 2012, doi: 10.3322/caac.20138.
- [7] S. N. Markovic *et al.*, "Malignant melanoma in the 21st century, part 1: Epidemiology, risk factors, screening, prevention, and diagnosis," in *Mayo Clinic Proceedings*, 2007, doi: 10.4065/82.3.364.
- [8] S. Gandini *et al.*, "Meta-analysis of risk factors for cutaneous melanoma: II. Sun exposure," *Eur. J. Cancer*, 2005, doi: 10.1016/j.ejca.2004.10.016.
- [9] J. Mark Elwood and J. Jopson, "Melanoma and sun exposure: An overview of published studies," *Int. J. Cancer*, 1997, doi: 10.1002/(SICI)1097-0215(19971009)73:2<198::AID-IJC6>3.0.CO;2-R.
- [10] A. Green *et al.*, "The association of use of sunbeds with cutaneous malignant melanoma and other skin cancers: A systematic review," *Int. J. Cancer*, 2007, doi: 10.1002/ijc.22453.
- [11] R. S. Stern, "The risk of melanoma in association with long-term exposure to PUVA," *J. Am. Acad. Dermatol.*, 2001, doi: 10.1067/mjd.2001.114576.
- [12] T. B. Fitzpatrick, "The Validity and Practicality of Sun-Reactive Skin Types I Through VI," *Arch. Dermatol.*, 1988, doi: 10.1001/archderm.1988.01670060015008.
- [13] S. J. Merrill, M. Subramanian, and D. E. Godar, "Worldwide cutaneous malignant melanoma incidences analyzed by sex, age, and skin type over time (1955–2007): Is HPV infection of androgenic hair follicular melanocytes a risk factor for developing melanoma exclusively in people of European-ancestry?," *Dermatoendocrinol.*, 2016, doi: 10.1080/19381980.2016.1215391.
- [14] J. W. Kelly and S. N. Shpall, "Number of melanocytic nevi as a major risk factor for malignant melanoma," *J. Am. Acad. Dermatol.*, 1987, doi: 10.1016/S0190-9622(87)70230-8.
- [15] J. J. Grob *et al.*, "Count of benign melanocytic nevi as a major indicator of risk for nonfamilial nodular and superficial spreading melanoma," *Cancer*, 1990, doi: 10.1002/1097-0142(19900715)66:2<387::AID-CNCR2820660232>3.0.CO;2-J.
- [16] A. J. Watt, S. V. Kotsis, and K. C. Chung, "Risk of melanoma arising in large congenital melanocytic nevi: A systematic review," *Plastic and Reconstructive Surgery*. 2004, doi: 10.1097/01.PRS.0000122209.10277.2A.

- [17] L. J. Loescher, J. D. Crist, and L. A. C. L. Siaki, "Perceived intrafamily melanoma risk communication," *Cancer Nurs.*, 2009, doi: 10.1097/NCC.0b013e31819ae11c.
- [18] M. Potrony *et al.*, "Update in genetic susceptibility in melanoma," *Annals of Translational Medicine*. 2015, doi: 10.3978/j.issn.2305-5839.2015.08.11.
- [19] E. Soura, P. J. Eliades, K. Shannon, A. J. Stratigos, and H. Tsao, "Hereditary melanoma: Update on syndromes and management Genetics of familial atypical multiple mole melanoma syndrome," *Journal of the American Academy of Dermatology*. 2016, doi: 10.1016/j.jaad.2015.08.037.
- [20] M. Rossi, C. Pellegrini, L. Cardelli, V. Ciciarelli, L. di Nardo, and M. C. Fagnoli, "Familial melanoma: diagnostic and management implications," *Dermatol. Pract. Concept.*, 2019, doi: 10.5826/dpc.0901a03.
- [21] J. Paluncic *et al.*, "Roads to melanoma: Key pathways and emerging players in melanoma progression and oncogenic signaling," *Biochimica et Biophysica Acta - Molecular Cell Research*. 2016, doi: 10.1016/j.bbamcr.2016.01.025.
- [22] J. A. Curtin *et al.*, "Distinct Sets of Genetic Alterations in Melanoma," *N. Engl. J. Med.*, 2005, doi: 10.1056/nejmoa050092.
- [23] S. Candido *et al.*, "Analysis of the B-RAFV600E mutation in cutaneous melanoma patients with occupational sun exposure," *Oncol. Rep.*, 2014, doi: 10.3892/or.2014.2977.
- [24] B. C. Bastian, "The molecular pathology of melanoma: An integrated taxonomy of melanocytic neoplasia," *Annu. Rev. Pathol. Mech. Dis.*, 2014, doi: 10.1146/annurev-pathol-012513-104658.
- [25] H. Davies *et al.*, "Mutations of the BRAF gene in human cancer," *Nature*, 2002, doi: 10.1038/nature00766.
- [26] G. Richtig *et al.*, "Beyond the BRAFV600E hotspot: biology and clinical implications of rare BRAF gene mutations in melanoma patients," *British Journal of Dermatology*. 2017, doi: 10.1111/bjd.15436.
- [27] P. T. C. Wan *et al.*, "Mechanism of activation of the RAF-ERK signaling pathway by oncogenic mutations of B-RAF," *Cell*, 2004, doi: 10.1016/S0092-8674(04)00215-6.
- [28] D. K. Morrison, "MAP kinase pathways," *Cold Spring Harb. Perspect. Biol.*, 2012, doi: 10.1101/cshperspect.a011254.
- [29] P. I. Poulidakos and N. Rosen, "Mutant BRAF melanomas-dependence and resistance," *Cancer Cell*. 2011, doi: 10.1016/j.ccr.2011.01.008.
- [30] R. W. Jenkins and R. J. Sullivan, " NRAS mutant melanoma: an overview for the clinician for melanoma management ," *Melanoma Manag.*, 2016, doi: 10.2217/mmt.15.40.
- [31] I. V. Fedorenko, G. T. Gibney, and K. S. M. Smalley, "NRAS mutant melanoma: Biological behavior and future strategies for therapeutic management," *Oncogene*. 2013, doi: 10.1038/onc.2012.453.
- [32] E. Shtivelman *et al.*, "Pathways and therapeutic targets in melanoma," *Oncotarget*, 2014, doi: 10.18632/oncotarget.1892.
- [33] J. E. Gershenwald *et al.*, "Melanoma staging: Evidence-based changes in the American Joint Committee on Cancer eighth edition cancer staging manual," *CA. Cancer J. Clin.*, 2017, doi: 10.3322/caac.21409.
- [34] American Cancer Society, "Cancer Facts & Figures 2022," *Atlanta Am. Cancer Soc.*, 2022.

- [35] R. M.A., S. A., S. R.A., and L. A.K.-Y., "BRAF inhibitors: From the laboratory to clinical trials," *Crit. Rev. Oncol. Hematol.*, 2014.
- [36] A. J. King *et al.*, "Dabrafenib; Preclinical Characterization, Increased Efficacy when Combined with Trametinib, while BRAF/MEK Tool Combination Reduced Skin Lesions," *PLoS One*, 2013, doi: 10.1371/journal.pone.0067583.
- [37] P. Koelblinger, O. Thuerigen, and R. Dummer, "Development of encorafenib for BRAF-mutated advanced melanoma," *Current Opinion in Oncology*. 2018, doi: 10.1097/CCO.0000000000000426.
- [38] T. R. Rheault *et al.*, "Discovery of dabrafenib: A selective inhibitor of Raf Kinases with antitumor activity against B-Raf-driven tumors," *ACS Med. Chem. Lett.*, 2013, doi: 10.1021/ml4000063.
- [39] E. W. Joseph *et al.*, "The RAF inhibitor PLX4032 inhibits ERK signaling and tumor cell proliferation in a V600E BRAF-selective manner," *Proc. Natl. Acad. Sci. U. S. A.*, 2010, doi: 10.1073/pnas.1008990107.
- [40] P. Savoia, P. Fava, F. Casoni, and O. Cremona, "Targeting the ERK signaling pathway in melanoma," *International Journal of Molecular Sciences*. 2019, doi: 10.3390/ijms20061483.
- [41] P. B. Chapman *et al.*, "Improved Survival with Vemurafenib in Melanoma with BRAF V600E Mutation," *N. Engl. J. Med.*, 2011, doi: 10.1056/nejmoa1103782.
- [42] P. B. Chapman *et al.*, "Vemurafenib in patients with BRAFV600 mutation-positive metastatic melanoma: Final overall survival results of the randomized BRIM-3 study," *Ann. Oncol.*, 2017, doi: 10.1093/annonc/mdx339.
- [43] A. Hauschild *et al.*, "Dabrafenib in BRAF-mutated metastatic melanoma: A multicentre, open-label, phase 3 randomised controlled trial," *Lancet*, 2012, doi: 10.1016/S0140-6736(12)60868-X.
- [44] J. A. Sosman *et al.*, "Survival in BRAF V600-Mutant Advanced Melanoma Treated with Vemurafenib," *N. Engl. J. Med.*, 2012, doi: 10.1056/nejmoa1112302.
- [45] G. Hatzivassiliou *et al.*, "RAF inhibitors prime wild-type RAF to activate the MAPK pathway and enhance growth," *Nature*, 2010, doi: 10.1038/nature08833.
- [46] P. I. Poulidakos, C. Zhang, G. Bollag, K. M. Shokat, and N. Rosen, "RAF inhibitors transactivate RAF dimers and ERK signalling in cells with wild-type BRAF," *Nature*, 2010, doi: 10.1038/nature08902.
- [47] K. H. T. Paraiso *et al.*, "Recovery of phospho-ERK activity allows melanoma cells to escape from BRAF inhibitor therapy," *Br. J. Cancer*, 2010, doi: 10.1038/sj.bjc.6605714.
- [48] "BRAF/MEK Combo Approved for Melanoma," *Cancer discovery*. 2018, doi: 10.1158/2159-8290.CD-NB2018-095.
- [49] A. K. S. Salama *et al.*, "Dabrafenib and trametinib in patients with tumors with BRAF V600E/K mutations: Results from the molecular analysis for therapy choice (MATCH) Arm H.," *J. Clin. Oncol.*, 2019, doi: 10.1200/jco.2019.37.15\_suppl.3002.
- [50] "FDA approves encorafenib and binimetinib in combination for unresectable or metastatic melanoma with BRAF mutations," *Case Med. Res.*, 2018, doi: 10.31525/fda1-ucm611981.htm.
- [51] L. Finn, S. N. Markovic, and R. W. Joseph, "Therapy for metastatic melanoma: The past, present, and future," *BMC Medicine*. 2012, doi: 10.1186/1741-7015-10-23.

- [52] S. A. Rosenberg *et al.*, "Prospective randomized trial of high-dose interleukin-2 alone or in conjunction with lymphokine-activated killer cells for the treatment of patients with advanced cancer," *J. Natl. Cancer Inst.*, 1993, doi: 10.1093/jnci/85.8.622.
- [53] R. Marconcini *et al.*, "Current status and perspectives in immunotherapy for metastatic melanoma," *Oncotarget*, 2018, doi: 10.18632/oncotarget.23746.
- [54] D. M. Pardoll, "The blockade of immune checkpoints in cancer immunotherapy," *Nature Reviews Cancer*. 2012, doi: 10.1038/nrc3239.
- [55] S. Hori, T. Nomura, and S. Sakaguchi, "Control of regulatory T cell development by the transcription factor Foxp3," *J. Immunol.*, 2017, doi: 10.1126/science.1079490.
- [56] S. Sivori, P. Vacca, G. Del Zotto, E. Munari, M. C. Mingari, and L. Moretta, "Human NK cells: surface receptors, inhibitory checkpoints, and translational applications," *Cellular and Molecular Immunology*. 2019, doi: 10.1038/s41423-019-0206-4.
- [57] P. Queirolo, A. Boutros, E. Tanda, F. Spagnolo, and P. Quaglino, "Immune-checkpoint inhibitors for the treatment of metastatic melanoma: a model of cancer immunotherapy," *Seminars in Cancer Biology*. 2019, doi: 10.1016/j.semcancer.2019.08.001.
- [58] P. A. Ascierto *et al.*, "Survival Outcomes in Patients with Previously Untreated BRAF Wild-Type Advanced Melanoma Treated with Nivolumab Therapy: Three-Year Follow-up of a Randomized Phase 3 Trial," *JAMA Oncol.*, 2019, doi: 10.1001/jamaoncol.2018.4514.
- [59] J. S. Weber *et al.*, "Nivolumab versus chemotherapy in patients with advanced melanoma who progressed after anti-CTLA-4 treatment (CheckMate 037): A randomised, controlled, open-label, phase 3 trial," *Lancet Oncol.*, 2015, doi: 10.1016/S1470-2045(15)70076-8.
- [60] C. Robert *et al.*, "Nivolumab in Previously Untreated Melanoma without BRAF Mutation," *N. Engl. J. Med.*, 2015, doi: 10.1056/nejmoa1412082.
- [61] P. A. Ascierto *et al.*, "Ipilimumab 10 mg/kg versus ipilimumab 3 mg/kg in patients with unresectable or metastatic melanoma: a randomised, double-blind, multicentre, phase 3 trial," *Lancet Oncol.*, 2017, doi: 10.1016/S1470-2045(17)30231-0.
- [62] F. S. Hodi *et al.*, "Nivolumab plus ipilimumab or nivolumab alone versus ipilimumab alone in advanced melanoma (CheckMate 067): 4-year outcomes of a multicentre, randomised, phase 3 trial," *Lancet Oncol.*, 2018, doi: 10.1016/S1470-2045(18)30700-9.
- [63] D. O. Khair *et al.*, "Combining immune checkpoint inhibitors: Established and emerging targets and strategies to improve outcomes in melanoma," *Frontiers in Immunology*. 2019, doi: 10.3389/fimmu.2019.00453.
- [64] S. Kakadia *et al.*, "Mechanisms of resistance to BRAF and MEK inhibitors and clinical update of us food and drug administration-approved targeted therapy in advanced melanoma," *OncoTargets and Therapy*. 2018, doi: 10.2147/OTT.S182721.
- [65] Y. Liu, X. Zhang, G. Wang, and X. Cui, "Triple Combination Therapy With PD-1/PD-L1, BRAF, and MEK Inhibitor for Stage III–IV Melanoma: A Systematic Review and Meta-Analysis," *Frontiers in Oncology*. 2021, doi: 10.3389/fonc.2021.693655.
- [66] R. Gutzmer *et al.*, "Atezolizumab, vemurafenib, and cobimetinib as first-line treatment for unresectable advanced BRAFV600 mutation-positive melanoma (IMspire150): primary analysis of the randomised, double-blind, placebo-controlled, phase 3 trial," *Lancet*, 2020, doi: 10.1016/S0140-6736(20)30934-X.
- [67] A. Sandru, S. Voinea, E. Panaitescu, and A. Blidaru, "Survival rates of patients with metastatic

- malignant melanoma," *J. Med. Life*, vol. 7, no. 4, pp. 572–576, 2014, [Online]. Available: <http://www.ncbi.nlm.nih.gov/pmc/articles/PMC4316142/>.
- [68] P. Savoia, P. Fava, T. Nardò, S. Osella-Abate, P. Quaglino, and M. G. Bernengo, "Skin metastases of malignant melanoma: A clinical and prognostic survey," *Melanoma Res.*, 2009, doi: 10.1097/CMR.0b013e32832ac775.
- [69] P. C. Tumei *et al.*, "Liver Metastasis and Treatment Outcome with Anti-PD-1 Monoclonal Antibody in Patients with Melanoma and NSCLC," *Cancer Immunol. Res.*, vol. 5, no. 5, pp. 417–424, May 2017, doi: 10.1158/2326-6066.CIR-16-0325.
- [70] O. Abdel-Rahman, "Clinical correlates and prognostic value of different metastatic sites in patients with malignant melanoma of the skin: a SEER database analysis," *J. Dermatolog. Treat.*, 2018, doi: 10.1080/09546634.2017.1360987.
- [71] J. C. Lee *et al.*, "Regulatory T cell control of systemic immunity and immunotherapy response in liver metastasis," *Sci. Immunol.*, 2020, doi: 10.1126/sciimmunol.aba0759.
- [72] A. Hauschild *et al.*, "Modeled Prognostic Subgroups for Survival and Treatment Outcomes in BRAF V600-Mutated Metastatic Melanoma: Pooled Analysis of 4 Randomized Clinical Trials," *JAMA Oncol.*, vol. 4, no. 10, pp. 1382–1388, Oct. 2018, doi: 10.1001/JAMAONCOL.2018.2668.
- [73] S. Paget, "THE DISTRIBUTION OF SECONDARY GROWTHS IN CANCER OF THE BREAST.," *Lancet*, 1889, doi: 10.1016/S0140-6736(00)49915-0.
- [74] D. L. Kinsey, "An experimental study of preferential metastasis," *Cancer*, 1960, doi: 10.1002/1097-0142(196007/08)13:4<674::AID-CNCR2820130405>3.0.CO;2-Q.
- [75] E. Ruoslahti and D. Rajotte, "An address system in the vasculature of normal tissues and tumors," *Annual Review of Immunology*. 2000, doi: 10.1146/annurev.immunol.18.1.813.
- [76] A. Müller *et al.*, "Involvement of chemokine receptors in breast cancer metastasis," *Nature*, 2001, doi: 10.1038/35065016.
- [77] F. C. L. Chow and K. S. H. Chok, "Colorectal liver metastases: An update on multidisciplinary approach," *World Journal of Hepatology*. 2019, doi: 10.4254/wjh.v11.i2.150.
- [78] I. J. Fidler, "The pathogenesis of cancer metastasis: the 'seed and soil' hypothesis revisited.," *Nat. Rev. Cancer*, 2003, doi: 10.1038/nrc1098.
- [79] C. Géraud, P. S. Koch, F. Damm, K. Schledzewski, and S. Goerdt, "The metastatic cycle: metastatic niches and cancer cell dissemination.," *J. Dtsch. Dermatol. Ges.*, pp. 1–8, 2014, doi: 10.1111/ddg.12451.
- [80] S. Valastyan and R. A. Weinberg, "Tumor metastasis: Molecular insights and evolving paradigms," *Cell*, vol. 147, no. 2, pp. 275–292, 2011, doi: 10.1016/j.cell.2011.09.024.
- [81] T. R. Geiger and D. S. Peeper, "Metastasis mechanisms," *Biochimica et Biophysica Acta - Reviews on Cancer*. 2009, doi: 10.1016/j.bbcan.2009.07.006.
- [82] J. P. Thiery, "Epithelial–mesenchymal transitions in tumour progression," *Nat. Rev. Cancer*, 2002, doi: 10.1038/nrc822.
- [83] G. Christofori, "New signals from the invasive front," *Nature*. 2006, doi: 10.1038/nature04872.
- [84] M. Jechlinger *et al.*, "Expression profiling of epithelial plasticity in tumor progression," *Oncogene*, 2003, doi: 10.1038/sj.onc.1206887.
- [85] M. A. Huber, N. Kraut, and H. Beug, "Molecular requirements for epithelial-mesenchymal transition during tumor progression," *Current Opinion in Cell Biology*. 2005, doi:

- 10.1016/j.ceb.2005.08.001.
- [86] J. Massague, "TGFbeta in Cancer.," *Cell*, 2008.
- [87] M. A. Huber *et al.*, "NF-κB is essential for epithelial-mesenchymal transition and metastasis in a model of breast cancer progression," *J. Clin. Invest.*, 2004, doi: 10.1172/jci21358.
- [88] R. Pardal, M. F. Clarke, and S. J. Morrison, "Applying the principles of stem-cell biology to cancer," *Nature Reviews Cancer*. 2003, doi: 10.1038/nrc1232.
- [89] J. Yang and R. A. Weinberg, "Epithelial-Mesenchymal Transition: At the Crossroads of Development and Tumor Metastasis," *Developmental Cell*. 2008, doi: 10.1016/j.devcel.2008.05.009.
- [90] I. Valyi-Nagy *et al.*, "Spontaneous and induced differentiation of human melanoma cells," *Int. J. Cancer*, 1993, doi: 10.1002/ijc.2910540125.
- [91] M. Y. Hsu, "Shifts in cadherin profiles between human normal melanocytes and melanomas," *J. Investig. Dermatology Symp. Proc.*, 1996.
- [92] L. M. Shih, D. E. Elder, M. Y. Hsu, and M. Herlyn, "Regulation of Mel-CAM/MUC18 expression on melanocytes of different stages of tumor progression by normal keratinocytes," *Am. J. Pathol.*, 1994.
- [93] G. Li, K. Satyamoorthy, and M. Herlyn, "N-cadherin-mediated intercellular interactions promote survival and migration of melanoma cells," *Cancer Res.*, 2001.
- [94] M. Sandig, E. B. Voura, V. I. Kalnins, and C. H. Siu, "Role of cadherins in the transendothelial migration of melanoma cells in culture," *Cell Motil. Cytoskeleton*, 1997, doi: 10.1002/(SICI)1097-0169(1997)38:4<351::AID-CM5>3.0.CO;2-6.
- [95] E. B. Voura, M. Sandig, and C. H. Siu, "Cell-cell interactions during transendothelial migration of tumor cells," *Microsc. Res. Tech.*, 1998, doi: 10.1002/(SICI)1097-0029(19981101)43:3<265::AID-JEMT9>3.0.CO;2-Z.
- [96] S. Xie *et al.*, "Expression of MCAM/MUC18 by human melanoma cells leads to increased tumor growth and metastasis," *Cancer Res.*, 1997.
- [97] J. L. Jones, J. E. Royall, and R. A. Walker, "E-cadherin relates to EGFR expression and lymph node metastasis in primary breast carcinoma," *Br. J. Cancer*, 1996, doi: 10.1038/bjc.1996.522.
- [98] R. Puches, J. Smolle, E. Rieger, H. P. Soyer, and H. Kerl, "Expression of cytoskeletal components in melanocytic skin lesions: An immunohistochemical study," *Am. J. Dermatopathol.*, 1991, doi: 10.1097/00000372-199104000-00006.
- [99] K. S. Hoek and C. R. Goding, "Cancer stem cells versus phenotype-switching in melanoma," *Pigment Cell and Melanoma Research*. 2010, doi: 10.1111/j.1755-148X.2010.00757.x.
- [100] M. Ghosh, X. Song, G. Mouneimne, M. Sidani, D. S. Lawrence, and J. S. Condeelis, "Cofilin Promotes Actin Polymerization and Defines the Direction of Cell Motility," *Science (80- )*, 2004, doi: 10.1126/science.1094561.
- [101] V. Sanz-Moreno, G. Gadea, H. Paterson, and C. J. Marshall, "Rac activation and inactivation control plasticity of tumour cell movement," *Eur. J. Cancer Suppl.*, 2008, doi: 10.1016/s1359-6349(08)71206-0.
- [102] A. Thies *et al.*, "Overexpression of the cell adhesion molecule L1 is associated with metastasis in cutaneous malignant melanoma," *Eur. J. Cancer*, 2002, doi: 10.1016/S0959-8049(02)00105-3.

- [103] M. Hortsch, "The L1 family of neural cell adhesion molecules: Old proteins performing new tricks," *Neuron*. 1996, doi: 10.1016/S0896-6273(00)80192-0.
- [104] E. B. Voura, R. A. Ramjeesingh, A. M. P. Montgomery, and C. H. Siu, "Involvement of integrin  $\alpha\beta3$  and cell adhesion molecule L1 in transendothelial migration of melanoma cells," *Mol. Biol. Cell*, 2001, doi: 10.1091/mbc.12.9.2699.
- [105] S. M. Frisch and H. Francis, "Disruption of epithelial cell-matrix interactions induces apoptosis," *J. Cell Biol.*, 1994, doi: 10.1083/jcb.124.4.619.
- [106] J. E. Meredith, B. Fazeli, and M. A. Schwartz, "The extracellular matrix as a cell survival factor," *Mol. Biol. Cell*, 1993, doi: 10.1091/mbc.4.9.953.
- [107] L. A. Liotta and E. Kohn, "Cancer and the homeless cell," *Nature*. 2004, doi: 10.1038/430973a.
- [108] S. M. Frisch, K. Vuori, E. Ruoslahti, and P. Y. Chan-Hui, "Control of adhesion-dependent cell survival by focal adhesion kinase," *J. Cell Biol.*, 1996, doi: 10.1083/jcb.134.3.793.
- [109] S. Atwell, C. Roskelley, and S. Dedhar, "The integrin-linked kinase (ILK) suppresses anoikis," *Oncogene*, 2000, doi: 10.1038/sj.onc.1203711.
- [110] G. Radeva *et al.*, "Overexpression of the integrin-linked kinase promotes anchorage-independent cell cycle progression," *J. Biol. Chem.*, 1997, doi: 10.1074/jbc.272.21.13937.
- [111] S. M. Janes and F. M. Watt, "New roles for integrins in squamous-cell carcinoma," *Nature Reviews Cancer*. 2006, doi: 10.1038/nrc1817.
- [112] W. Guo and F. G. Giancotti, "Integrin signalling during tumour progression," *Nature Reviews Molecular Cell Biology*. 2004, doi: 10.1038/nrm1490.
- [113] G. W. McLean, N. O. Carragher, E. Avizienyte, J. Evans, V. G. Brunton, and M. C. Frame, "The role of focal-adhesion kinase in cancer - A new therapeutic opportunity," *Nature Reviews Cancer*. 2005, doi: 10.1038/nrc1647.
- [114] N. K. Haass, K. S. M. Smalley, L. Li, and M. Herlyn, "Adhesion, migration and communication in melanocytes and melanoma," *Pigment Cell Research*. 2005, doi: 10.1111/j.1600-0749.2005.00235.x.
- [115] J. Perea Paizal, S. H. Au, and C. Bakal, "Squeezing through the microcirculation: survival adaptations of circulating tumour cells to seed metastasis," *British Journal of Cancer*. 2021, doi: 10.1038/s41416-020-01176-x.
- [116] H. Q. Le *et al.*, "Mechanical regulation of transcription controls Polycomb-mediated gene silencing during lineage commitment," *Nat. Cell Biol.*, 2016, doi: 10.1038/ncb3387.
- [117] A. Tajik *et al.*, "Transcription upregulation via force-induced direct stretching of chromatin," *Nat. Mater.*, 2016, doi: 10.1038/nmat4729.
- [118] H. A. Cognart, J. L. Viovy, and C. Villard, "Fluid shear stress coupled with narrow constrictions induce cell type-dependent morphological and molecular changes in SK-BR-3 and MDA-MB-231 cells," *Sci. Rep.*, 2020, doi: 10.1038/s41598-020-63316-w.
- [119] D. M. Brown and E. Ruoslahti, "Metadherin, a cell surface protein in breast tumors that mediates lung metastasis," *Cancer Cell*, 2004, doi: 10.1016/S1535-6108(04)00079-0.
- [120] K. J. Luzzi *et al.*, "Multistep nature of metastatic inefficiency: Dormancy of solitary cells after successful extravasation and limited survival of early micrometastases," *Am. J. Pathol.*, 1998, doi: 10.1016/S0002-9440(10)65628-3.
- [121] V. L. Morris, E. E. Schmidt, I. C. MacDonald, A. C. Groom, and A. F. Chambers, "Sequential

- steps in hematogenous metastasis of cancer cells studied by in vivo videomicroscopy," *Invasion and Metastasis*. 1997.
- [122] G. N. Naumov *et al.*, "Persistence of solitary mammary carcinoma cells in a secondary site: A possible contributor to dormancy," *Cancer Res.*, 2002.
- [123] L. Holmgren, M. S. O'reilly, and J. Folkman, "Dormancy of micrometastases: Balanced proliferation and apoptosis in the presence of angiogenesis suppression," *Nat. Med.*, 1995, doi: 10.1038/nm0295-149.
- [124] M. S. O'Reilly *et al.*, "Angiostatin: A novel angiogenesis inhibitor that mediates the suppression of metastases by a lewis lung carcinoma," *Cell*, 1994, doi: 10.1016/0092-8674(94)90200-3.
- [125] C. M. Koebel *et al.*, "Adaptive immunity maintains occult cancer in an equilibrium state," *Nature*, 2007, doi: 10.1038/nature06309.
- [126] J. C. Berger, D. J. Vander Griend, V. L. Robinson, J. A. Hickson, and C. W. Rinker-Schaeffer, "Metastasis suppressor genes: From gene identification to protein function and regulation," *Cancer Biology and Therapy*. 2005, doi: 10.4161/cbt.4.8.1865.
- [127] P. S. Steeg, "Metastasis suppressors alter the signal transduction of cancer cells," *Nature Reviews Cancer*. 2003, doi: 10.1038/nrc967.
- [128] M. A. Gimbrone, S. B. Leapman, R. S. Cotran, and J. Folkman, "Tumor dormancy in vivo by prevention of neovascularization," *J. Exp. Med.*, 1972, doi: 10.1084/jem.136.2.261.
- [129] R. Kalluri, "Basement membranes: Structure, assembly and role in tumour angiogenesis," *Nature Reviews Cancer*. 2003, doi: 10.1038/nrc1094.
- [130] G. Bergers and L. E. Benjamin, "Tumorigenesis and the angiogenic switch," *Nature Reviews Cancer*. 2003, doi: 10.1038/nrc1093.
- [131] D. Hanahan and J. Folkman, "Patterns and emerging mechanisms of the angiogenic switch during tumorigenesis," *Cell*. 1996, doi: 10.1016/S0092-8674(00)80108-7.
- [132] C. Murdoch, M. Muthana, S. B. Coffelt, and C. E. Lewis, "The role of myeloid cells in the promotion of tumour angiogenesis," *Nature Reviews Cancer*. 2008, doi: 10.1038/nrc2444.
- [133] G. L. Semenza, "Targeting HIF-1 for cancer therapy," *Nature Reviews Cancer*. 2003, doi: 10.1038/nrc1187.
- [134] M. Bar-Eli, "Role of interleukin-8 in tumor growth and metastasis of human melanoma," *Pathobiology*, 1999, doi: 10.1159/000028045.
- [135] R. K. Jain, "Normalization of tumor vasculature: An emerging concept in antiangiogenic therapy," *Science*. 2005, doi: 10.1126/science.1104819.
- [136] J. Poisson *et al.*, "Liver sinusoidal endothelial cells: Physiology and role in liver diseases," *Journal of Hepatology*. 2017, doi: 10.1016/j.jhep.2016.07.009.
- [137] R. N. Kaplan *et al.*, "VEGFR1-positive haematopoietic bone marrow progenitors initiate the pre-metastatic niche," *Nature*, vol. 438, no. 7069, pp. 820–827, 2005, doi: 10.1038/nature04186.VEGFR1-positive.
- [138] B. Psaila and D. Lyden, "The metastatic niche: adapting the foreign soil.," *Nat. Rev. Cancer*, vol. 9, no. 4, pp. 285–293, 2009, doi: 10.1038/nrc2621.
- [139] B. Seubert *et al.*, "Tissue inhibitor of metalloproteinases (TIMP)-1 creates a premetastatic niche in the liver through SDF-1/CXCR4-dependent neutrophil recruitment in mice,"

*Hepatology*, 2015, doi: 10.1002/hep.27378.

- [140] C. D. Hermann *et al.*, "TIMP1 expression underlies sex disparity in liver metastasis and survival in pancreatic cancer," *J. Exp. Med.*, 2021, doi: 10.1084/jem.20210911.
- [141] D. Wang, H. Sun, J. Wei, B. Cen, and R. N. DuBois, "CXCL1 is critical for premetastatic niche formation and metastasis in colorectal cancer," *Cancer Res.*, 2017, doi: 10.1158/0008-5472.CAN-16-3199.
- [142] B. F evrier and G. Raposo, "Exosomes: Endosomal-derived vesicles shipping extracellular messages," *Current Opinion in Cell Biology*. 2004, doi: 10.1016/j.ceb.2004.06.003.
- [143] C. Th ery, L. Zitvogel, and S. Amigorena, "Exosomes: Composition, biogenesis and function," *Nature Reviews Immunology*. 2002, doi: 10.1038/nri855.
- [144] H. Peinado *et al.*, "Melanoma exosomes educate bone marrow progenitor cells toward a pro-metastatic phenotype through MET.," *Nat. Med.*, vol. 18, no. 6, pp. 883–91, 2012, doi: 10.1038/nm.2753.
- [145] J. L. Hood, S. San Roman, and S. A. Wickline, "Exosomes released by melanoma cells prepare sentinel lymph nodes for tumor metastasis," *Cancer Res.*, 2011, doi: 10.1158/0008-5472.CAN-10-4455.
- [146] Y. Shao *et al.*, "Colorectal cancer-derived small extracellular vesicles establish an inflammatory premetastatic niche in liver metastasis," *Carcinogenesis*, 2018, doi: 10.1093/carcin/bgy115.
- [147] O. V. Glinskii, V. H. Huxley, G. V. Glinsky, K. J. Pienta, A. Raz, and V. V. Glinsky, "Mechanical entrapment is insufficient and intercellular adhesion is essential for metastatic cell arrest in distant organs," *Neoplasia*, 2005, doi: 10.1593/neo.04646.
- [148] C. R. Gardner, A. J. Wasserman, and D. L. Laskin, "Liver macrophage-mediated cytotoxicity toward mastocytoma cells involves phagocytosis of tumor targets," *Hepatology*, 1991, doi: 10.1002/hep.1840140219.
- [149] H. Matsumura *et al.*, "Kupffer cells decrease metastasis of colon cancer cells to the liver in the early stage," *Int. J. Oncol.*, 2014, doi: 10.3892/ijo.2014.2662.
- [150] L. G. Bay on, M. A. Izquierdo, I. Sirovich, N. Van Rooijen, R. H. J. Beelen, and S. Meijer, "Role of Kupffer cells in arresting circulating tumor cells and controlling metastatic growth in the liver," *Hepatology*, 1996, doi: 10.1053/jhep.1996.v23.pm0008621157.
- [151] A. M. Khatib, M. Kontogiannea, L. Fallavollita, B. Jamison, S. Meterissian, and P. Brodt, "Rapid induction of cytokine and E-selectin expression in the liver in response to metastatic tumor cells," *Cancer Res.*, 1999.
- [152] A. M. Khatib, L. Fallavollita, E. V. Wancewicz, B. P. Monia, and P. Brodt, "Inhibition of hepatic endothelial E-selectin expression by C-raf antisense oligonucleotides blocks colorectal carcinoma liver metastasis," *Cancer Res.*, 2002.
- [153] A. Mielgo and M. C. Schmid, "Liver tropism in cancer: The hepatic metastatic niche," *Cold Spring Harb. Perspect. Med.*, 2020, doi: 10.1101/cshperspect.a037259.
- [154] B. Costa-Silva *et al.*, "Pancreatic cancer exosomes initiate pre-metastatic niche formation in the liver," *Nat. Cell Biol.*, 2015, doi: 10.1038/ncb3169.
- [155] K. Taura *et al.*, "Hepatic Stellate Cells Secrete Angiopoietin 1 That Induces Angiogenesis in Liver Fibrosis," *Gastroenterology*, 2008, doi: 10.1053/j.gastro.2008.07.065.
- [156] E. Olaso *et al.*, "Proangiogenic role of tumor-activated hepatic stellate cells in experimental

- melanoma metastasis," *Hepatology*, 2003, doi: 10.1053/jhep.2003.50068.
- [157] B. L. Copple, S. Bai, L. D. Burgoon, and J. O. Moon, "Hypoxia-inducible factor-1 $\alpha$  regulates the expression of genes in hypoxic hepatic stellate cells important for collagen deposition and angiogenesis," *Liver Int.*, 2011, doi: 10.1111/j.1478-3231.2010.02347.x.
- [158] A. I. Thompson, K. P. Conroy, and N. C. Henderson, "Hepatic stellate cells: Central modulators of hepatic carcinogenesis," *BMC Gastroenterology*. 2015, doi: 10.1186/s12876-015-0291-5.
- [159] S. Stremitzer *et al.*, "Immune phenotype and histopathological growth pattern in patients with colorectal liver metastases," *Br. J. Cancer*, vol. 122, no. 10, pp. 1518–1524, May 2020, doi: 10.1038/S41416-020-0812-Z.
- [160] H. E. Grossniklaus, Q. Zhang, S. You, C. McCarthy, S. Heegaard, and S. E. Coupland, "Metastatic ocular melanoma to the liver exhibits infiltrative and nodular growth patterns," *Hum. Pathol.*, vol. 57, pp. 165–175, 2016, doi: 10.1016/j.humpath.2016.07.012.
- [161] P. J. Van Dam *et al.*, "International consensus guidelines for scoring the histopathological growth patterns of liver metastasis," *Br. J. Cancer*, vol. 117, no. 10, p. 1427, Nov. 2017, doi: 10.1038/BJC.2017.334.
- [162] E. Latacz *et al.*, "Can medical imaging identify the histopathological growth patterns of liver metastases?," *Semin. Cancer Biol.*, 2021, doi: 10.1016/j.semcancer.2020.07.002.
- [163] P. B. Vermeulen *et al.*, "Liver metastases from colorectal adenocarcinomas grow in three patterns with different angiogenesis and desmoplasia," *J. Pathol.*, 2001, doi: 10.1002/path.966.
- [164] R. Barnhill *et al.*, "Replacement and desmoplastic histopathological growth patterns in cutaneous melanoma liver metastases: frequency, characteristics, and robust prognostic value," *J. Pathol. Clin. Res.*, vol. 6, no. 3, pp. 195–206, Jul. 2020, doi: 10.1002/CJP2.161.
- [165] S. Frentzas *et al.*, "Vessel co-option mediates resistance to anti-angiogenic therapy in liver metastases," *Nat. Med.*, vol. 22, no. 11, pp. 1294–1302, Nov. 2016, doi: 10.1038/NM.4197.
- [166] J. S. Mumm and R. Kopan, "Notch signaling: From the outside in," *Developmental Biology*. 2000, doi: 10.1006/dbio.2000.9960.
- [167] E. C. Lai, "Notch signaling: Control of cell communication and cell fate," *Development*. 2004, doi: 10.1242/dev.01074.
- [168] M. Baron, "An overview of the Notch signalling pathway," *Seminars in Cell and Developmental Biology*. 2003, doi: 10.1016/S1084-9521(02)00179-9.
- [169] L. W. Ellisen *et al.*, "TAN-1, the human homolog of the Drosophila Notch gene, is broken by chromosomal translocations in T lymphoblastic neoplasms," *Cell*, 1991, doi: 10.1016/0092-8674(91)90111-B.
- [170] A. P. Weng *et al.*, "Activating mutations of NOTCH1 in human T cell acute lymphoblastic leukemia," *Science (80-. )*, 2004, doi: 10.1126/science.1102160.
- [171] S. Majumder, J. S. Crabtree, T. E. Golde, L. M. Minter, B. A. Osborne, and L. Miele, "Targeting Notch in oncology: the path forward," *Nature Reviews Drug Discovery*. 2021, doi: 10.1038/s41573-020-00091-3.
- [172] D. Banerjee *et al.*, "Notch suppresses angiogenesis and progression of hepatic metastases," *Cancer Res.*, vol. 75, no. 8, pp. 1592–1602, 2015, doi: 10.1158/0008-5472.CAN-14-1493.
- [173] E. Wieland *et al.*, "Endothelial Notch1 Activity Facilitates Metastasis," *Cancer Cell*, vol. 31, no.

- 3, pp. 355–367, 2017, doi: 10.1016/j.ccell.2017.01.007.
- [174] H. Ishibashi, M. Nakamura, A. Komori, K. Migita, and S. Shimoda, “Liver architecture, cell function, and disease,” *Seminars in Immunopathology*. 2009, doi: 10.1007/s00281-009-0155-6.
- [175] A. Kalra and F. Tuma, *Physiology, Liver*. 2018.
- [176] T. Matsumoto and M. Kawakami, “The unit-concept of hepatic parenchyma--a re-examination based on angioarchitectural studies.,” *Acta Pathol. Jpn.*, 1982.
- [177] H. F. Teutsch, D. Schuerfeld, and E. Groezinger, “Three-dimensional reconstruction of parenchymal units in the liver of the rat,” *Hepatology*, 1999, doi: 10.1002/hep.510290243.
- [178] G. Xie, L. Wang, X. Wang, L. Wang, and L. D. DeLeve, “Isolation of periportal, midlobular, and centrilobular rat liver sinusoidal endothelial cells enables study of zoned drug toxicity,” *Am. J. Physiol. - Gastrointest. Liver Physiol.*, 2010, doi: 10.1152/ajpgi.00302.2010.
- [179] T. Kietzmann, “Metabolic zonation of the liver: The oxygen gradient revisited,” *Redox Biology*. 2017, doi: 10.1016/j.redox.2017.01.012.
- [180] A. Blouin, R. P. Bolender, and E. R. Weibel, “Distribution of organelles and membranes between hepatocytes and nonhepatocytes in the rat liver parenchyma. A stereological study,” *J. Cell Biol.*, 1977, doi: 10.1083/jcb.72.2.441.
- [181] L. Qin and J. M. Crawford, “Anatomy and Cellular Functions of the Liver,” in *Zakim and Boyer’s Hepatology*, 2018.
- [182] P. D. Wilkinson *et al.*, “The Polyploid State Restricts Hepatocyte Proliferation and Liver Regeneration in Mice,” *Hepatology*, 2019, doi: 10.1002/hep.30286.
- [183] R. J. Schulze, M. B. Schott, C. A. Casey, P. L. Tuma, and M. A. McNiven, “The cell biology of the hepatocyte: A membrane trafficking machine,” *Journal of Cell Biology*. 2019, doi: 10.1083/jcb.201903090.
- [184] A. Treyer and A. Müsch, “Hepatocyte polarity,” *Compr. Physiol.*, 2013, doi: 10.1002/cphy.c120009.
- [185] R. Gebhardt, F. Gaunitz, and D. Mecke, “Heterogeneous (positional) expression of hepatic glutamine synthetase: features, regulation and implications for hepatocarcinogenesis,” *Adv. Enzyme Regul.*, 1994, doi: 10.1016/0065-2571(94)90007-8.
- [186] A. Braeuning *et al.*, “Differential gene expression in periportal and perivenous mouse hepatocytes,” *FEBS J.*, 2006, doi: 10.1111/j.1742-4658.2006.05503.x.
- [187] K. B. Halpern *et al.*, “Single-cell spatial reconstruction reveals global division of labour in the mammalian liver,” *Nature*, 2017, doi: 10.1038/nature21065.
- [188] C. Torre, C. Perret, and S. Colnot, “Transcription dynamics in a physiological process:  $\beta$ -Catenin signaling directs liver metabolic zonation,” *International Journal of Biochemistry and Cell Biology*. 2011, doi: 10.1016/j.biocel.2009.11.004.
- [189] A. Geerts, “History, heterogeneity, developmental biology, and functions of quiescent hepatic stellate cells,” *Seminars in Liver Disease*. 2001, doi: 10.1055/s-2001-17550.
- [190] R. Blomhoff and H. K. Blomhoff, “Overview of retinoid metabolism and function,” *Journal of Neurobiology*. 2006, doi: 10.1002/neu.20242.
- [191] F. Tacke and R. Weiskirchen, “Update on hepatic stellate cells: Pathogenic role in liver fibrosis and novel isolation techniques,” *Expert Review of Gastroenterology and Hepatology*. 2012,

doi: 10.1586/egh.11.92.

- [192] H. Reynaert, D. Urbain, and A. Geerts, "Regulation of sinusoidal perfusion in portal hypertension," *Anat. Rec.*, 2008, doi: 10.1002/ar.20669.
- [193] D. C. Rockey, "Characterization of endothelin receptors mediating rat hepatic stellate cell contraction," *Biochem. Biophys. Res. Commun.*, 1995, doi: 10.1006/bbrc.1995.1247.
- [194] H. Senoo, "Structure and function of hepatic stellate cells," *Medical Electron Microscopy*. 2004, doi: 10.1007/s00795-003-0230-3.
- [195] E. Mormone, J. George, and N. Nieto, "Molecular pathogenesis of hepatic fibrosis and current therapeutic approaches," *Chem. Biol. Interact.*, 2011, doi: 10.1016/j.cbi.2011.07.001.
- [196] T. Amann *et al.*, "Activated hepatic stellate cells promote tumorigenicity of hepatocellular carcinoma," *Cancer Sci.*, 2009, doi: 10.1111/j.1349-7006.2009.01087.x.
- [197] D. Thabut and V. Shah, "Intrahepatic angiogenesis and sinusoidal remodeling in chronic liver disease: New targets for the treatment of portal hypertension?," *Journal of Hepatology*. 2010, doi: 10.1016/j.jhep.2010.07.004.
- [198] M. Naito, G. Hasegawa, and K. Takahashi, "Development, differentiation, and maturation of kupffer cells," *Microsc. Res. Tech.*, 1997, doi: 10.1002/(SICI)1097-0029(19971115)39:4<350::AID-JEMT5>3.0.CO;2-L.
- [199] L. J. Dixon, M. Barnes, H. Tang, M. T. Pritchard, and L. E. Nagy, "Kupffer cells in the liver," *Compr. Physiol.*, 2013, doi: 10.1002/cphy.c120026.
- [200] C. Ju *et al.*, "Protective role of kupffer cells in acetaminophen-induced hepatic injury in mice," *Chem. Res. Toxicol.*, 2002, doi: 10.1021/tx0255976.
- [201] P. Ramachandran and J. P. Iredale, "Macrophages: Central regulators of hepatic fibrogenesis and fibrosis resolution," *Journal of Hepatology*. 2012, doi: 10.1016/j.jhep.2011.10.026.
- [202] L. E. Nagy, "The role of innate immunity in alcoholic liver disease," *Alcohol Res. Curr. Rev.*, 2015.
- [203] S. W. Wen, E. I. Ager, and C. Christophi, "Bimodal role of Kupffer cells during colorectal cancer liver metastasis," *Cancer Biol. Ther.*, 2013, doi: 10.4161/cbt.24593.
- [204] M. Siwicki *et al.*, "Resident Kupffer cells and neutrophils drive liver toxicity in cancer immunotherapy," *Sci. Immunol.*, 2021, doi: 10.1126/sciimmunol.abi7083.
- [205] H. G. Augustin and G. Y. Koh, "Organotypic vasculature: From descriptive heterogeneity to functional pathophysiology," *Science*. 2017, doi: 10.1126/science.aal2379.
- [206] S. Shetty, P. F. Lalor, and D. H. Adams, "Liver sinusoidal endothelial cells — gatekeepers of hepatic immunity," *Nature Reviews Gastroenterology and Hepatology*. 2018, doi: 10.1038/s41575-018-0020-y.
- [207] K. K. Sørensen, J. Simon-Santamaria, R. S. McCuskey, and B. Smedsrød, "Liver sinusoidal endothelial cells," *Compr. Physiol.*, 2015, doi: 10.1002/cphy.c140078.
- [208] A. Couvelard, J. Y. Scoazec, M. C. Dauge, A. F. Binguier, F. Potet, and G. Feldmann, "Structural and functional differentiation of sinusoidal endothelial cells during liver organogenesis in humans," *Blood*, 1996, doi: 10.1182/blood.v87.11.4568.bloodjournal87114568.
- [209] T. J. Walter, A. E. Cast, K. A. Huppert, and S. S. Huppert, "Epithelial VEGF signaling is required in the mouse liver for proper sinusoid endothelial cell identity and hepatocyte zonation in vivo," *Am. J. Physiol. - Gastrointest. Liver Physiol.*, 2014, doi: 10.1152/ajpgi.00426.2013.

- [210] K. Matsumoto, H. Yoshitomi, J. Rossant, and K. S. Zaret, "Liver organogenesis promoted by endothelial cells prior to vascular function," *Science (80-. )*, 2001, doi: 10.1126/science.1063889.
- [211] C. Géraud *et al.*, "GATA4-dependent organ-specific endothelial differentiation controls liver development and embryonic hematopoiesis," *J. Clin. Invest.*, vol. 127, no. 3, pp. 1–16, 2017, doi: 10.1172/JCI90086.
- [212] P. S. Koch, K. H. Lee, S. Goerdt, and H. G. Augustin, "Angiodiversity and organotypic functions of sinusoidal endothelial cells," *Angiogenesis*. 2021, doi: 10.1007/s10456-021-09780-y.
- [213] E. Wisse, "An electron microscopic study of the fenestrated endothelial lining of rat liver sinusoids," *J. Ultrastructure Res.*, 1970, doi: 10.1016/S0022-5320(70)90150-4.
- [214] F. Braet, R. de Zanger, M. Baekeland, E. Crabbé, P. van der Smissen, and E. Wisse, "Structure and dynamics of the fenestrae-associated cytoskeleton of rat liver sinusoidal endothelial cells," *Hepatology*, 1995, doi: 10.1016/0270-9139(95)90427-1.
- [215] E. Wisse, R. B. de Zanger, K. Charels, P. van der Smissen, and R. S. McCuskey, "The liver sieve: Considerations concerning the structure and function of endothelial fenestrae, the sinusoidal wall and the space of disse," *Hepatology*, 1985, doi: 10.1002/hep.1840050427.
- [216] K. Szafranska, L. D. Kruse, C. F. Holte, P. McCourt, and B. Zapotoczny, "The wHole Story About Fenestrations in LSEC," *Frontiers in Physiology*. 2021, doi: 10.3389/fphys.2021.735573.
- [217] K. B. Halpern *et al.*, "Paired-cell sequencing enables spatial gene expression mapping of liver endothelial cells," *Nat. Biotechnol.*, vol. 36, no. 10, p. 962, 2018, doi: 10.1038/nbt.4231.
- [218] T. Wakabayashi *et al.*, "CD157 Marks Tissue-Resident Endothelial Stem Cells with Homeostatic and Regenerative Properties," *Cell Stem Cell*, 2018, doi: 10.1016/j.stem.2018.01.010.
- [219] J. Bonnardel *et al.*, "Stellate Cells, Hepatocytes, and Endothelial Cells Imprint the Kupffer Cell Identity on Monocytes Colonizing the Liver Macrophage Niche," *Immunity*, 2019, doi: 10.1016/j.immuni.2019.08.017.
- [220] L. Planas-Paz *et al.*, "The RSPO-LGR4/5-ZNRF3/RNF43 module controls liver zonation and size," *Nat. Cell Biol.*, 2016, doi: 10.1038/ncb3337.
- [221] T. Leibing *et al.*, "Angiocrine Wnt signaling controls liver growth and metabolic maturation in mice," *Hepatology*, vol. 68, no. 2, pp. 707–722, Aug. 2018, doi: 10.1002/HEP.29613.
- [222] R. Ma, A. S. Martínez-Ramírez, T. L. Borders, F. Gao, and B. Sosa-Pineda, "Metabolic and non-metabolic liver zonation is established non-synchronously and requires sinusoidal Wnts," *Elife*, 2020, doi: 10.7554/eLife.46206.
- [223] B. Wang, L. Zhao, M. Fish, C. Y. Logan, and R. Nusse, "Self-renewing diploid Axin2 + cells fuel homeostatic renewal of the liver," *Nature*, 2015, doi: 10.1038/nature14863.
- [224] B. Smedsrød *et al.*, "Hepatic sinusoidal cells in health and disease: Update from the 14th International Symposium," *Liver International*. 2009, doi: 10.1111/j.1478-3231.2009.01979.x.
- [225] K. K. Sørensen *et al.*, "The scavenger endothelial cell: A new player in homeostasis and immunity," *American Journal of Physiology - Regulatory Integrative and Comparative Physiology*. 2012, doi: 10.1152/ajpregu.00686.2011.
- [226] K. Schledzewski *et al.*, "Deficiency of liver sinusoidal scavenger receptors stabilin-1 and -2 in mice causes glomerulofibrotic nephropathy via impaired hepatic clearance of noxious blood factors," *J. Clin. Invest.*, 2011, doi: 10.1172/JCI44740.

- [227] K. Elvevold, J. Simon-Santamaria, H. Hasvold, P. McCourt, B. Smedsrød, and K. K. Sørensen, "Liver sinusoidal endothelial cells depend on mannose receptor-mediated recruitment of lysosomal enzymes for normal degradation capacity," *Hepatology*, 2008, doi: 10.1002/hep.22527.
- [228] S. Shetty, P. F. Lalor, and D. H. Adams, "Lymphocyte recruitment to the liver: Molecular insights into the pathogenesis of liver injury and hepatitis," *Toxicology*. 2008, doi: 10.1016/j.tox.2008.08.003.
- [229] D. A. Patten *et al.*, "SCARF-1 promotes adhesion of CD4+ T cells to human hepatic sinusoidal endothelium under conditions of shear stress," *Sci. Rep.*, 2017, doi: 10.1038/s41598-017-17928-4.
- [230] D. A. Patten *et al.*, "Human liver sinusoidal endothelial cells promote intracellular crawling of lymphocytes during recruitment: A new step in migration," *Hepatology*, 2017, doi: 10.1002/hep.28879.
- [231] P.-S. Koch *et al.*, "Angiocrine Bmp2 signaling in murine liver controls normal iron homeostasis," *Blood*, vol. 129, no. 4, pp. 415–420, 2016, doi: 10.1182/blood-2016-07-729822.
- [232] S. Canali *et al.*, "Endothelial cells produce bone morphogenetic protein 6 required for iron homeostasis in mice," *Blood*, 2017, doi: 10.1182/blood-2016-06-721571.
- [233] B. Sen Ding *et al.*, "Inductive angiocrine signals from sinusoidal endothelium are required for liver regeneration," *Nature*, 2010, doi: 10.1038/nature09493.
- [234] J. C. Mathison and R. J. Ulevitch, "Lipopolysaccharide in Rabbits Localization of Intravenously Injected The Clearance, Tissue Distribution, and Cellular," *J. Immunol.* , 1979.
- [235] T. Areschoug and S. Gordon, "Scavenger receptors: Role in innate immunity and microbial pathogenesis," *Cellular Microbiology*. 2009, doi: 10.1111/j.1462-5822.2009.01326.x.
- [236] U. Gazi and L. Martinez-Pomares, "Influence of the mannose receptor in host immune responses," *Immunobiology*. 2009, doi: 10.1016/j.imbio.2008.11.004.
- [237] M. Martin-Armas, J. Simon-Santamaria, I. Pettersen, U. Moens, B. Smedsrød, and B. Sveinbjørnsson, "Toll-like receptor 9 (TLR9) is present in murine liver sinusoidal endothelial cells (LSECs) and mediates the effect of CpG-oligonucleotides," *J. Hepatol.*, 2006, doi: 10.1016/j.jhep.2005.09.020.
- [238] J. Wu *et al.*, "Toll-like receptor-induced innate immune responses in non-parenchymal liver cells are cell type-specific," *Immunology*, 2010, doi: 10.1111/j.1365-2567.2009.03179.x.
- [239] A. W. Lohse *et al.*, "Antigen-presenting function and B7 expression of murine sinusoidal endothelial cells and Kupffer cells," *Gastroenterology*, 1996, doi: 10.1053/gast.1996.v110.pm8613007.
- [240] P. A. Knolle *et al.*, "Induction of cytokine production in naive CD4+ T cells by antigen-presenting murine liver sinusoidal endothelial cells but failure to induce differentiation toward T(h1) cells," *Gastroenterology*, 1999, doi: 10.1016/S0016-5085(99)70508-1.
- [241] C. Wiegand, C. Frenzel, J. Herkel, K. J. Kallen, E. Schmitt, and A. W. Lohse, "Murine liver antigen presenting cells control suppressor activity of CD4+CD25+ regulatory T cells," *Hepatology*, 2005, doi: 10.1002/hep.20756.
- [242] C. Kurts, B. W. S. Robinson, and P. A. Knolle, "Cross-priming in health and disease," *Nature Reviews Immunology*. 2010, doi: 10.1038/nri2780.
- [243] A. Schurich *et al.*, "Distinct kinetics and dynamics of cross-presentation in liver sinusoidal

- endothelial cells compared to dendritic cells," *Hepatology*, 2009, doi: 10.1002/hep.23075.
- [244] N. von Oppen *et al.*, "Systemic antigen cross-presented by liver sinusoidal endothelial cells induces liver-specific CD8 T-cell retention and tolerization," *Hepatology*, 2009, doi: 10.1002/hep.22795.
- [245] J. J. Maher, "Cell-specific expression of hepatocyte growth factor in liver: Upregulation in sinusoidal endothelial cells after carbon tetrachloride," *J. Clin. Invest.*, 1993, doi: 10.1172/JCI116451.
- [246] L. Wang, X. Wang, G. Xie, L. Wang, C. K. Hill, and L. D. DeLeve, "Liver sinusoidal endothelial cell progenitor cells promote liver regeneration in rats," *J. Clin. Invest.*, 2012, doi: 10.1172/JCI58789.
- [247] F. Schaffner and H. Popper, "Capillarization of Hepatic Sinusoids in Man," *Gastroenterology*, 1963, doi: 10.1016/S0016-5085(63)80130-4.
- [248] L. D. Deleve, X. Wang, and L. Wang, "VEGF-sdf1 recruitment of CXCR7+ bone marrow progenitors of liver sinusoidal endothelial cells promotes rat liver regeneration," *Am. J. Physiol. - Gastrointest. Liver Physiol.*, 2016, doi: 10.1152/ajpgi.00056.2016.
- [249] G. Xie *et al.*, "Role of differentiation of liver sinusoidal endothelial cells in progression and regression of hepatic fibrosis in rats," *Gastroenterology*, 2012, doi: 10.1053/j.gastro.2011.12.017.
- [250] T. Horn, P. Christoffersen, and J. H. Henriksen, "Alcoholic liver injury: Defenestration in noncirrhotic livers—a scanning electron microscopic study," *Hepatology*, 1987, doi: 10.1002/hep.1840070117.
- [251] M. Pasarín *et al.*, "Sinusoidal endothelial dysfunction precedes inflammation and fibrosis in a model of NAFLD," *PLoS One*, 2012, doi: 10.1371/journal.pone.0032785.
- [252] R. Bataller and D. A. Brenner, "Erratum: Liver fibrosis (Journal of Clinical Investigation (2005) 115 (209-218) DOI:10.1172/JCI200524282)," *Journal of Clinical Investigation*. 2005, doi: 10.1172/JCI200524282C1.
- [253] S. L. Friedman, "Liver fibrosis - From bench to bedside," *Journal of Hepatology, Supplement*. 2003, doi: 10.1016/S0168-8278(02)00429-4.
- [254] P. Ginès, A. Cárdenas, V. Arroyo, and J. Rodés, "Management of Cirrhosis and Ascites," *N. Engl. J. Med.*, 2004, doi: 10.1056/nejmra035021.
- [255] A. L. Wilkinson, M. Qurashi, and S. Shetty, "The Role of Sinusoidal Endothelial Cells in the Axis of Inflammation and Cancer Within the Liver," *Frontiers in Physiology*. 2020, doi: 10.3389/fphys.2020.00990.
- [256] H. H. Wang *et al.*, "B16 melanoma cell arrest in the mouse liver induces nitric oxide release and sinusoidal cytotoxicity: A natural hepatic defense against metastasis," *Cancer Res.*, 2000.
- [257] H. Yanagida *et al.*, "Hepatic ischemia/reperfusion upregulates the susceptibility of hepatocytes to confer the induction of inducible nitric oxide synthase gene expression," *Shock*, 2006, doi: 10.1097/01.shk.0000223130.87382.73.
- [258] K. Vekemans, F. Braet, D. Muylaert, and E. Wisse, "Nitric oxide from rat liver sinusoidal endothelial cells induces apoptosis in IFN  $\gamma$ -sensitized CC531s colon carcinoma cells," *J. Hepatol.*, 2004, doi: 10.1016/j.jhep.2004.03.026.
- [259] A. M. Clark, B. Ma, D. L. Taylor, L. Griffith, and A. Wells, "Liver metastases: Microenvironments and ex-vivo models," *Exp. Biol. Med.*, 2016, doi: 10.1177/1535370216658144.

- [260] P. Auguste, L. Fallavollita, N. Wang, J. Burnier, A. Bikfalvi, and P. Brodt, "The host inflammatory response promotes liver metastasis by increasing tumor cell arrest and extravasation," *Am. J. Pathol.*, 2007, doi: 10.2353/ajpath.2007.060886.
- [261] J. Ou *et al.*, "Endothelial cell-derived-fibronectin extra domain A promotes colorectal cancer metastasis via inducing epithelialmesenchymal transition," *Carcinogenesis*, 2014, doi: 10.1093/carcin/bgu090.
- [262] L. R. Kelland, "'Of mice and men': Values and liabilities of the athymic nude mouse model in anticancer drug development," *Eur. J. Cancer*, 2004, doi: 10.1016/j.ejca.2003.11.028.
- [263] J. K. Peterson and P. J. Houghton, "Integrating pharmacology and in vivo cancer models in preclinical and clinical drug development," *Eur. J. Cancer*, 2004, doi: 10.1016/j.ejca.2004.01.003.
- [264] S. J. Huh, S. Liang, A. Sharma, C. Dong, and G. P. Robertson, "Transiently entrapped circulating tumor cells interact with neutrophils to facilitate lung metastasis development," *Cancer Res.*, 2010, doi: 10.1158/0008-5472.CAN-09-4442.
- [265] A. Sharma, N. R. Trivedi, M. A. Zimmerman, D. A. Tuveson, C. D. Smith, and G. P. Robertson, "Mutant V599EB-Raf regulates growth and vascular development of malignant melanoma tumors," *Cancer Res.*, 2005, doi: 10.1158/0008-5472.CAN-04-2423.
- [266] C. Khanna and K. Hunter, "Modeling metastasis in vivo," *Carcinogenesis*. 2005, doi: 10.1093/carcin/bgh261.
- [267] D. Herlyn *et al.*, "In Vitro Properties of Human Melanoma Cells Metastatic in Nude Mice," *Cancer Res.*, 1990.
- [268] F. J. Huang *et al.*, "Molecular basis for the critical role of suppressor of cytokine signaling-1 in melanoma brain metastasis," *Cancer Res.*, 2008, doi: 10.1158/0008-5472.CAN-08-1429.
- [269] J. C. Becker, R. Houben, D. Schrama, H. Voigt, S. Ugurel, and R. A. Reisfeld, "Mouse models for melanoma: A personal perspective," *Experimental Dermatology*. 2010, doi: 10.1111/j.1600-0625.2009.00986.x.
- [270] S. P. Flanagan, "'Nude', a new hairless gene with pleiotropic effects in the mouse," *Genet. Res.*, 1966, doi: 10.1017/S0016672300010168.
- [271] M. J. Bosma and A. M. Carroll, "The scid mouse mutant: Definition, characterization, and potential uses," *Annual Review of Immunology*. 1991, doi: 10.1146/annurev.iy.09.040191.001543.
- [272] O. F. Kuzu, F. D. Nguyen, M. A. Noory, and A. Sharma, "Current State of Animal (Mouse) Modeling in Melanoma Research," *Cancer Growth Metastasis*, 2015, doi: 10.4137/cgm.s21214.
- [273] M. Herlyn and M. Fukunaga-Kalabis, "What is a good model for melanoma," *Journal of Investigative Dermatology*. 2010, doi: 10.1038/jid.2009.441.
- [274] K. Nakamura, N. Yoshikawa, Y. Yamaguchi, S. Kagota, K. Shinozuka, and M. Kunitomo, "Characterization of mouse melanoma cell lines by their mortal malignancy using an experimental metastatic model," *Life Sci.*, 2002, doi: 10.1016/S0024-3205(01)01454-0.
- [275] L. van der Weyden *et al.*, "Genome-wide in vivo screen identifies novel host regulators of metastatic colonization," *Nature*, vol. 541, no. 7636, pp. 233–236, 2017, doi: 10.1038/nature20792.
- [276] M. H. Jenkins *et al.*, "Multiple murine BRAF(V600E) melanoma cell lines with sensitivity to

- PLX4032," *Pigment Cell Melanoma Res.*, vol. 27, no. 3, pp. 495–501, 2014, doi: 10.1111/PCMR.12220.
- [277] T. Bald *et al.*, "Ultraviolet-radiation-induced inflammation promotes angiotropism and metastasis in melanoma," *Nat.* 2014 5077490, vol. 507, no. 7490, pp. 109–113, Feb. 2014, doi: 10.1038/nature13111.
- [278] M. H. Jenkins *et al.*, "Multiple murine BRAFV600E melanoma cell lines with sensitivity to PLX4032," *Pigment Cell Melanoma Res.*, 2014, doi: 10.1111/pcmr.12220.
- [279] E. Pérez-Guijarro, C. P. Day, G. Merlino, and M. R. Zaidi, "Genetically engineered mouse models of melanoma," *Cancer*. 2017, doi: 10.1002/cncr.30684.
- [280] P. HANINEC and J. VACHTENHEIM, "Tyrosinase Protein Is Expressed Also in Some Neural Crest Derived Cells Which Are Not Melanocytes," *Pigment Cell Res.*, 1988, doi: 10.1111/j.1600-0749.1988.tb00129.x.
- [281] J. Ackermann, M. Fruttschi, K. Kaloulis, T. McKee, A. Trumpp, and F. Beermann, "Metastasizing melanoma formation caused by expression of activated N-RasQ61K on an INK4a-deficient background," *Cancer Res.*, 2005, doi: 10.1158/0008-5472.CAN-04-2970.
- [282] N. Dhomen *et al.*, "Inducible expression of V600EBraf using tyrosinase-driven Cre recombinase results in embryonic lethality," *Pigment Cell Melanoma Res.*, 2010, doi: 10.1111/j.1755-148X.2009.00662.x.
- [283] M. Bosenberg *et al.*, "Characterization of melanocyte-specific inducible Cre recombinase transgenic mice," *Genes. (United States)*, 2006, doi: 10.1002/dvg.20205.
- [284] V. K. Goel *et al.*, "Melanocytic nevus-like hyperplasia and melanoma in transgenic BRAFV600E mice," *Oncogene*, 2009, doi: 10.1038/onc.2009.95.
- [285] N. Dhomen *et al.*, "Oncogenic Braf Induces Melanocyte Senescence and Melanoma in Mice," *Cancer Cell*, 2009, doi: 10.1016/j.ccr.2009.02.022.
- [286] W. Damsky *et al.*, "mTORC1 activation blocks brafV600E-induced growth arrest but is insufficient for melanoma formation," *Cancer Cell*, 2015, doi: 10.1016/j.ccell.2014.11.014.
- [287] V. Umansky and A. Sevko, "Ret transgenic mouse model of spontaneous skin melanoma: Focus on regulatory T cells," *Pigment Cell Melanoma Res.*, 2013, doi: 10.1111/pcmr.12104.
- [288] M. Kato *et al.*, "Transgenic mouse model for skin malignant melanoma," *Oncogene* 1998 1714, vol. 17, no. 14, pp. 1885–1888, Oct. 1998, doi: 10.1038/sj.onc.1202077.
- [289] S. A. Wohlfeil *et al.*, "Hepatic endothelial notch activation protects against liver metastasis by regulating endothelial-tumor cell adhesion independent of angiocrine signaling," *Cancer Res.*, vol. 79, no. 3, pp. 598–610, Feb. 2019, doi: 10.1158/0008-5472.CAN-18-1752/653416/AM/HEPATIC-ENDOTHELIAL-NOTCH-ACTIVATION-PROTECTS.
- [290] L. C. Murtaugh, B. Z. Stanger, K. M. Kwan, and D. A. Melton, "Notch signaling controls multiple steps of pancreatic differentiation," *Proc. Natl. Acad. Sci. U. S. A.*, 2003, doi: 10.1073/pnas.2436557100.
- [291] I. Augustin *et al.*, "Loss of epidermal evi/wls results in a phenotype resembling psoriasiform dermatitis," *J. Exp. Med.*, 2013, doi: 10.1084/jem.20121871.
- [292] L. Van Der Weyden *et al.*, "Genome-wide in vivo screen identifies novel host regulators of metastatic colonization," *Nature*, 2017, doi: 10.1038/nature20792.
- [293] S. A. Wohlfeil *et al.*, "Angiogenic and molecular diversity determine hepatic melanoma

- metastasis and response to anti-angiogenic treatment," *J. Transl. Med.*, vol. 20, no. 1, Dec. 2022, doi: 10.1186/S12967-022-03255-4.
- [294] J. Gracia-Sancho, E. Caparrós, A. Fernández-Iglesias, and R. Francés, "Role of liver sinusoidal endothelial cells in liver diseases," *Nature Reviews Gastroenterology and Hepatology*. 2021, doi: 10.1038/s41575-020-00411-3.
- [295] X. Luo *et al.*, "Autophagic degradation of caveolin-1 promotes liver sinusoidal endothelial cells defenestration article," *Cell Death Dis.*, 2018, doi: 10.1038/s41419-018-0567-0.
- [296] Q. Sun *et al.*, "Notch1 promotes hepatitis B virus X protein-induced hepatocarcinogenesis via Wnt/ $\beta$ -catenin pathway," *Int. J. Oncol.*, 2014, doi: 10.3892/ijo.2014.2537.
- [297] A. Benedicto, I. Romayor, and B. Arteta, "Role of liver ICAM-1 in metastasis," *Oncology Letters*. 2017, doi: 10.3892/ol.2017.6700.
- [298] J. Saleh, "Murine models of melanoma," *Pathol. Res. Pract.*, vol. 214, no. 9, pp. 1235–1238, 2018, doi: 10.1016/j.prp.2018.07.008.
- [299] W. S. Chan, C. M. Page, J. R. Maclellan, and G. A. Turner, "The growth and metastasis of four commonly used tumour lines implanted into eight different sites: Evidence for site and tumour effects," *Clin. Exp. Metastasis*, 1988, doi: 10.1007/BF01782483.
- [300] C. R. Lindsay *et al.*, "P-Rex1 is required for efficient melanoblast migration and melanoma metastasis," *Nat. Commun.*, 2011, doi: 10.1038/ncomms1560.
- [301] N. R. Adler *et al.*, "Tumour mutation status and sites of metastasis in patients with cutaneous melanoma," *Br. J. Cancer*, vol. 117, no. 7, pp. 1026–1035, Sep. 2017, doi: 10.1038/BJC.2017.254.
- [302] R. Rabbie *et al.*, "The mutational landscape of melanoma brain metastases presenting as the first visceral site of recurrence," *Br. J. Cancer*, 2021, doi: 10.1038/s41416-020-01090-2.
- [303] S. Paku, L. Kopper, and P. Nagy, "Development of the vasculature in 'pushing-type' liver metastases of an experimental colorectal cancer," *Int. J. Cancer*, 2005, doi: 10.1002/ijc.20886.
- [304] M. Tulesin *et al.*, "Vascular Remodeling Is a Crucial Event in the Early Phase of Hepatocarcinogenesis in Rodent Models for Liver Tumorigenesis," *Cells*, 2022, doi: 10.3390/cells11142129.
- [305] C. Géraud *et al.*, "Unique Cell Type-Specific Junctional Complexes in Vascular Endothelium of Human and Rat Liver Sinusoids," *PLoS One*, vol. 7, no. 4, p. e34206, Apr. 2012, doi: 10.1371/JOURNAL.PONE.0034206.
- [306] C. M. Carreira *et al.*, "LYVE-1 is not restricted to the lymph vessels: Expression in normal liver blood sinusoids and down-regulation in human liver cancer and cirrhosis," *Cancer Res.*, 2001.
- [307] C. Korn and H. G. Augustin, "Mechanisms of Vessel Pruning and Regression," *Developmental Cell*. 2015, doi: 10.1016/j.devcel.2015.06.004.
- [308] K. Yoshimura *et al.*, "Integrin  $\alpha$ 2 mediates selective metastasis to the liver," *Cancer Res.*, 2009, doi: 10.1158/0008-5472.CAN-09-0315.
- [309] R. B. Rebhun, H. Cheng, J. E. Gershenwald, D. Fan, I. J. Fidler, and R. R. Langley, "Constitutive expression of the  $\alpha$ 4 integrin correlates with tumorigenicity and lymph node metastasis of the B16 murine melanoma," *Neoplasia*, 2010, doi: 10.1593/neo.91604.
- [310] A. Garofalo *et al.*, "Involvement of the Very Late Antigen 4 Integrin on Melanoma in Interleukin 1-augmented Experimental Metastases," *Cancer Res.*, 1995.

- [311] R. Huang and E. K. Rofstad, "Integrins as therapeutic targets in the organ-specific metastasis of human malignant melanoma," *Journal of Experimental and Clinical Cancer Research*. 2018, doi: 10.1186/s13046-018-0763-x.
- [312] A. Meves *et al.*, "Tumor cell adhesion as a risk factor for sentinel lymph node metastasis in primary cutaneous melanoma," *J. Clin. Oncol.*, vol. 33, no. 23, pp. 2509–2515, 2015, doi: 10.1200/JCO.2014.60.7002.
- [313] A. Takeda *et al.*, "Role of angiogenesis in the development and growth of liver metastasis," *Annals of Surgical Oncology*. 2002, doi: 10.1245/aso.2002.9.7.610.
- [314] S. P. Pitroda *et al.*, "Author Correction: Integrated molecular subtyping defines a curable oligometastatic state in colorectal liver metastasis," *Nat. Commun.*, 2018, doi: 10.1038/s41467-018-07303-w.
- [315] J. Liu *et al.*, "Molecular dissection of CRC primary tumors and their matched liver metastases reveals critical role of immune microenvironment, EMT and angiogenesis in cancer metastasis," *Sci. Rep.*, 2020, doi: 10.1038/s41598-020-67842-5.
- [316] S. M. Wilhelm *et al.*, "BAY 43-9006 exhibits broad spectrum oral antitumor activity and targets the RAF/MEK/ERK pathway and receptor tyrosine kinases involved in tumor progression and angiogenesis," *Cancer Res.*, 2004, doi: 10.1158/0008-5472.CAN-04-1443.
- [317] T. Eisen *et al.*, "Sorafenib in advanced melanoma: A Phase II randomised discontinuation trial analysis," *Br. J. Cancer*, 2006, doi: 10.1038/sj.bjc.6603291.
- [318] M. Toledo, F. Penna, S. Busquets, F. J. López-Soriano, and J. M. Argilés, "Distinct behaviour of sorafenib in experimental cachexia-inducing tumours: The role of STAT3," *PLoS One*, 2014, doi: 10.1371/journal.pone.0113931.
- [319] A. Lazaris *et al.*, "Vascularization of colorectal carcinoma liver metastasis: insight into stratification of patients for anti-angiogenic therapies," *J. Pathol. Clin. Res.*, 2018, doi: 10.1002/cjp2.100.
- [320] C. Giovannini *et al.*, "Molecular and proteomic insight into Notch1 characterization in hepatocellular carcinoma," *Oncotarget*, 2016, doi: 10.18632/oncotarget.9203.
- [321] K. Zhang, P. Wong, C. Salvaggio, A. Salhi, I. Osman, and B. Bedogni, "Synchronized Targeting of Notch and ERBB Signaling Suppresses Melanoma Tumor Growth through Inhibition of Notch1 and ERBB3," *J. Invest. Dermatol.*, 2016, doi: 10.1016/j.jid.2015.11.006.
- [322] D. A. Venkatesh, K. S. Park, A. Harrington, L. Miceli-Libby, J. K. Yoon, and L. Liaw, "Cardiovascular and hematopoietic defects associated with notch1 activation in embryonic tie2-expressing populations," *Circ. Res.*, 2008, doi: 10.1161/CIRCRESAHA.108.177808.
- [323] A. Trindade *et al.*, "Overexpression of delta-like 4 induces arterialization and attenuates vessel formation in developing mouse embryos," *Blood*, 2008, doi: 10.1182/blood-2007-09-112748.
- [324] F. P. Limbourg, K. Takeshita, F. Radtke, R. T. Bronson, M. T. Chin, and J. K. Liao, "Essential role of endothelial Notch1 in angiogenesis," *Circulation*, vol. 111, no. 14, pp. 1826–1832, 2005, doi: 10.1161/01.CIR.0000160870.93058.DD.
- [325] J. L. Duan *et al.*, "Endothelial Notch activation reshapes the angiocrine of sinusoidal endothelia to aggravate liver fibrosis and blunt regeneration in mice," *Hepatology*, 2018, doi: 10.1002/hep.29834.
- [326] L. Wang *et al.*, "Disruption of the transcription factor recombination signal-binding protein-Jk (RBP-J) leads to veno-occlusive disease and interfered liver regeneration in mice," *Hepatology*,

2009, doi: 10.1002/hep.22579.

- [327] M. T. Dill *et al.*, "Disruption of Notch1 induces vascular remodeling, intussusceptive angiogenesis, and angiosarcomas in livers of mice," *Gastroenterology*, vol. 142, no. 4, pp. 967-977.e2, 2012, doi: 10.1053/j.gastro.2011.12.052.
- [328] H. Cuervo, C. M. Nielsen, D. A. Simonetto, L. Ferrell, V. H. Shah, and R. A. Wang, "Endothelial notch signaling is essential to prevent hepatic vascular malformations in mice," *Hepatology*, vol. 64, no. 4, pp. 1302–1316, Oct. 2016, doi: 10.1002/HEP.28713.
- [329] L. D. DeLeve, X. Wang, and Y. Guo, "Sinusoidal endothelial cells prevent rat stellate cell activation and promote reversion to quiescence," *Hepatology*, 2008, doi: 10.1002/hep.22351.
- [330] C. Souilhol and P. C. Evans, "Notching Up Vascular Inflammation," *Arteriosclerosis, Thrombosis, and Vascular Biology*. 2018, doi: 10.1161/ATVBAHA.118.310856.
- [331] I. Christiansen, C. Gidlöf, K. M. Kälkner, H. Hagberg, H. Bennmarker, and T. Tötterman, "Elevated serum levels of soluble ICAM-1 in non-Hodgkin's lymphomas correlate with tumour burden, disease activity and other prognostic markers," *Br. J. Haematol.*, 1996, doi: 10.1046/j.1365-2141.1996.00377.x.
- [332] E. A. Kotteas *et al.*, "Soluble ICAM-1 levels in small-cell lung cancer: Prognostic value for survival and predictive significance for response during chemotherapy," *Med. Oncol.*, 2013, doi: 10.1007/s12032-013-0662-0.
- [333] A. Benedicto *et al.*, "Liver sinusoidal endothelial cell ICAM-1 mediated tumor/endothelial crosstalk drives the development of liver metastasis by initiating inflammatory and angiogenic responses," *Sci. Rep.*, 2019, doi: 10.1038/s41598-019-49473-7.
- [334] D. Alexiou *et al.*, "Serum levels of E-selectin, ICAM-1 and VCAM-1 in colorectal cancer patients: Correlations with clinicopathological features, patient survival and tumour surgery," *Eur. J. Cancer*, 2001, doi: 10.1016/S0959-8049(01)00318-5.
- [335] S. Ghislin, D. Obino, S. Middendorp, N. Boggetto, C. Alcaide-Loridan, and F. Deshayes, "LFA-1 and ICAM-1 expression induced during melanoma-endothelial cell co-culture favors the transendothelial migration of melanoma cell lines in vitro," *BMC Cancer*, 2012, doi: 10.1186/1471-2407-12-455.
- [336] T. Ozdemir, P. Zhang, C. Fu, and C. Dong, "Fibrin serves as a divalent ligand that regulates neutrophil-mediated melanoma cells adhesion to endothelium under shear conditions," *Am. J. Physiol. - Cell Physiol.*, 2012, doi: 10.1152/ajpcell.00346.2011.
- [337] A. Benedicto, J. Marquez, A. Herrero, E. Olaso, E. Kolaczowska, and B. Arteta, "Decreased expression of the  $\beta$ 2 integrin on tumor cells is associated with a reduction in liver metastasis of colorectal cancer in mice," *BMC Cancer*, 2017, doi: 10.1186/s12885-017-3823-2.
- [338] M. Winkler *et al.*, "Endothelial GATA4 controls liver fibrosis and regeneration by preventing a pathogenic switch in angiocrine signaling," *J. Hepatol.*, 2021, doi: 10.1016/j.jhep.2020.08.033.
- [339] Dietsch, B., Weller, C., Sticht, C. et al. Hepatic passaging of NRAS-mutant melanoma influences adhesive properties and metastatic pattern. *BMC Cancer* 23, 436 (2023). <https://doi.org/10.1186/s12885-023-10912-4>

## Acknowledgements

First, I would like to express my deepest gratitude to my second supervisor Prof. Dr. Cyrill Géraud for giving me the opportunity to perform my doctoral thesis in the “Arbeitsgruppe der Sektion Klinische und Molekulare Dermatologie”, for the supervision of my work and ongoing support throughout my PhD Thesis.

This thesis would not have been possible without the support of Dr. Sebastian Wohlfeil. I am extremely grateful for his supervision, help with design and performance of experiments, data analysis and support in all respects of my PhD Thesis.

Furthermore, I would like to express my appreciation to Prof. Dr. Peter Angel for being my first supervisor, for reviewing this thesis and for support and scientific input during the Thesis Advisory Committee (TAC) meetings.

I further would like to thank Prof. Dr. Thomas Wieland for being the chairperson and Prof. Dr. Viktor Umansky for being an examiner.

I am also thankful to Prof. Dr. Adelheid Cerwenka for being part of my TAC and scientific input during annual TAC meetings.

This thesis would not have been possible without funding of the Deutsche Forschungsgemeinschaft (DFG). I would like to thank all members of the Research Training Group 2099 “Hallmarks of Skin Cancer” for the organization of lecture series, conferences, summer schools, scientific input and support of my thesis.

Special thanks to Ina Schäfer and the LIMA Core facility for support with microscopic imaging.

I am also grateful for the support by Cathleen Fichtner, Camela Jost, Maria Muciek and Elisabeth Wühl for conducting histopathological stainings, for running the autotechnicon and for analysis of plasma levels at the core facility of the ZMF at the UMM.

Special thanks to the animal caretakers of the animal facility of the UMM H111 and H21 for the care of the mice and assistance in animal breeding.

I’m also thankful to Dr. Carsten Sticht for support with RNA sequencing and Data analysis.

Thanks, should also go to Jochen Weber, Hiltrud Schönhaber, Stefanie Riester and Christof Dormann for technical support and general support in all concerns regarding laboratory work. Special thanks also to Dr. Kai Schledzewski for support with animal breeding and genotyping, as well as technical support and scientific input.

I would like to extend my sincere thanks to all former and actual lab members of the “AG Angiodiversität und Organfunktion” and the “Arbeitsgruppe der Sektion Klinische und Molekulare Dermatologie”. I especially like to thank Céline Weller and Bianca Dietsch for scientific and personal support throughout my PhD Thesis.

Lastly, I’d like to thank my family and friends that always supported me. Especially I would like to thank my parents for their support throughout my studies and my husband Florian, who always supported and encouraged me. Special thanks to my daughters Wilhelmina and Ophelia, that remind me every day that there is so much more in life than just science. Many thanks to my friend Anna, for having the best time together during our studies and for personal advice and support during my PhD thesis.

# Appendix

## List of Figures

Figure 1 Cumulative survival in malignant melanoma in presence or absence of liver metastasis.....	- 11 -
Figure 2 The metastatic cascade.....	- 12 -
Figure 3 Hexagonal structure of the hepatic lobules in the liver.....	- 21 -
Figure 4 Morphology of LSEC.....	- 24 -
Figure 5 Scheme of the melanoma model.....	- 31 -
Figure 6 Melanoma cell lines.....	- 53 -
Figure 7 Metastatic efficiency and number of hepatic metastases of melanoma cell lines. .....	- 54 -
Figure 8 Histopathological analysis of hepatic metastases.....	- 57 -
Figure 9 Immunofluorescence staining of intratumoral blood vessels.....	- 59 -
Figure 10 Immunofluorescence stainings.....	- 61 -
Figure 11 Immunofluorescence staining of extracellular matrix proteins.....	- 64 -
Figure 12 RNA sequencing analysis.....	- 65 -
Figure 13 Generation of $Clec4g-Cre^{tg/wt}; Rosa26^{N1ICD-IRES-GFP}$ ( $NICD^{OE-HEC}$ ) and verification of endothelial Cre activity.....	- 67 -
Figure 14 Hepatic endothelial notch activation protects from metastasis.....	- 69 -
Figure 15 Characterization of adult $NICD^{OE-HEC}$ mice.....	- 71 -
Figure 16 Plasma analysis of 8-week-old mice after 4 hours of fasting.....	- 72 -
Figure 17 Analysis of endothelial zonation of $NICD^{OE-HEC}$ mice.....	- 73 -
Figure 18 Immunofluorescence staining of extracellular matrix proteins.....	- 75 -
Figure 19 Immunofluorescence staining of hepatic stellate cells and VE-Cadherin..	- 76 -
Figure 20 Metabolic zonation of $NICD^{OE-HEC}$ mice.....	- 78 -
Figure 21 Metastatic susceptibility of $Wls^{HEK-KO}$ mice.....	- 79 -
Figure 22 Immunofluorescence staining of adhesion molecules.....	- 80 -

## List of Tables

<b>Table 1. Unconjugated antibodies</b> .....	- 36 -
<b>Table 2. Conjugated antibodies</b> .....	- 37 -
<b>Table 3. Primes for genotyping</b> .....	- 37 -
<b>Table 4. Mouse strains</b> .....	- 41 -
<b>Table 5. Cell lines</b> .....	- 42 -
<b>Table 6. Metastatic sites upon WT31 tail vein injection</b> .....	- 56 -

## List of Abbreviations

ALCAM	activated leukocyte cell adhesion molecule
ALT	alanine transaminase
ARG1	arginase 1
$\alpha$ SMA	alpha smooth muscle actin
AST	aspartate aminotransferase
ATG5	Autophagy related 5
ATP	adenosine triphosphate
BMDCs	bone marrow derived cells
BMP	bone morphogenetic protein
BRAF	v-Raf murine sarcoma viral oncogene homolog B1
BSA	bovine serum albumin
CD	Cluster of differentiation
CDK4	cyclin dependent kinase 4
CDKN2A/p16	Cyclin Dependent Kinase Inhibitor 2A
cGMP	cyclic guanosine monophosphate
CHE	cholinesterase
CRC	colorectal carcinoma
CT	computed tomography
CTLA-4	Cytotoxic T-Lymphocyte-Associated Protein 4
CXCL12	C-X-C motif chemokine ligand 12
CXCR4	C-X-C motif chemokine receptor 4
CYP	Cytochrome P
DAPI	4',6-diamidino-2-phenylindole
DII4	delta-like 4
DMBA	Dimethylbenzanthracene
DMEM	Dulbecco's Modified Eagle Medium
DNA	deoxyribonucleic acid
dNTP	desoxynukleosidtriphosphate
EC	endothelial cells
EDTA	Ethylenediaminetetraacetic acid
EGF	epidermal growth factor

EGFR	epidermal growth factor receptor
EMT	epithelial-mesenchymal transition
ERK	Extracellular-signal regulated kinase
FAK	focal adhesion kinase
FBS	fetal bovine serum
FCS	fetal calf serum
FDA	Food and Drug Administration
FGF	fibroblast growth factor
FoxP3	Forkhead box protein P3
GATA4	GATA binding protein 4
GEO	gene expression omnibus
GLDH	Glutamate dehydrogenase
GluI	glutamine synthetase
GOBP	gene ontology biological processes
GTP	guanosine triphosphate
HCV	hepatitis C virus
H&E	hematoxylin & eosin
HEC	hepatic endothelial cells
HEPES	4-(2-hydroxyethyl)-1-piperazineethanesulfonic acid
HGF	hepatocyte growth factor
HIER	heat-induced epitope retrieval
HIF1-alpha	hypoxia-inducible factor-1 subunit alpha
HIM-Melanoma	High and intermediate metastatic melanoma
HSCs	hepatic stellate cells
ICAM 1	intercellular adhesion molecule
ICI	immune checkpoint inhibition
IFNY	interferon gamma
KRAS	Kirsten rat sarcoma virus
L1-CAM	L1 cell adhesion molecule
LM-Melanoma	Low metastatic melanoma
LPS	lipopolysaccharide
LSEC	liver sinusoidal endothelial cells
LSm	like Sm proteins

Lyve-1	lymphatic vessel endothelial hyaluronan receptor-1
MAPK	mitogen activated protein kinase
MCAM/MUC18	Melanoma Cell Adhesion Molecule
MEK	Mitogen-activated protein kinase kinase
MHC	major histocompatibility complex
miRNA	micro RNA
MMPs	Matrix metalloproteinases
MRI	magnetic resonance imaging
NASH	nonalcoholic steatohepatitis
NCAM	Neural cell adhesion molecule
NEAA	Non-essential amino acids
NEDD9	Neural Precursor Cell Expressed, Developmentally Down-Regulated 9
NF-1	neurofibromin-1
NFkB	nuclear factor k-light-chain-enhancer of activated B cells)
NICD	notch1 intracellular domain
NO	nitrogen oxide
NK-cells	natural killer cells
ORA	Over-representation analysis
PBS	phosphate buffered saline
PCR	polymerase chain reaction
PECAM	Platelet/endothelial cell adhesion molecule
PFA	Paraformaldehyde
PD1	programmed cell death protein 1
PDGF	platelet derived growth factor
PD-L1	programmed death-ligand 1
Pdxl	podocalyxin
POT1	Protection of Telomeres 1
PRRs	pattern recognition receptors
PTEN	Phosphatase and Tensin homolog
Raf	rat fibrosarcoma
RAS	Rat sarcoma
RBP-J Region	Recombination Signal Binding Protein For Immunoglobulin Kappa J

Rho	Ras homologous
RNA	ribonucleic acid
ROS	reactive oxygen species
RPMI	Roswell Park Memorial Institute
Rspo3	R-Spondin 3
RTKs	receptor tyrosine kinases
SCARF-1	scavenger receptor class F member 1
sGC	Soluble guanylyl cyclase
cGMP	cyclic guanosine monophosphate
TERT	Telomerase Reverse Transcriptase
TGF $\beta$	Transforming growth factor beta
TIMPs	Tissue inhibitors of metalloproteinases
TNF $\alpha$	Tumor necrosis factor alpha
TRP2	Tyrosinase related protein 2
Tyr-Promoter	tyrosinase-promoter
US	United States
UV	ultraviolet
VCAM-1	vascular cell adhesion molecule 1
VE-Cadherin	Vascular endothelial cadherin
VEGF-A	Vascular endothelial growth factor A
VEGFR3	Vascular Endothelial Growth Factor Receptor 3
WNT	Wingless/Integrated
ZMF	Zentrum für medizinische Forschung

